UNIVERSITY OF SOUTHERN QUEENSLAND

BEHAVIOUR OF FIBRE COMPOSITE PILES FOR TIMBER PILE REHABILITATION

A Dissertation submitted by

Chamila S. Sirimanna

B.Sc. Eng (Hons), PG Dip (Structural Design)

For the award of

Master of Engineering Research (MENR)

Supervisory Team

Dr. Mainul Islam
Assoc Prof. Thiru Aravinthan
Dr. Weena Lokuge

2011

ABSTRACT

Fibre composites have inherent material properties that are better than other existing materials such as steel, timber, or concrete in numerous environments. In the marine and ground-zone environments in particular, fibre composite materials can be selected for their corrosion, rot, and pest resistance, as well as high strength-to-weight ratio. The advantages of fibre composites over traditional construction materials, is their high strength, light weight, less corrosive, durable, and most importantly, no decay / deterioration by natural organisms, which is the dominant problem for timber piles used in water front structures.

This research project, focused on the development of a system for decayed timber piles replacement, for piers, jetties, bridges and boardwalks, using fibre composite technology to enable rehabilitation of the structures, as well as new construction, by using Glass Fibre Reinforced Polymer (GFRP) tubular pile and connector.

Three objectives were considered to examine the structural behaviour of GFRP tubular piles and connector used for novel timber pile rehabilitation technique. As the first objective, the effects of various loading scenarios on the capacity of the GFRP hollow tubular piles were investigated.

Then as a second objective, numerical simulations were performed using the finite element analysis approach to verify experiments, and study the behaviour of the overall pile rehabilitation system. Based on the results of these numerical simulations, further research areas were highlighted for filler material development, which was used to fill the space between the GFRP connector and the existing timber pile. Due to durability, pumpability, workability and compressive strength requirements, polyester resin based filler development was chosen.

As the third objective, appropriate polyester based filler materials were developed for the GFRP tubular connector, to transfer the vertical load from the super structure, to the original timber stump, by the connector. A research program has been initiated to improve the fundamental understanding of this rehabilitation concept. A new polyester based filler material has been considered to provide the working knowledge required for its broad utilisation.

Fibre composites have not been used in this specific manner previously. While there have been fibre composite wraps developed, these are not the replacement systems, and have inherent weaknesses in their application, being more difficult to install, and needing

to be highly tailored to specific instances. The concept developed, tested and verified in this study is viable for general timber pile rehabilitations in piers / jetties with reasonable factor of safety and will be possible to extended rural two lane timber bridges. The results of this research, reveals a system, designed from an engineering perspective, relatively simple to install. Further, it is favourably disposed to mass production processes, to gain efficiencies of scale. Finally, this targeted research project, uncovers a timber pile rehabilitation system, capable of accepting the full working loads, while also ensuring a life span of some 50-100 years, with minimal maintenance.

CERTIFICATION OF DISSERTATION

I hereby certify that the ideas, experimental work, results, analyses, software and conclusions reported in this dissertation are entirely my own effort, except where otherwise acknowledged. I also hereby certify that the work is original and has not been previously submitted for any other award, except where otherwise acknowledged.

_____   _____

Signature of Candidate   Date

ENDORSEMENT

_____   _____

(Dr. Mainul Islam)

_____   _____

(Assoc Prof. Thiru Aravinthan)

_____   _____

(Dr. Weena Lokuge)

Signature of Supervisor/s   Date

PUBLICATIONS ARISING FROM THE RESEARCH

During the research process, a number of papers have been published, based on the work presented in this thesis. They are listed here for reference.

Publication in the Refereed Journal:

1. **Sirimanna**, **C.S.**, Islam, M.M., & Aravinthan, T. (2011). Polymer Based Filler Materials as Infill for GFRP Pile Connector. *Key Engineering Materials*, Vols. 471- 472, pp.763-768.

2. **Sirimanna, C.S.**, Lokuge, W., Islam, M.M., & Aravinthan, T. (2012). Compressive Strength Characterization of Polyester Based Fillers. *Advanced Materials Research*, Vols. 410, pp.32-35.

Publications at International Conferences:

1. **Sirimanna, C.S.**, Islam, M.M., & Aravinthan, T. (2010). Preliminary Development of Polymer Based Filling Materials for GFRP Confinement. *Twenty-first Australasian Conference on the Mechanics of Structures and Materials (ACMSM21)*, December 07-10, 2010, Melbourne, Australia. pp.445-451

2. Guades, E.J., **Sirimanna, C.S.,** Aravinthan, T., & Islam, M.M. (2010). Behaviour of fibre reinforced polymer (FRP) tubular pile under axial compression load. *Twenty-first Australasian Conference on the Mechanics of Structures and Materials (ACMSM21)*, December 07-10, 2010, Melbourne, Australia. pp.457-463.

3. Lokuge, W., Aravinthan, T., **Sirimanna, C.S.**, & Islam, M.M. (2011). Influence of Fly Ash Proportions on Properties of Polymer Concrete with Polyester Resin. *The Concrete Institute of Australia's 25th Biennial Conference* to be held on October 12-14, 2011 in Perth, West Australia.

ACKNOWLEDGEMENTS

The undertaking and completion of this study would not have been possible without the help and assistance of a number of significant people, to whom I wish to express my sincere gratitude and appreciation.

To my supervisory team –

Dr. Mainul Islam – Thank you for sharing with me your knowledge and support, and in the giving of your time to edit and review this work.

A/Prof. Thiru Aravinthan – Thank you for first recognising my potential, and providing me with invaluable insight and assistance in the many facets of this work, and for the generosity of your time in reviewing this dissertation.

Dr. Weena Lokuge – Thank you for your expertise, and invaluable guidance in the numerous aspects of this work.

To my wife, Dulmini – Thank you so much for your love and support through the ups and downs, and for allowing and encouraging me to pursue this goal.

To my Parents – Thank you for your constant support, and for giving me the initial motivation to become an engineer.

To the CEEFC team – Thank you for teaching me the skills I required to produce the experimental specimens for my study. Your valuable assistance and advice saved me many hours, and I gratefully acknowledge your part in this work. Many thanks, especially to my fellow postgraduates, who have willingly provided ongoing support and wonderful friendship.

To Mr. Norm Watt (Managing Director), and other staff members of BAC Technologies Pty. Ltd, for essential support during this research, and for the provision samples for testing, all of which is greatly appreciated.

To others, who played a part in this work, regardless of the size of their contribution, I offer my sincere appreciation.

.

TABLE OF CONTENTS

Chapter 4 NUMERICAL SIMULATIONS OF THE OVERALL
BEHAVIOUR OF GFRP PILE SYSTEMS

Chapter 6   CONCLUSIONS

LIST OF FIGURES

LIST OF TABLES

NOMENCLATURE

Term	Definition
D	Diameter of the confined core
E	Young's modulus
Ec	modulus of elasticity of concrete
E_f	Modulus of elasticity of the FRP system in the hoop direction
Eo	Ratio between maximum stress (f_o) and strain at maximum stress (ε_o)
F	Vertical load at a middle of beam
f_{cp}	The confining pressure provided by the FRP system
f_f	Ultimate strength of the FRP system in the hoop direction
I	2nd moment of inertia of Biaxial fibre in the pile
L	Support span
M	Applied moment
m_b	Mass of flask fills with water
m_c	Mass of flask with sand sample + water
m_m	Mass of oven dry sand sample
m_s	Mass of Saturated surface dry Sand sample
t_f	Thickness of the FRP system
V	Total volume
V_{FA}	Volume of Fly ash
V_{In}	Volume of Initiator
V_{Re}	Volume of Resin
V_{Sa}	Volume of Sand
W	Total weight of samples
W_{FA}	Weight of Fly ash
W_{In}	Weight of Initiator
W_{Re}	Weight of Resin
W_{Sa}	Weight of Sand
y	Distance from neutral axis
v_a	Air voids in sand mix
v_m	Volume in material (sand)
ρ	Bulk density of sand
ρ_{FA}	Density of Fly ash
ρ_{In}	Density of Initiator
ρ_m	Material density of sand
ρ_{Re}	Density of Resin
ρ_{Sa}	Density of Sand
ρ_w	Density of water at specific temperature
σ_c	Compressive strength at failure
ϵ_f	Ultimate strain of the FRP system
$\epsilon_{t(hoop)}$	Ultimate strain of the core in hoop direction

Chapter 1

INTRODUCTION

1.1 Introduction

Timber piles are widely used to support buildings, bridges, trestles, wharves and a variety of other structures. Australia has a large number of timber bridges which require ongoing maintenance and rehabilitation. The approximate numbers of timber bridges around some of the Australian States are shown in Table 1.1:

Table 1.1: Population of timber bridges in Australia (Irene Scott, 2002)

State	local council owned	state road authority owned	state rail authority owned
NSW	4000	150	700
QLD	3000	500	
WA	3000		
VIC	600	25	
TAS	100		

These figures indicate that there are a large number of timber bridges within the local government regions. The serviceability of these bridges are affected due to the age and minimal level of maintenance. Timber piles have been traditionally used in many bridges for piers, especially when loose granular materials are present. Locally available wood piles provide a low-cost foundation system. As an organic material, timber may be subjected to decay and deterioration by natural organisms. Untreated wood piles are subjected to deterioration from marine borers, crustaceans, fungi, and other sources (Figure1.1). For this reason, many wood piles have been treated in the past with preservatives, like creosote, or chromated copper arsenate (CCA) (Lopez-Anido 2003). With time, preservatives are leached from the wood, and thus deterioration begins within the treated wood piles, similar to that of untreated wood piles. When wood piles deteriorate, the conventional repair process is to dismantle the pier, extract the deteriorated piles, drive in new piles, and rebuild the pier over the new piles. In addition, treated extracted piles may need to undergo special disposal procedures.

For some facilities, especially when a road bridge sits on piers, extraction of deteriorated piles, and driving down new piles, can be difficult and costly. In these cases, replacing deteriorated portions with new piles, becomes a sought after alternative. Replacements are possible, since the portion of the pile below the mud-line, is normally fully intact. The major deterioration occurs in the portion of the pile in the inter-tidal zone, and the splash zone (above high-tide) [Figure 1.2 (a)].

(a)   (b)
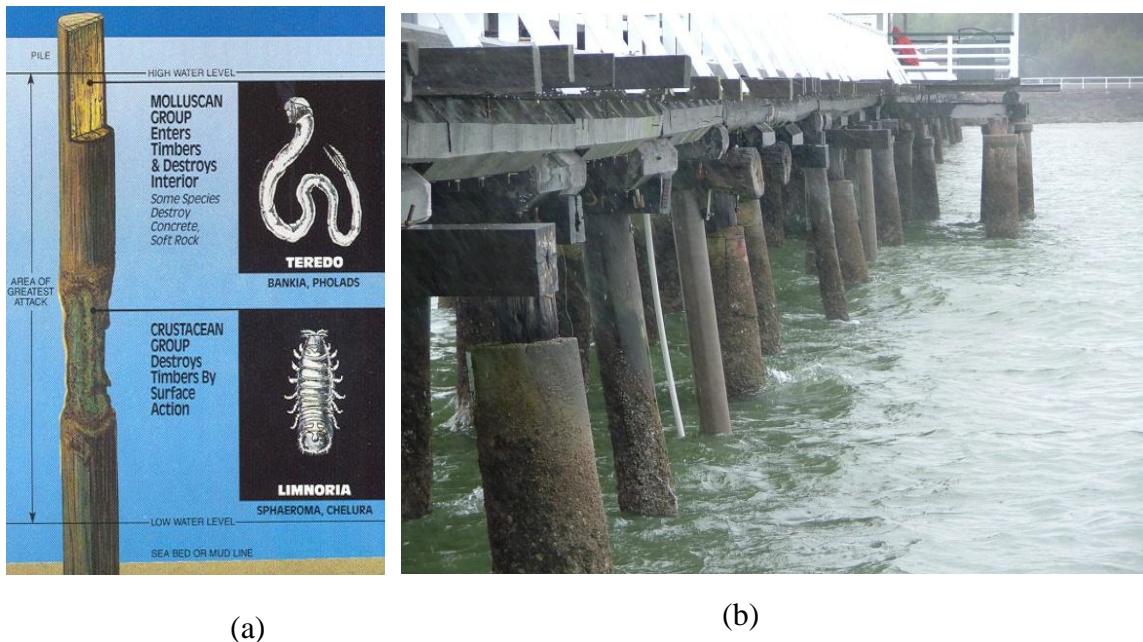
Figure 1.1: (a) Types of marine borers attack, in the pile (www.georgehenn.com), (b) Decayed timber pile in Shorncliffe Pier, Brisbane

In response to this problem, an innovative technique for the repair of these decayed timber piles is being evaluated by the Centre of Excellence in Engineered Fibre Composites (CEEFC), University of Southern Queensland, Australia, with the collaboration of BAC Technologies Pty Ltd. The replacement system consists of a new pile made out of Glass Fibre Reinforced Polymer (GFRP), and a GFRP tubular connector [Figure 1.2 (b)]. The connector is used to join the existing timber pile to the new pile. To simplify the construction, the connector is first inserted onto the existing timber stump [Figure 1.2(c)]. Then, the new pile is inserted into the connector, and both lifted, until they become attached to the head stock. After that, the void between the connector and existing timber pile was filled with a suitable filler material, to transfer the vertical load from the connector to the original stump [Figure 1.2(d). The use of the GFRP system provides an advantage over other conventional materials due to their high-strength to weight ratio, resistance to corrosion, durability and ease of installation.
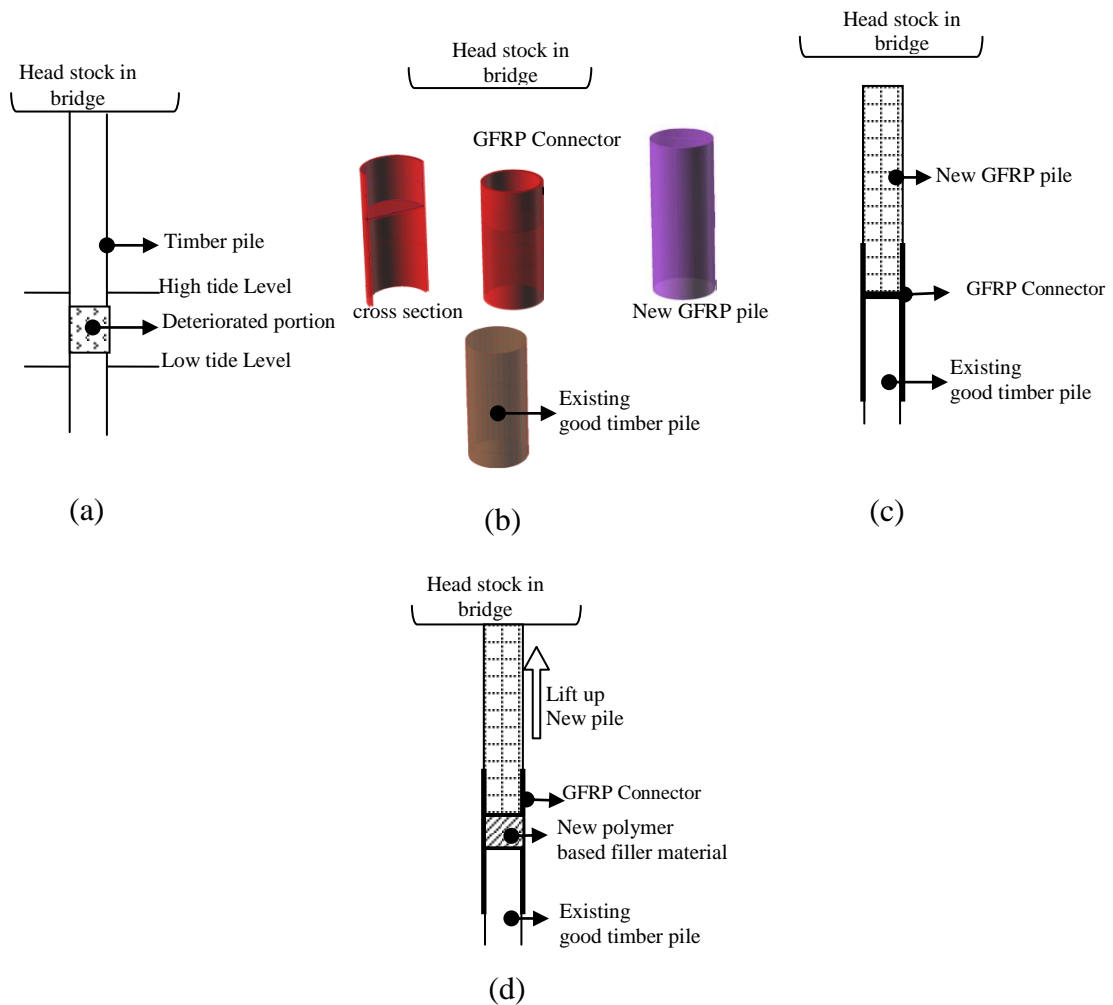
Figure 1.2: (a) General layout of the deteriorated timber pile, (b) Typical components used in pile rehabilitation, (c) Installing FRP connector and new pile in to the remaining non deteriorated timber pile, (d) Filling new polymer base filler material in to the connector.

To evaluate the performance and effectiveness of the proposed repair scheme, an experimental program has been conducted at the structural laboratories at the University of Southern Queensland.

1.2 Objectives

The main objectives of this research project are to examine the structural behaviour of Glass Fibre Reinforced Polymer (GFRP) tubular piles used for novel timber pile rehabilitation technique. The main three aspects considered in the study are:

I. To examine the effect of various loading scenarios on the capacity of the GFRP hollow tubular piles. Extensive experimental investigations were conducted to identify behaviour of GFRP hollow piles under different loadings.

II. Develop a comprehensive numerical simulation model using Finite Element Analysis (FEA) approach to study both experimental and overall behaviour of GFRP pile, followed by the connector under different loadings. Based on the results of these numerical simulations, further research areas are highlighted for polymer based filler development.

III. Development of appropriate polymer based filler material for the GFRP tubular connector, to transfer the vertical load from super structure, to the original timber stump, by the connector. This third objective includes investigations of suitable polymer based filler mixes, mix design approaches, and mathematical model to represent the behaviour of unconfined polymer based fillers, under compression loadings.

1.3   Scope of the study

The scope of this study involves an experimental investigation, and FEA modelling to examine the effectiveness of GFRP piles used for innovative decayed timber piles method of repair, by using the GFRP connector and polymer based fillers. The study encompasses: characterising the behaviour of the fibre composite laminates in flexure, tension, compression and shear, which are the building blocks of the GFRP pile. The experimental program includes testing of two full-scale piles having outer diameters of 300 mm and 470 mm respectively, for compression, bending and combine loadings.

In polymer based filler materials development, sample mixes were considered, based on trial weight percentages, and the volumetric analysis approach, comprising of different proportions of polyester resin, fly ash, and sand.   Material parameters, such as compressive strength, stiffness, shrinkage, split tensile strength, modulus of rupture, flexural modulus, and gel time, were achieved from the experimental investigation. The focus of the study was to determine the existence (or absence) of relationships, rather than their precise nature. Over 100 individual tests were completed, to examining the behaviour of polyester based fillers. This strategic investigation provides the platform to further undertake a large number of subsequent detailed investigations. Consequently, caution has been exercised in the analysis and interpretation of data, because much more testing will be required to better establish, and verify detailed relationships.

1.4 Structure of the dissertation

The thesis is organised in the following format:

Chapter 2: This chapter presents a review of previous studies of timber pile rehabilitation techniques, found in other literature. The mechanics of unconfined and confined concrete, and how it affects the axial compressive performance, is also briefly discussed. All of which is related to the proposed pile repair technique. In addition, a general summary of polymer concrete, and its mechanical properties are reviewed, with the goal of understanding more about the behaviour of polymer base fillers.

Chapter 3: This chapter presents the experimental program analysis, and interpretation of results, including coupon laminates, and full-scale pile testings. Details of the repair technique, materials used, fabrication process, and the different parameters, are evaluated and discussed.

Chapter 4: Numerical simulation of the experimental program, overall behaviours of the 300 mm external diameter GFRP pile, followed by the connector, is discussed relative to the FEA approach. In addition, the 470 mm external diameter GFRP pile performance will be assessed, by using the FEA model against a two lane timber bridge loadings, under class 4 road classification in AS 5100.7-2004. Also filler material inside the connector was simulated to identify filler behaviour against bridge loadings.

Chapter 5: Development of polymer based filler material for the GFRP connectors is presented in this chapter. Detailed investigations of polyester fillers were done using trial weight percentages, and the volumetric analysis approach. Mechanical properties, such as compressive strength, flexural modulus, split tensile strength, modulus of rupture, etc., are evaluated to identify the behaviour of polymer base fillers under different loadings. Compressive strength versus age curves, are established for different mix proportions of polymer fillers, against the volumetric analysis approach. Axial stress - strain mathematical model for normal strength

concrete was re-evaluated to identify any similarities of unconfined polymer based fillers with different fly ash regions.

Chapter 6: This chapter provides a summary and conclusions of the study. Recommendations for future research are also highlighted in this chapter.

Chapter 2

REVIEW OF TIMBER PILE REHABILITATION WITH ALTERNATIVE MATERIALS

2.1 Introduction

This section presents a review of published timber pile repair studies. The repair methodologies discussed include: pile splicing, cutting and posting, grout injection, concrete jackets, and FRP composite shells. Proposed novel timber pile rehabilitation techniques utilise GFRP piles, GFRP connectors, and polymer based filler material as major components. This filler material is used for filling in between the connector and the existing timber pile. When considering overall behaviour of the system against different loadings, the GFRP connector will act as a confinement to the filler. This scenario could be the same as concrete confined with FRP layers. Therefore the use of confining FRP systems to enhance the axial compressive performance of concrete columns will be discussed. Test data on confined concrete columns has formed a basis for the development of equations, describing the mechanics of unconfined and confined concrete. Several of these equations are presented in this chapter, and with appropriate modifications, may be applicable for investigating stress strain behaviour of unconfined polymer base filler material. In addition, a general summary of polymer concrete, and its properties are presented to obtain a macro view about polymer base fillers.

2.2 Damage zones in timber piles

Timber piles that support piers or other marine structures are driven into the mud, and extend above to the deck or structure they support. The vertical variation of exposure condition of the timber pile, allows the creation of different micro-environment zones, as shown in Figure 2.1 (US Army Corps of Engineers et al., 2001).

This exposure variation affects the type and extent of damage produced by marine organisms. A typical damage profile in the different zones of a timber pile is illustrated in Figure 2.2. Similar to the case of corroded steel piles in marine structures, (Coburn, 2000), inspection of marine timber piles indicate the presence of

five different zones: Atmospheric, splash, tidal, continuously submerged, and soil. Timber pile damage, due to marine organisms in each zone, is assessed.
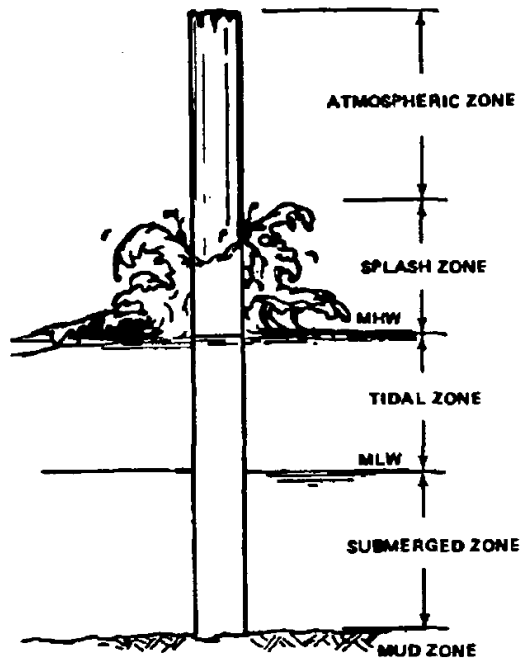
Figure 2.1: Exposure zones of marine timber piles (US army corps of engineers et al. 2001)
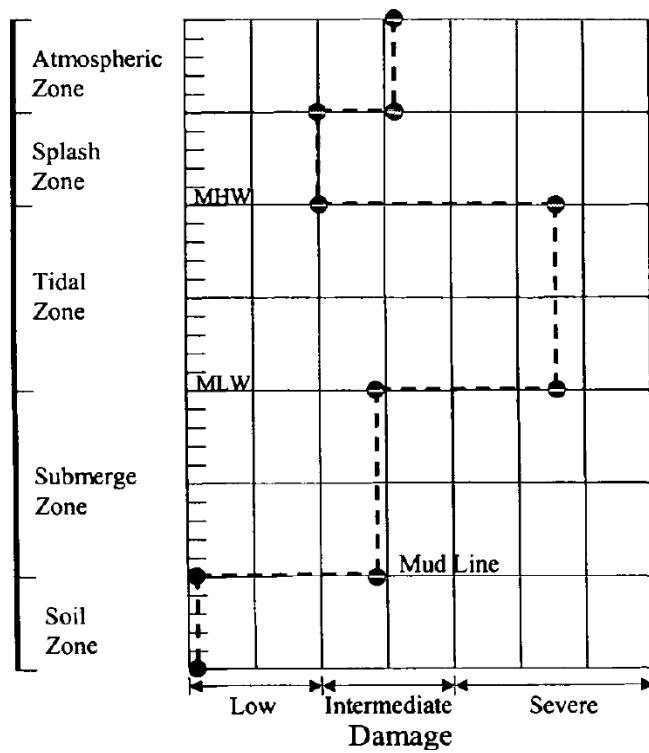
Figure 2.2: Typical damage profile of a timber pile (US army corps of engineers et al. 2001)

2.2.1 Atmospheric Zone

The atmospheric zone is the top portion of the timber pile, which is above the splash zone. This zone is accessible for maintenance and repair. In this zone, the presence of fresh water from the rain and oxygen creates a favourable environment for the growth of fungi. Fungal spores could exist inside the timber in an inert state for years. When the conditions in this zone are favourable, fungi will grow and start decaying the timber, working their way from the inside to the outer surface. Timber piles are often vulnerable to fungal attack in their centre portion, because preservative treatments do not penetrate all the way into the timber section. Marine borers will not attack the timber in the atmospheric zone, since they cannot survive in this environment.

2.2.2 Splash Zone

The mean high water level at the bottom, and the atmospheric zone at the top, delimit the splash zone. The timber pile surface is exposed to continuous water spray. This zone is accessible for maintenance and repair at low tide, with some limitations. Although this zone is subjected to continued salt water spray, it is possible for fungi to survive and damage the timber, because there is adequate oxygen, and the salinity is not very high. Fungal activity will probably be lower in this zone, since the conditions are not the most favourable.

2.2.3 Tidal Zone

The tidal zone is delimited by the mean low water level, and the mean high water level. This zone is exposed to cycles of water immersion. This zone is accessible for maintenance and repair at low tide, with difficulty. The tidal zone is typically the most heavily attacked zone of a timber pile. In this zone, marine borers such as shipworms and Gribble attack the timber, and cause significant damage. The conditions in this zone seem to be the most favourable for the marine borers to flourish. The presence of salt water and oxygen is a necessity for the survival of marine borers. If the mud line is above the mean low water level, then the attack is most severe at the mud line. In the case of Gribble, a significant reduction in the cross section at the mud line can be observed.

2.2.4 Continuously Submerged Zone

The continuously submerged zone extends between the mud line and the mean low water level. This zone is permanently under water. If the mud line is above the mean low water level, then this zone does not exist. This zone is only accessible for maintenance and repair with cofferdams or specialised underwater techniques. Marine borers such as shipworms and Gribble can attack the timber since salt water and oxygen are available at this zone. However, the attack and the extent of damage may not be as severe as the damage in the tidal zone.

2.2.5 Soil Zone

The soil zone is the zone below the mud line. Generally, this zone does not require maintenance. In this zone there is no oxygen available, which prevents the survival of marine borers. For this reason, timber piles below the mud line are usually in good condition.

Compared to the above zones, the tidal zone is more vulnerable to marine borer attacks, causing significant timber damage. Therefore waterfront timber pile systems, located in this tidal zone require continual examination, and to undergo appropriate repairs and/or rehabilitation.

2.3 Previous studies on timber pile rehabilitation

Very few experimental studies on the repair and rehabilitation of decayed timber piles are available in publications and modern day literature. However, a few repair methodologies were used in the past, including splicing, cutting and posting, grout injection, and concrete jackets.

There are many factors which may affect the selection of a repair method, including the strength and durability of the repaired pile, access to the existing pile, disruption of structural functions due to pile repair activities in remote locations, and the availability of craftworkers, materials, and equipment. Although cost tends to be the overriding factor in the selection of an appropriate repair method, strength and durability of the repaired pile is also an important factor. Ideally, the repair scheme should restore the timber pile to its original strength.
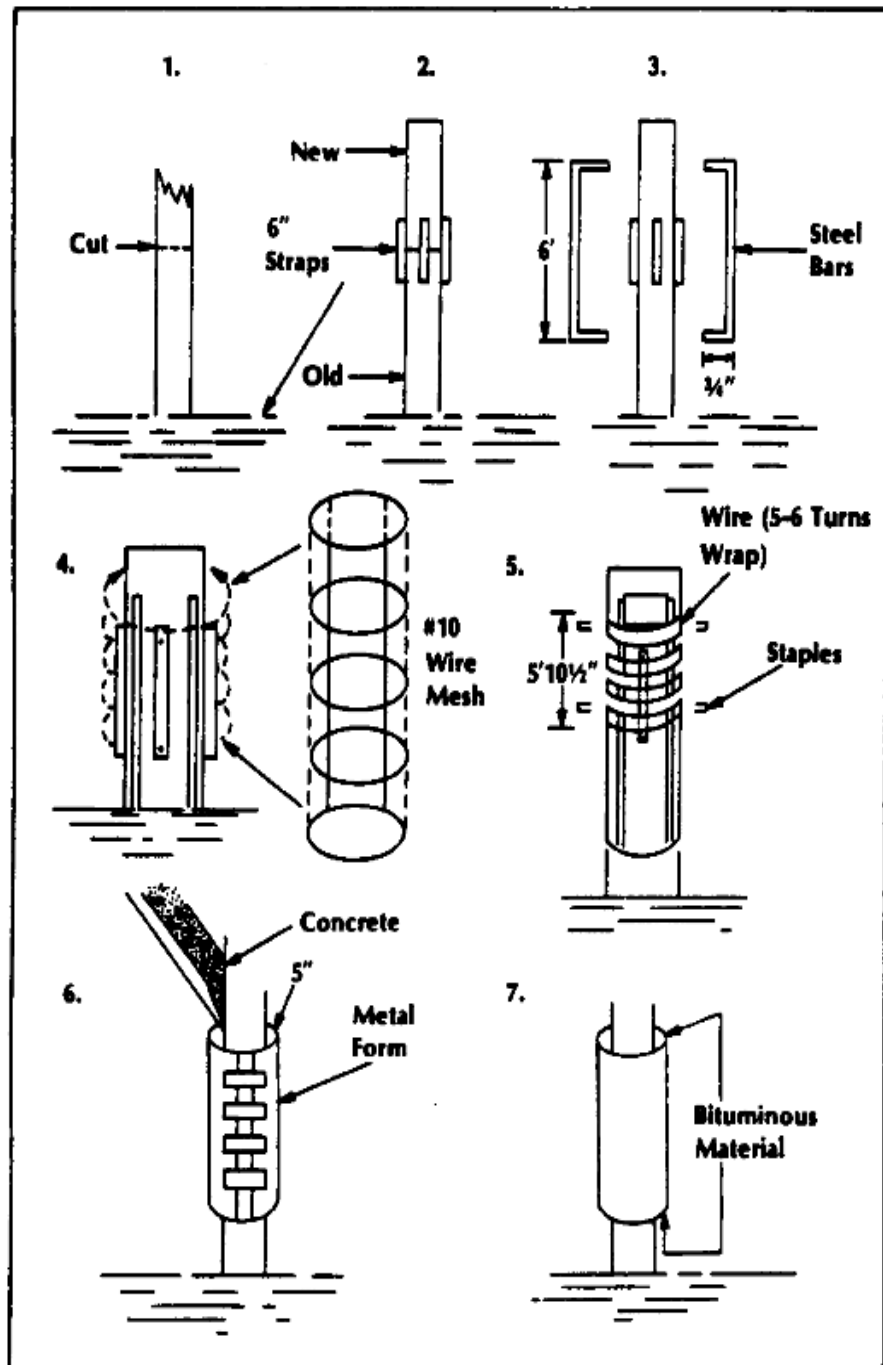
Figure 2.3: Timber pile repair scheme by splicing using reinforced concrete [US ARMY FM 5-134 (1985)]

Repair by pile splicing involves the addition of new materials and connectors, such as attaching a new section of timber pile to the existing pile, bolting or splicing sections of steel, or adding steel or timber bracing. A typical splicing repair scheme is shown in steps one through seven in Figure 2.3 (US ARMY (1985): FM 5-134). As shown in Figure 2.3, the deteriorated upper portion of the pile is removed and a new section of pile is installed and spliced to the existing timber below. If long,

unsupported piles are spliced using new timber, the flexural strength at the splice is typically much less than that of the original pile.

A stronger splice can be obtained with a reinforced concrete encasement as shown in Figure 2.3. However, the complexity of the technique, the amount of additional material required, and the long term durability of the repair are the main concerns.

Cutting and posting is a repair technique that is similar to pile splicing, and involves cutting out the damaged section of pile and replacing it with a new section of timer pile. The extent of damage in the existing pile is first determined by drilling. The deteriorated pile section is then cut perpendicular to the longitudinal axis of the pile and removed. A jack is used to provide temporary support to the structure above. A new length of timber pile of similar diameter is then cut and placed into position, as shown in Figure 2.4. The new piece of timber is spiked or bolted to the existing pile and a relatively weak connection is formed. To increase the capacity of the repaired pile, a low viscosity epoxy may be pressure injected through a predrilled port connecting the new piece to the existing timber pile, as shown in Figure 2.4.
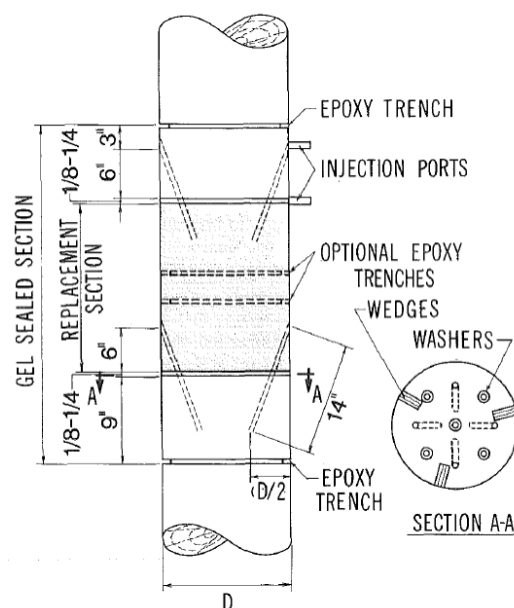
Figure 2.4: Schematic of cutting and posting timber pile repair (Avent, 1989)

The effectiveness of the cutting and posting repair procedure using epoxy injection was evaluated by Avent, (1989), both experimentally, and in a field repair application on a bridge with timber piles. Avent reported that the repair procedure can restore the axial strength of timber piles to their original design strength. However, the flexural strength of the piles can be restored to only about one-half the

original design capacity. The injection of cementitious grout into voids in decayed timber piles is a repair technique that was explored by Ritter, (1990). The procedure involved treating the existing timber to prevent further decay, then drilling various holes and pumping the grout through hose nozzles into the drilled holes. According to Railway Track and Structures (1973), this procedure is expected to add 15 – 20 years of service life to the piles. If the pile damage is less severe, epoxy injection can be used to effectively repair the pile. Reinforced concrete jackets have also been used to repair damaged timber piles. As shown in Figure 2.5, reinforcement is first placed in the annular space between the deteriorated timber pile and the formwork, followed by concrete injection. Concrete jackets have also been formed using a 25 mm - 50 mm thick coating of shotcrete, reinforced with a wire mesh. Precast concrete jackets have also been used for timber pile repair applications.
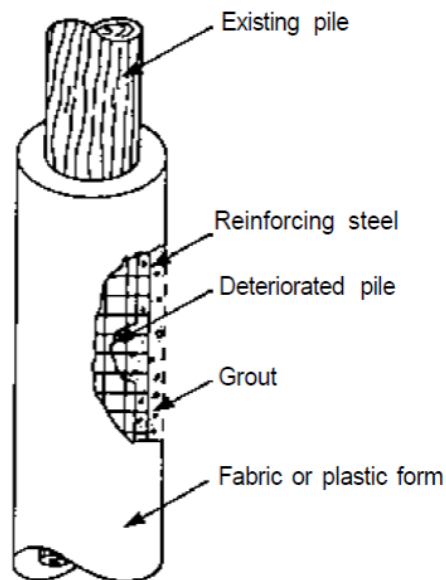
Figure 2.5: Reinforced concrete jacket for pile augmentation (Ritter, 1990)

Since concrete is prone to deterioration from environmental effects such as the acids, alkalies or salts found in ground water, there is a concern regarding the durability of reinforced concrete jackets.

Alternate freezing and thawing cycles accelerate the deterioration, since any water in the voids or cracks creates an expansive force when freezing, with further cracking and spalling. Cracking and spalling may lead to exposure and corrosion of the reinforcing steel, including the loss of the relatively thin concrete cross-section.

The process of external strengthening typically involves: filling the cracks and holes, surface preparation, primer application (primer usually consists of resin

applied to the timber), wetting the FRP fabric with resin, and the application of this FRP fabric to the member.

Applying FRP composite wraps to deteriorated timber members is a widely accepted practice for strengthening structural members. The fabric wraps are usually applied in layers to provide a maximum gain in strength and stiffness. Plate bonding is also a popular alternative to the application of composite fibres/fabrics to strengthen timber members. Plates are normally bonded using epoxies. However, due to the creosote treatment of timber, some epoxies do not bond well. It is extremely important to achieve optimum bonding between the timber substrate, and the FRP composite. Therefore, plate bonding to creosote-treated members with phenolic based adhesives compatible with the timber substrate, is not an acceptable alternative for rehabilitating timber railroad bridges.

GangaRao et al. (1996), conducted research on timber beams, strengthened with a Glass Fibre Reinforced Composite (GFRP) wrap. The wrap surrounded the four longitudinal faces of the beam. One group of timber cross ties was wrapped with a GFRP fabric, placed parallel to the longitudinal axis, and one group was wrapped perpendicular (transverse) to the longitudinal axis. To minimise the amount of fabric used per tie, only one layer of GFRP was used. The GFRP wrap successfully increased the modulus of elasticity (MOE) by 14 – 41% and the modulus of rupture (MOR) by 14 – 31%. Ductility of the beams was also maintained as the ties could carry additional loading, experiencing more deformation relative to other beams that were not wrapped.

Repair of timber piles using prefabricated FRP composite shells was investigated by Lopez, (2005). This method employed an FRP composite encasement or shield that encapsulates and splices the deteriorated portion of the pile. The development of the encasement was based on experience, with appropriate technologies in the structural FRP composites field, combined with the needs for timber pile protection and strengthening observed in the field inspection and survey. The shield is made of bonded thin and flexible FRP composite prefabricated cylindrical shells that deliver the required strength to repair damaged timber piles. The shells are fabricated in a quality-controlled composites manufacturing facility. The cylindrical shells have a slit or opening along their length, which enables them to be opened and placed around the deteriorated timber pile. Since it is advantageous to encase the pile with a series of overlapping shells, the minimum number of FRP

composite shells required is two. However, additional shells can be added, depending on the structural restoration needs. The slit in each cylindrical shell is staggered to avoid lines of weakness through the entire shield. (Figure 2.6)
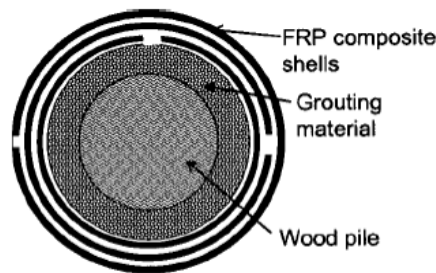
Figure 2.6: Cross section of timber pile repaired with fibre-reinforced polymer composite shells (Lopez, 2005).

In this repair method, the space between the FRP composite shield, and the timber pile is filled with a grouting material which does not provide a structural bond with the timber pile. It does however, provide interlocking (friction) between the timber pile, and the FRP composite shells. Since the grout is not expected to completely seal the timber core, seawater saturates the pile, creating a layer of stagnant water, potentially limiting the oxygen supply. Assuming a lack of oxygen, marine borers already inside the timber pile would be expected to die, and new borers would be prevented from attacking the timber pile.

As proposed in the present study, GFRP pile and connector can be an attractive replacement solution, and fibre composites have not been used in this specific manner previously. While there have been fibre composite wraps developed and shown in literature reviews, these are not replacement systems, and posses inherent weaknesses in their application, being more difficult to install, and needing to be highly tailored to specific purposes. This research, designed from an engineering perspective to be relatively simple to install, will be able to be mass produced to gain efficiencies of scale, and bearing the full working loads, while also ensuring a life span of 50-100 years, with minimal maintenance.

2.4   Review of polymer concrete

This proposed novel rehabilitation approach is required to develop polymer based filler materials for the FRP connector. The FRP connector will act as a confinement for the filler. This filler material is used for filling between the connector and the existing timber pile. This filler must have a good workability, less curing time, fair

compressive capacity, and reasonable pump ability qualities. For durability considerations, concrete was less suitable material for GFRP. Therefore, a review of the polymer concrete is very important, to understand the behaviour of the new polymer based filler materials.

Polymer Concrete (PC) is a composite material in which the aggregate is bound together in a matrix form with a polymer binder. The composites do not contain a hydrated cement phase, although Portland cement can be used as an aggregate or filler. PC composites possess a unique combination of properties, dependent upon the formulation (Fontana and Bartholomew, 1981). These include:

a) Rapid curing at ambient temperatures from -18 to $+40^{o}$C (0 to 104°F).

b) High tensile, flexural, and compressive strengths.

c) Good adhesion to most surfaces.

d) Good long-term durability relative to cycles of freezing and thawing.

e) Low permeability to water and aggressive solutions.

f) Good chemical resistance.

g) Light weight.

Polymer concretes have been used for:

a) Patching material for Portland cement concrete (Dimmick, 1985).

b) Skid-resistant protective overlays and wearing surfaces on concrete (Fontana and Bartholomew, 1981; Dimmick, 1994; Dimmick, 1996).

c) Structural and decorative construction panels

d) Sewer pipes, equipment vaults, drainage channels, etc.

e) Linings in carbon-steel pipes for geothermal applications

f) Swimming pool and patio decking.

These widely divergent uses clearly indicate that no single commercially available product could be compounded to perform all of these tasks well. Therefore, the term PC should never suggest only one product, but rather a family of products. Application and performance of PC is dependent upon the specific polymeric binder, as well as the type of aggregate, and its gradation.

Copolymerization techniques allow the production of a variety of binders with a wide range of physical properties. The user of PC should insist on field and engineering performance data to support laboratory data, whenever possible.

Concrete-polymer composite materials can be classified into three types:

1.) PC;

2.) Polymer cement concrete PCC;

3.) Polymer-impregnated concrete – PIC (Fowler, 1999; Blaga, and Beaudoin, 1985).

PC is a composite material consisting of fine or coarse aggregates and micro filler which are bound together in a matrix of polymer. The composite does not contain a hydrated cement paste. Fibres of different types (carbon or glass fibre, polypropylene fibres, natural fibres, etc.), can be included in the polymer concrete matrix (Reis and Ferreira, 2004, Reis, 2006, San-José and Manso, 2006). The PCC is a modified concrete in which part (10–15% by weight) of the cement binder is replaced by a synthetic organic polymer. The PIC is made by impregnation of precast Portland cement concrete with low viscosity monomers that are converted to a polymer under the influence of physical or chemical agents (Blaga and Beaudoin,1985).

Aggregates include silicate products, quartz, crushed stone, chalk, gravel, limestone, granite, clay, expanded glass, and metallic fillers (Muthukumar et al., 2003).

2.4.1 General Properties

Polymer concrete consists of a mineral filler (for example, an aggregate) and a polymer binder (which may be a thermoplastic, but more frequently, it is a thermosetting polymer).When sand is used as filler, the composite is referred to as a polymer mortar. Other fillers include crushed stone, gravel, limestone, chalk, condensed silica fume (silica flour, silica dust), granite, quartz, clay, expanded glass, and metallic fillers. Generally, any dry, non-absorbent, solid material can be used as filler.

To produce PC, a monomer or a prepolymer (i.e., a product resulting from the partial polymerization of a monomer), a hardener (cross-linking agent), and a catalyst are mixed with the filler. Other ingredients added to the mix include plasticisers, and fire retardants. Sometimes, silane coupling agents are used to increase the bond

strength between the polymer matrix and the filler. To achieve the full potential of polymer concrete products for certain applications, various fibre reinforcements are used. These include glass fibre, glass fibre-based mats, fabrics and metal fibres. Setting and development times for maximum strength can be readily varied from a few minutes to several hours by adjusting the temperature, and the catalyst system. The amount of polymer binder used is generally small, and it is usually determined by the size of the filler. Normally the polymer content will range from 5 to 15 percent of the total weight, but if the filler is fine, up to 30 percent may be required. Polymer concrete composites have generally good resistance to attack from chemicals and other corrosive agents. They have very low water sorption properties, good resistance to abrasion, and marked freeze-thaw stability. Also, the greater strength of polymer concrete in comparison to that of Portland cement concrete permits the use of up to 50 percent less material. This puts polymer concrete on a competitive basis with cement concrete in certain special applications.

Table 2.1: General properties of polymer concrete (CBD-242, ACI 548.5R-94)

General properties	Type of Polymer Concrete				
	Epoxy polymer concrete	Polyester polymer concrete	Methacrylates polymer concrete	Furan polymer	Portland cement concrete
Working life, gel time (min)	30-60	10-60	20-40	Not available	40-50
Cure time	3 hr @ 21^0C	1-5 hr	1-3 hr	Not available	7 days -30% strength
Tensile strength(MPa)	10	10	7-14	7-8	1.5-3.5
Compressive strength (MPa)	33	28	14-62	48-64	13-35
Flexural strength	14	14	9-21	-	2-8
Modulus of elasticity, compressive(MPa)	$0.6\text{-}1.0 \times 10^3$	$0.6\text{-}1.0 \times 10^3$	$0.34\text{-}6.9 \times 10^3$	-	20-30
Density, kg/dm³	2.0-2.4	2.0-2.4	2.0-2.4	1.6-1.7	1.9-2.5
Poisson Ratio	0.30	0.16-0.30	0.22-0.33	-	0.15-0.20
Thermal compatibility*	10 cycles	Not available	Not available	Not available	Not available

The chemical resistance and physical properties are generally determined by the nature of the polymer binder to a greater extent, rather than by the type and the amount of filler. In turn, the properties of the matrix polymer are highly dependent

on time and the temperature to which it is exposed. Most polymeric materials undergo degradation on exposure to UV radiation and aggressive chemicals. Vipulanandan, and Paul, (1991), have investigated degradation of polymer concrete without fibre reinforcement. They found that polymer concrete specimens immersed in alkaline solutions lost considerable strength after even short exposures. Water is also known to cause degradation of polymer concrete.

Table 2.2: General characteristics and applications of polymer concrete products (Blaga and Beaudoin, 1985)

Type of Binder Used in PC	General Characteristics	Typical Applications
Poly(methyl methacrylate)	Low tendency to absorb water; thus high freezethaw resistance; low rate of shrinkage during and after setting; very good chemical resistance and outdoor durability.	Used in the manufacture of stair units, facade plates, sanitary products for curb stones.
Polyester	Relatively strong, good adhesion to other materials, good chemical and freezethaw resistance, but have high-setting and postsetting shrinkage.	Because of lower cost, widely used in panels for public and commercial buildings, floor tiles, pipes, stairs, various precast and cast-in applications in construction works.
Epoxy	Strong adhesion to most building materials; low shrinkage; superior chemical resistance; good creep and fatigue resistance; low water sorption.	Epoxy polymer products are relatively costly; they are mainly used in special applications, including use in mortar for industrial flooring, skid-resistant overlays in highways, epoxy plaster for exterior walls and resurfacing of deteriorated structures.
Furan-based polymer	Composite materials with high resistance to chemicals (most acidic or basic aqueous media), strong resistance to polar organic liquids such as ketones, aromatic hydrocarbons, and chlorinated compounds.	Furan polymer mortars and grouts are used for brick (e.g. carbon brick, red shale brick, etc.) floors and linings that are resistant to chemicals, elevated temperatures and thermal shocks.

Polymer concretes have greatly improved resistance to chemicals, including hydrochloric acid, alkaline and sulphate solutions, which are present in industrial environments. Polyester polymer concrete is more acid-resistant than the epoxy polymer concrete; it is, however, less resistant to alkalis than epoxy polymer concrete.(R.D. Browne et al. ,1975)

The viscoelastic properties of the polymer binder lead to high creep values. This is a factor in the restricted use of PC in structural applications. Its deformation response is highly variable depending on formulation. The elastic moduli may range from 20 to about 50 GPa, the tensile failure strain being usually 1%. Shrinkage strains vary with the polymer used: high for polyester and low for typical properties of polymer concrete. A wide variety of monomers and prepolymers are used to produce PC. The polymers most frequently used are based on four types of monomers or prepolymer systems: methyl methacrylates (MMA), polyester prepolymer-styrene, epoxide prepolymer hardener (cross-linking monomer) and furfuryl alcohol.

In the past decade, most research study focused on stress strain behaviour of concrete wrapped with FRP confinement. There was an absence of study on confinement and unconfinement behaviour of polymer based filler material. Therefore, studies of the confinement and unconfinement effect of the concrete, helps with understanding the behaviour of the new polymer base filler materials.

2.5   Review of confined and unconfined concrete under compression loadings

2.5.1 Stress - strain relationship for confined and unconfined concrete

In recent years, the repair and rehabilitation of concrete columns using fibre reinforced polymer (FRP) sheets has become increasingly popular. Typically, FRP sheets are wrapped around the column, overlapped, and bonded to themselves, resulting in effective confinement which enhances the axial capacity of the column (Picher et al., 1996).

As a concrete column is uni-axially compressed along its longitudinal axis, the Poisson effect induces transverse strain that results in radial expansion of the concrete. At low levels of longitudinal strain, the concrete behaves elastically, and the transverse strain is related proportionally to the longitudinal strain by Poisson's ratio. At a critical value of longitudinal stress, typically 75-80% of the concrete strength, (f'_c), additional cracks forming in the concrete paste between the aggregates, result in a large increase in transverse strain with a relatively small increase in longitudinal stress. This rapid increase in transverse strain results in an

equally rapid volumetric expansion. This behaviour of unconfined concrete is illustrated by the stress-strain curves provided in Figure 2.7 (MacGregor, 2005).
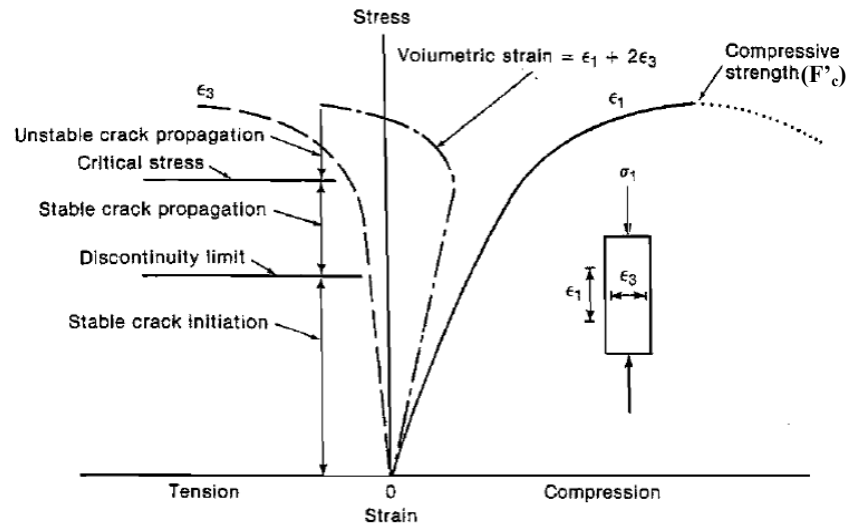
Figure 2.7: Stress-strain curves for longitudinal and transverse direction for uniaxial compression (MacGregor, 2005).

By wrapping the axially loaded concrete with a continuous confining FRP system, the transverse expansion of the concrete is restrained by the fibres. This resistance provides a confining pressure to the concrete. At low levels of longitudinal stress, the transverse strains are so low that the confining FRP system induces little confinement. However, at longitudinal stress levels above the critical stress which is 75-80% of the concrete strength, (f'_c), the dramatic increase in transverse strain engages the confining FRP system and the confining pressure becomes significant. The effect of the confining pressure is to induce a triaxial state of stress in the concrete. It is generally understood that concrete under triaxial compressive stress exhibits superior behaviour in both strength and ductility when compared to concrete in uniaxial compression (MacGregor, 2005). If the wrap is applied under the water, effect of wrapping could reduce passive confinement.

The stress Vs strain behaviour of concrete columns confined by an FRP system and subjected to axial load can be divided into three distinct regions, which can be seen in Figure 2.8.

In the first region, the behaviour of confined concrete is similar to that of unconfined concrete, since the confining effect of the FRP system has not yet been activated by the lateral expansion of the concrete core. Near the peak stress of the unconfined concrete, the confined concrete reaches a state of unstable volumetric

growth caused by excessive cracking. At this stage, the confining FRP system is activated, and starts to gradually restrain the rapid lateral expansion of the column. This region of the response is characterised by a transitional curve near the unconfined concrete strength, (f'$_c$). Finally, the third region is when the confining FRP system is fully activated, and the stiffness is generally stabilised at an approximately constant rate. The response in this region is mainly dependent on the linear elastic behaviour of the confining FRP system (Mirmiran et al., 1997).
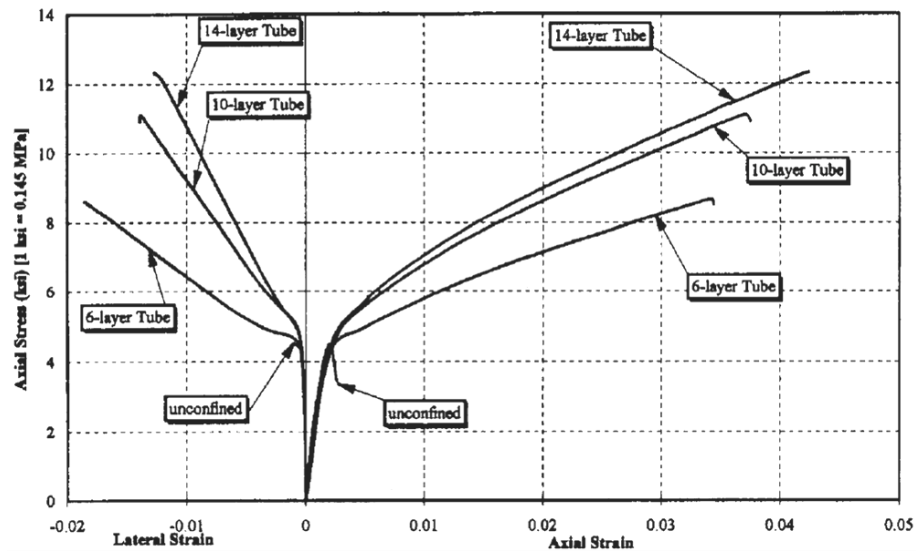
Figure 2.8: Experimental stress–strain curves for unconfined and confined concrete (Mirmiran, et al. 1997).

The reduced effectiveness of confinement for concrete cylinders with void cores was also examined during an experimental study conducted by Fam, (2000). Fam examined the axial capacity of GFRP tubes, totally and partially filled with concrete. Fam reported that although the void core offers material savings and a reduced self-weight, the maximum confined strength is reduced when compared to totally filled GFRP tubes. A reduction in strength with increasing void size was observed. This behaviour was attributed to the fact that the void core allows an inward displacement, or a degree-of-freedom for the concrete, as it expands under axial compression. However, if the central void is maintained by an inner GFRP tube, the confinement effectiveness is improved and could approach that of a totally concrete filled GFRP tube Fam, (2000).

Fam, (2001) tested two identical GFRP tubes filled with concrete, having a compressive strength, f'$_c$, of 58 MPa, but with different void core sizes. While the overall diameter of both tubes was 219 mm, the first tube had a 95 mm diameter void core, and the other tube had a 133 mm diameter void core. Fam reported that the

maximum stress in the concrete shell with the 95 mm diameter void core slightly exceeded the compressive strength of the unconfined concrete, f'$_c$, while the tube with the larger 133 mm diameter void core failed at a stress level of only about 0.91 f'$_c$.

The behaviour of Concrete filled fibre-reinforced polymers (FRP) tube (CFFT) concrete circular columns under concentric and eccentric loading was also examined by Hamdy, (2009). Ten unconfined cylinders, eight CFFT columns and two control steel spiral reinforcement concrete columns were cast and tested under concentric and eccentric loading. Four CFFT columns loaded with different eccentricity 15, 30, 45 and 60 mm from the centre of the columns. The behaviour of the concrete filled GFRP tubes is significantly affected by the eccentric load. The test results indicate that by increasing the thickness of the GFRP tubes a significant improvement is achieved in the confinement efficiency. The confinement provided by the GFRP tubes improves both the load-carrying capacity and the ductility of the concrete columns under concentric load.

2.5.2 Mathematical models for confined and unconfined concrete

The mechanics of confinement, which were developed based on confined concrete column tests, may be applicable to confined polymer base filler, used for timber pile repair with some modifications. The confining pressure provided by the FRP system is a function of the stiffness of the FRP and the expansion of the concrete or grout in the transverse direction. Therefore, to quantify the behaviour of concrete or grout confined by FRP system, it is necessary to determine the confining pressure provided by the FRP system. Figure 2.9 illustrates the confining action provided by an FRP system applied with the continuous fibres oriented in the transverse or hoop direction.
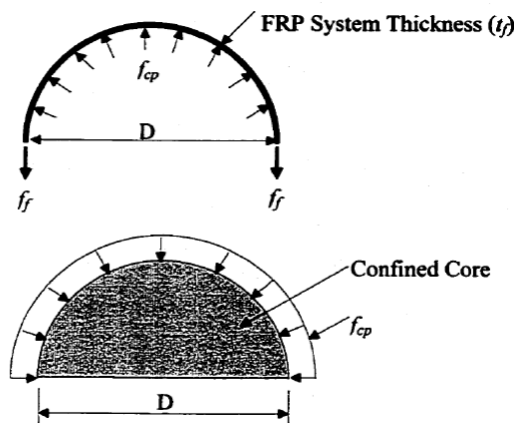
Figure 2.9: Internal and external Forces on the FRP system and concrete core (MacGregor, 2005)

The mechanics of confinement is dependent upon two factors, the tendency of the concrete or grout to dilate, and the radial stiffness of the FRP system restraining the dilation. Consequently, two conditions must always be satisfied: firstly, geometric compatibility between the core and the confining FRP system, and secondly, equilibrium of forces in the free-body diagram, as shown in Figure 2.9. According to the first condition, strain compatibility dictates that the strain in the confining FRP system is equal to the transverse strain of the concrete or grout. This leads to the following relationship:

$$\epsilon_f = \epsilon_{t(hoop)} \text{---------------------------------- (2.1)}$$

The second equilibrium condition leads to the following relationship:

$$f_{cp} = \frac{2f_f t_f}{D} \text{------------------------------------ (2.2)}$$

$$f_{cp} = \frac{2E_f \epsilon_{t(hoop)} t_f}{D} \text{---------------------------- (2.3)}$$

Where:

D = diameter of the confined core

E_f = modulus of elasticity of the FRP system in the hoop direction

f_{cp} = the confining pressure provided by the FRP system

f_f = ultimate strength of the FRP system in the hoop direction

t_f = thickness of the FRP system

ϵ_f= ultimate strain of the FRP system

$\epsilon_{t(hoop)}$= ultimate strain of the core in hoop direction

Various researchers have attempted to develop a generalised model to quantify the effect of confinement on the strength and ductility of concrete. The model proposed by Mander et al. (1988), is however, the most widely used. Although this model was originally developed for conventional reinforced concrete columns, it can be used to model the behaviour of concrete columns confined by a steel or FRP system. Stress-strain curves for confined and unconfined concrete based on Mander's model are shown in Figure 2.10.
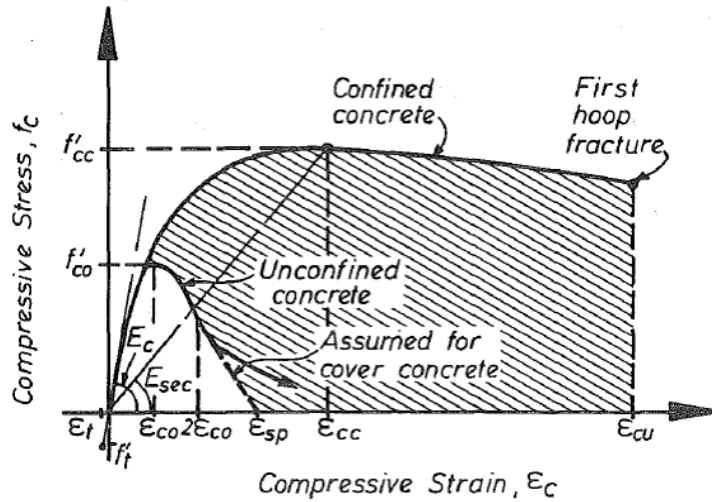
Figure 2.10: Stress-strain model proposed for monotonic loading of confined and unconfined concrete (Mander et al., 1988)

Mander et al. (1988), first proposed a unified stress – strain approach for confined concrete which is applicable to both circular and rectangular shaped sections subject to axial compressive load. The confinement model proposed by Mander is based on a constant confining pressure, f_{cp}, acting during the entire loading history. The failure strain of the confined concrete is sought by an energy balance approach. The basis of this approach is that the additional ductility available in confined concrete is due to the energy stored in the confining member. Therefore to establish the first confining hoop fracture, the total strain energy in the confining member is equated with the increase in strain energy of the confined concrete over its unconfined value.

The increased compressive strength of the concrete, due to the confining pressure provided by the FRP system is a function of the unconfined strength, and the confining pressure, f_{cp}. Hence the increased concrete strength can be quantified using the following equation proposed by Mander et al. (1988).

$$f'_{cc} = f'_{c}\left[2.254\sqrt{1 + \frac{7.94f_{cp}}{f'_{c}}} - \frac{2f_{cp}}{f'_{c}} - 1.254\right] \text{------------------ (2.4)}$$

The peak strain of the confined concrete, is a function of the peak strain of the unconfined concrete, and is given by Equation (5).

$$\epsilon'_{cc} = \epsilon'_{co}\left[1 + 5\left(\frac{f'_{cc}}{f'_{c}} - 1\right)\right] \text{-------------------------- (2.5)}$$

By using Equations (2.1) through (2.5), the confined compressive strength of concrete or grout can be predicted.

Carreira, and Chu, (1985), proposed a model for plain concrete in compression. This is the modifications made by using Popovics (1973) model. In these two models (σ_1, $\varepsilon 1$) are the coordinates of any point in the stress strain curve, ε_{co} is the peak axial strain of unconfined concrete strength, f_c, ε_{cc} is the peak axial strain of confined concrete strength. These models have one continuous function for both ascending and descending branches.

$$f_c \frac{\varepsilon_1}{\varepsilon_{co}} \left(\frac{n}{n-1+(\varepsilon_1/\varepsilon_{co})^n} \right) \qquad \text{Popovics (1973)} \text{ ------- (2.6)}$$

$$\frac{f_{cc}(\varepsilon_1/\varepsilon_{co})^\beta}{\beta-1+(\varepsilon_1/\varepsilon_{co})^\beta} \qquad \text{Carreira and Chu (1985)} \text{ --- (2.7)}$$

The model was proven to be valid from the experimental studies carried out for a wide range of concrete (60 to 120 MPa). Modifications to these unconfined and confine concrete models may be necessary to study behaviour of new polymer base filler material in a GFRP pile connector. Also additional test data would be required to calibrate the model.

2.6 Summary

From the literature review, it could be identified that the proposed novel timber rehabilitation / replacement approach has never been used in timber pile rehabilitation. Comparatively, very few researches have been instigated to study decayed pile rehabilitation. Previous research has focused on pile splicing, cutting and posting, grout injection, concrete jackets and FRP composite shells. Therefore exploring the overall behaviour of this new pile replacement / rehabilitation technique is essential and important. In the past two decades, most researches have investigated confined and unconfined affects of concrete. There is an absence of study in this area on polymer base filler material. Understanding and investigation of this polymer based fillers behaviour is important, because, in this novel timber pile rehabilitation / replacement approach, all vertical super structure loads transfer through this filler. Therefore this entire research programme is designed and planned to fill this research gap.

Chapter 3

BEHAVIOUR OF HOLLOW GFRP PILES

3.1 Introduction

Fibre composites have inherent material properties that are better than other materials, such as steel, timber or concrete in numerous environments. In the marine and ground-zone environments in particular, fibre composite materials can be selected for their corrosion, rot and pest resistance, as well as their high strength-to-weight ratio. This research aims to develop a system for pile replacement for piers, jetties, bridges, and boardwalks, by using fibre composite to enable replacement of those items for rehabilitation of the structures, as well as new construction. BAC Technologies Pty Ltd, and Centre of Excellence in Engineered Fibre Composites (CEEFC) USQ, are in collaboration as part of Proof of Concept funding by Queensland Government on GFRP Pile for new civil infrastructure and the replacement of existing piles in jetties, piers, and bridges.

Common standard pile diameters available for the timber bridges and jetties are 180, 210, 230, 280,300 and 450 mm (www.hardwood.timber.net.au) In most of the Queensland jetties and bridges, pile diameters vary from 250 mm to 450 mm (Timber bridge maintenance manual, 2005). Initially this new concept was intended to be applied to the Shorncliffe Jetty, which belongs to the Brisbane City Council, and then it was planned to extend the new concept into rural area bridges under class 4 road classification according to AS 5100.7-2004- Bridge Design Code.
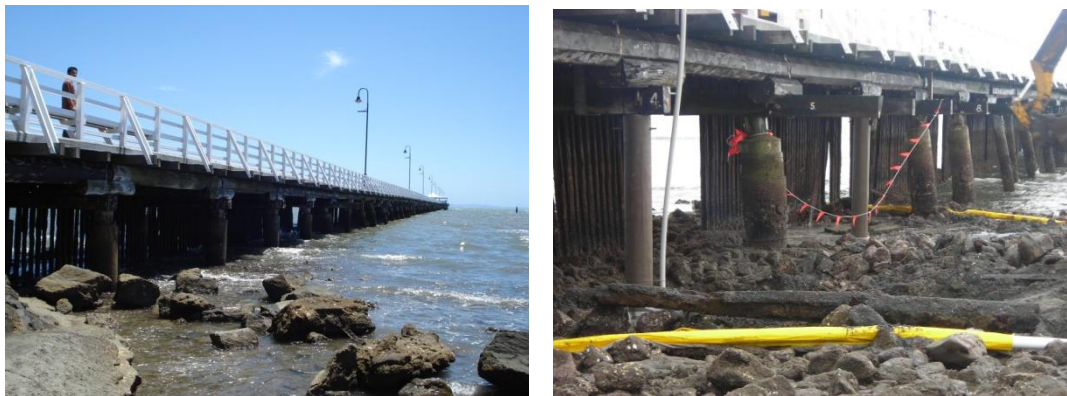
Figure 3.1: Deteriorated piles in Shorncliffe pier, Brisbane

According to Figure 3.1, most of the timber piles were deteriorated as a result of marine borer attack. Brisbane City Council wanted to introduce an innovative new pile replacement scheme without disturbing superstructure functions. To study the behaviour of piles for rehabilitation, 300 and 470 mm outer diameter full scale GFRP pile specimens were considered, which represent most common pile diameters in the Shorncliffe jetty and common standard pile diameters in two lanes timber bridge (Timber bridge maintenance manual, 2005) respectively. The main objective of this study program was to evaluate the performance and suitability of GFRP pile as a replacement, or rehabilitation of timber pile.

3.2   The repair technique

3.2.1 Proposed repair method using GFRP composite pile and connector

The available wood pile protection, restoration and rehabilitation methods have limited applicability in most cases. Plastic wraps can protect against marine borers in some cases, but they cannot be used to restore structural capacity. Steel jackets can corrode, especially in the marine environment, and concrete encasement can develop problems with spalling. Fibre-reinforced composite jackets installed in halves have bonded longitudinal joints that may limit the ability of the pile encasement to deliver circumferential confinement. On the other hand, application of wet fabric reinforcement underwater can be difficult, and proper curing of the resin may not be achieved.

The wood pile rehabilitation method proposed in this research utilises a GFRP composite pile and connector that replace the deteriorated portion of the pile. The GFRP pile development was based on experience with appropriate technologies in the structural FRP composites field (Kshirsagar et al. 2000, Lopez- Anido and Karbhari 2000, Lopez Anido, et al. 2000, Lopez-Anido and Xu 2002), combined with the needs for wood pile protection, durability and strengthening observed in the field inspection, survey, and literature review. The connector was used to join existing timber pile and new pile. To simplify the construction, the connector was inserted onto the existing fully intact timber stump. Then, new pile was inserted into the connector, and both lifted up, until attached to the super structure (head stock for bridge). After that, the void in between the connector and the existing timber pile was filled with new filler material to transfer the vertical load from the connector, to

the original stump. Development of this new polymer based filler material was important and will be further discussed in Chapter 5.

3.2.2 Fabrication of GFRP pile specimens and connector

300 and 470 mm diameter full scale pile specimens were manufactured using a resin infusion method. Resin infusion, also called vacuum infusion, utilises a vacuum bag to de-bulk or compact a parts complete laminate ply schedule of reinforcements and core materials laid onto the mould. After de-bulking, the resin is allowed to be infused by the vacuum to completely wet-out the reinforcements and eliminate all air voids in the laminate structure. High quality composite parts made from a wide range of fibre and resin combinations can be utilised to infuse laminates up to six inches thick. Typical resins used are polyester, vinyl ester, and epoxy, with many being UV cure initiated. For this full scale pile manufacture process vinyl ester resin was used. This process added benefits which include eliminating weaker secondary bonds. While the vacuum infusion-enabling adhesive is primarily used for fibre glass, its cross-linking properties with resin, also provides greater inter-laminar shear strength for glass fibre materials. Pigmented gel coats provide the parts surface finish, and often a hand lay-up skin laminate may be fabricated to allow fabricators to walk on gel coated surface, while loading the dry reinforcement laminate ply schedule and vacuum bag. A total of 20 layers of 600 g/m2 biaxial glass fibre and 6 layers of XF Soric were used based on the following layup arrangement having an overall thickness of 22 mm (from the inside to outside of the pile wall). Individual biaxial and XF Soric layers were having 0.5 mm, 2 mm thickness respectively. XF Soric is a core material for closed mould processing techniques like infusion. It is a polyester non-woven which contains pressure stable cells which are separated by canals. The cells keep their thickness in the infusion process. XF has large canals which allow quick resin flow and reduced resin takes up. Figure 3.2 and 3.3 shows the manufacturing process of the GFRP pile, and connector.

Table 3.1: Layup arrangements of both 300 mm and 470 mm external diameter GFRP piles

Number of Layers	4	2	1	2	1	1	1	1	13	Total tickness (mm)
Type	Biaxial	Soric	Biaxial	Soric	Biaxial	Soric	Biaxial	Soric	Biaxial	
Thickness (mm)	2	4	0.5	4	0.5	2	0.5	2	6.5	22

Note: 0^0 biaxial fibres were aligned to the pile axis.

Figure 3.2: Manufacture process of the pile (Courtesy of BAC Technologies Pty Ltd)

The final proposed laminates layup for the connector is given below;

1. 8 layers 600/225 gsm Biax/CSM glass (inner top)
2. 8 layers 600/225 gsm Biax/CSM glass (inner bottom)
3. 12 layers 600/225 gsm Biax/CSM glass (outer) and shown in Figure 3.3 (b).

In this study programme, only 300 mm and 470 mm GFRP pile behaviour is investigated. The pile connector behaviour will be discussed as part of whole system behaviour by numerical simulation in Chapter 4. To investigate the behaviour of GFRP piles, three types of tests were conducted.

- Laminate testings such as fibre fraction, tensile, compression, shear and flexural tests were performed with three different glass fibre orientations, such as: uni-axial, biaxial and double-bias fibres, which are the building blocks of the pile.

- Compression testing was performed on 300 mm and 470 mm external diameter short piles to evaluate axial loading capacity.

- Combined axial and bending test and pure three point bending test were conducted on full scale pile to verify the combined axial and flexural loading capacity as well as pure bending capacity. More detailed information about the testing will be described in this chapter.

(a)

Inner Top Laminates

Polymer Base Filler Location

Outer Laminates

Inner Bottom Laminates

Outer Laminates

Inner Laminates

Old Timber Pile

(b)

(c)
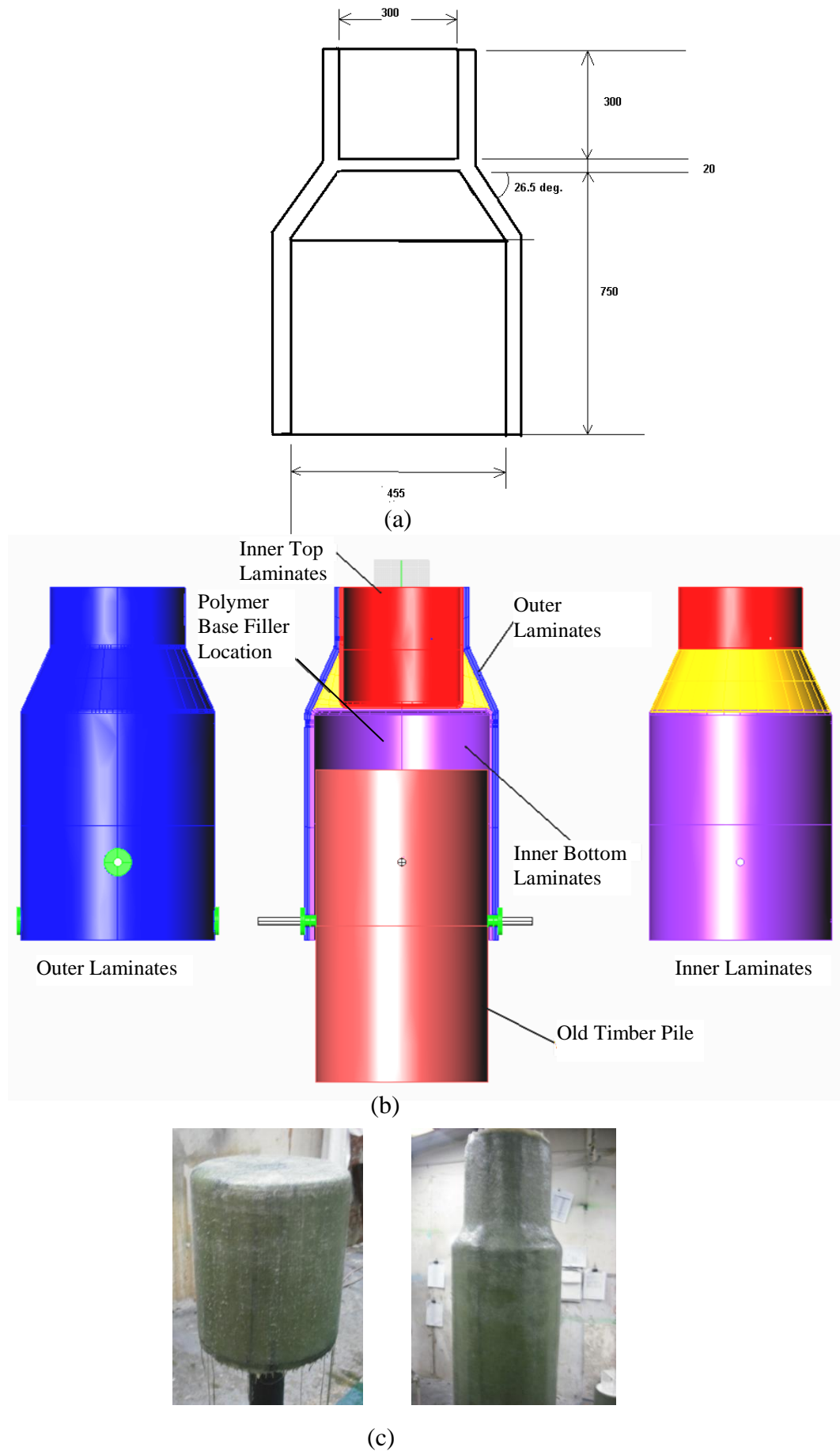
Figure 3.3: (a) Basic dimensions of the connector, (b) Laminates arrangement in connector, (c) Manufacturing process of GFRP connector (Courtesy of BAC Technologies Pty Ltd)

3.3 Determination of laminate properties

The test specimen for the fibre composite laminate is cut from the laboratory size panel, which was fabricated by hand lay-up process. Experimental characterisation of the fibre composite laminates has been performed using fibre fraction, flexure, tensile, compressive and shear tests. The details of the specimen for characterisation of the behaviour of the fibre composite laminates are listed in Table3.3. (Please see Appendix A for detail test results).

Table 3.2: Number of specimens for Laminate characterisation

Type of test	Test standard	No. of coupons			General Dimensions of coupons (mm)		
		Uni Axial		Biaxial			
		0°	90^0		length	width	thickness
Fibre Fraction	ISO 1172:1999	3		3	25	25	2.7
Flexural	ISO 14125:1998(E)/	5	5	5	80	15	2.7
Tensile	ISO 527-4/2/2:1997	5	5	5	300	25	2.7
Compressive	ISO 14126(1999)	5	5	5	140	12.75	2.6
Shear	ASTM D5379M-98	5	5	5	75	20	2.7

3.3.1 Fibre fraction test

The specimens were contained in a crucible, and were placed in a furnace degraded, leaving only GFRP reinforcement, and no filler was used. Once the resin was completely removed, analysis of the laminate was performed on the burnout remains. This method is known as the Fibre Fraction Test or burnout process. The burning method has been considered a simple and effective way to determine the volume fraction of cured resin composite materials, but in many cases, it has shown some limitations when fillers have been added to the material. The fillers which may be partially burned out, or not burned out at all by the burnout process, stay with the glass fibre. This causes difficulties in determining the fibre volume. Until now there has been no standard approach to separate fillers from the resin, and glass fibre from structural composites (Binshan S. Y et al. 1995). In this work there was no fillers added to the GFRP pile produced. The burnout tests shows that the fibre composite laminates have a glass fibre content around, 71% for uni-axial and 65% for bi-axial by weight.

3.3.2 Tensile properties

The tensile test of the laminates was conducted following the ISO 527-4/2/2:1997 standards. Five specimens, each being cut from the longitudinal (0-degree uni axial), transverse (90-degree uni axial,) and longitudinal (0-degree biaxial) directions were prepared and tested to determine the tensile strength and modulus of elasticity. The specimens were tested in tension using an Avery testing machine (capacity 530 kN) with a loading rate of 1mm/min. All the tensile specimens were properly instrumented with an extensometer (25 mm axial gauge length) to measure the Poisson's Ratio. The extensometer was removed from the specimen when longitudinal strain reached 3000 microstrains to prevent any damage to the equipment. The ends of the test specimen were carefully clamped onto the testing jaws to prevent slipping at the gripping area and prevent the premature fracture at the grip. All specimens were tested up to failure to determine the ultimate tensile strength and the failure mode. The tensile modulus, ultimate tensile stress and the failure modes of the tensile specimens were evaluated.
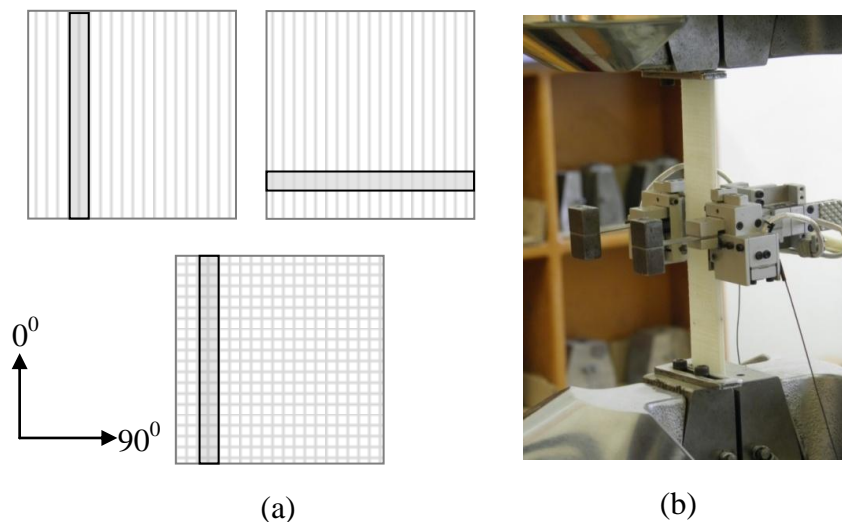
Figure 3.4 (a) Cutting directions of laminate specimens, (b) Tensile test setup with extensometer

3.3.3 Flexural properties

The flexural test of the laminates was conducted following the ISO 14125:1998(E)/Method A/Class II Fibre-Reinforced Plastic Composites standards. The fibre composite laminates was simply supported and was tested under 3-point loading. The span was set at approximately 16 times the thickness of the laminates. The load was applied at midspan of the specimen at a constant rate of 1 mm/min. The

load and midspan deflection were recorded up to failure to determine the strength and elastic properties of the laminates under flexural loading. The failure mode was also observed after each test. The flexural strength was calculated at the maximum applied load. The flexural modulus was then calculated from the linear portion of the stress-strain curve at the midspan of the specimen.
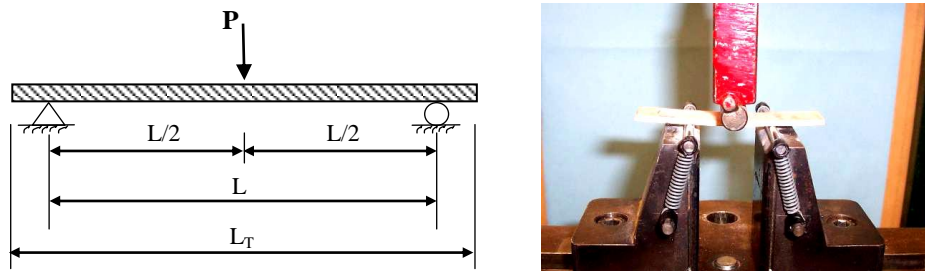
Figure 3.5: Flexural test setup

3.3.4 Compressive properties in the in-plane direction

The compressive test of the laminates was carried out following the ISO 14126(1999)-Fibre-Reinforced Plastic Composites. Specimens that were cut along the longitudinal (0-degree uni axial), transverse (90-degree uni axial), and longitudinal (0-degree biaxial) directions were loaded on the end in a universal testing machine by the Wyoming Modified Celanese Compression test fixture at the rate of 1 mm / min until failure. The specimen was compressed and the subsequent deformation at various loads was recorded. The compressive stress was calculated by dividing the applied load with the average cross-sectional area of the specimen.

3.3.5 Shear properties by the V-notched beam method (Iosipescu shear test)

The shear test of the laminates was conducted following the ASTM D5379 / D 5379M-98 standards. Five coupon specimens each from the longitudinal (0-degree uni axial), transverse (90-degree uni axial) and longitudinal (0-degree biaxial) directions of the fibre composite laminates with symmetrically located v-notches were used as the test specimens. The specimen was loaded in a universal testing machine by the Iosipescu shear test fixture at a constant head speed of 2mm/min. Three specimens from each type were provided with resistance strain gauges oriented at $+45^o$ to the loading axis bonded in the middle of the specimen to determine its shear response. The load, strains and displacement were recorded into the data acquisition System 5000.

The shear stress is calculated by dividing the applied load with the area of the notched section. The shear strains is determined from the indicated normal strains of the +45° strain gauges.
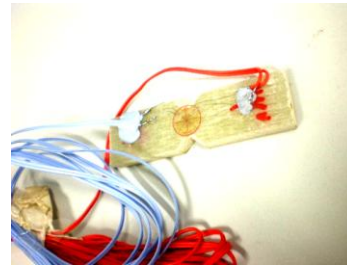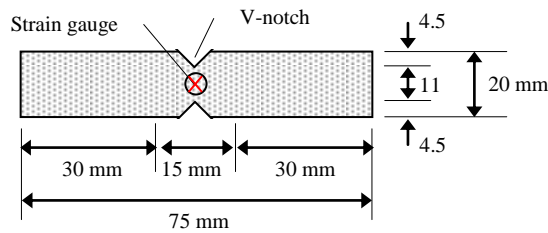
(a) Specimen for shear test
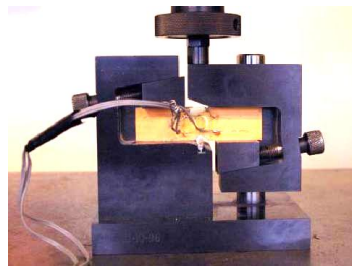
(b) Iosipescu shear test fixture

Figure 3.6: Shear test set-up

3.3.6 Summary of laminates test results

The average value and the standard deviation for the strength and elastic properties of the fibre composite laminates determined from the different coupon tests are summarised in Tables 3.3. Detailed test results for laminates and relevant information are given in Appendix A.

Table 3.3: Characteristics of single glass fibre laminate

Test	Property	Uni-Axial				Bi-Axial	
		Longitudinal direction		Transverse direction			
		Ave:	Std Dev	Ave:	Std Dev	Ave:	Std Dev
Flexure	Flexural modulus (MPa) Peak stress (MPa) Strain at peak	29921 763.41 0.0276	688 47.56 0.16	8763 72.94 0.025	349 9.07 0.74	14493 486.94 0.0406	943 23.68 0.46
Tensile	Tensile modulus (MPa) Peak stress (MPa) Poisson's ratio	40259 786.90 0.269	469 34 0.006	11101 41.99 0.082	782 4.56 0.005	27996 343.84 0.151	544 25.87 0.016
Compression	Peak stress (MPa)	469.44	15.63	120.90	10.68	300.64	24.46
Shear	Shear modulus (MPa) Peak stress (MPa) Strain at peak	3245.84 51.53 0.0402	110.85 2.08 0.12	2850.5 35.8 0.0285	130.85 2.36 0.10	3101.25 50.00 0.0398	98.75 3.8 0.15
Fibre fraction (%)		71.28				64.78	

The biaxial and uni-axial glass fibre laminates have fibre fraction of 64.78% and 71.28% by weight, respectively. In the Table 3.3, all the elastic properties have been determined by considering the linear approximation in according to the ISO and ASTM standards.

3.4 Compression tests on hollow GFRP piles

300 mm and 470 mm external diameter GFRP pile sections were selected for the compression tests. Specimen length was measured as 230 mm and 1000 mm respectively to make it as short compression pile sections. 300 mm external diameter GFRP tubular pile was checked against the Shorncliffe pier loadings supplied by Brisbane City Council. 470 mm external diameter GFRP pile was checked against rural area bridges under class 4 road classification in AS 5100.7-2004.

3.4.1 Compression test on 300 mm external diameter short hollow GFRP pile

Compression test was performed on short 300 mm external diameter FRP composite pile to evaluate its behaviour under axial compression load excluding the effect of buckling. Compression test on short pile was conducted using a 500 kN loading capacity AVERY testing machine. To protect pile circumference edges from compressive crushing, a piece of plywood was placed on both ends of the specimen. The specimen was loaded up to a maximum load of 414 kN at a rate of 2 mm / min. Four unidirectional strain gages were positioned at the mid-height of the specimen. Collections and recordings of data were generated using Systems 5000 data logger connected to the upper load cell and strain gages. This simulates a sufficient axial load including dead and live loads on a pile in the actual Shorncliffe pier structure. Specimen dimensions and test set up were arranged as shown in Figure 3.7.

(a)   (b)
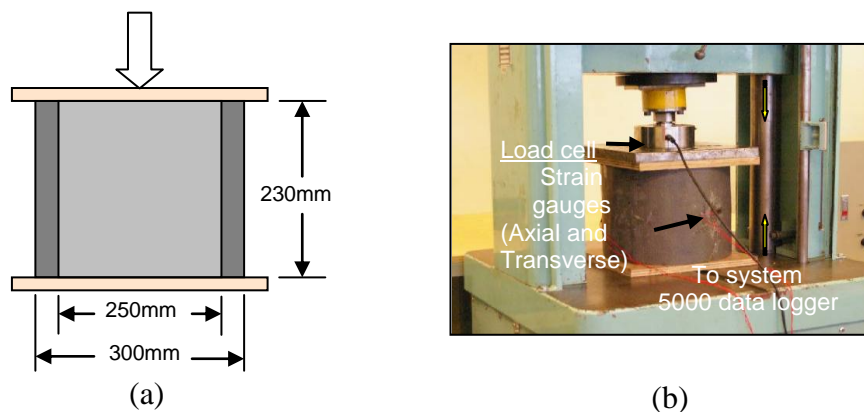
Figure 3.7: Compression test setup arrangements for 300 mm external diameter pile

A compressive proof load of 414kN was applied to the pile axially. There was no evidence of damage during loading. Result of compression testing on a 230 mm short pile is given in Table 3.3 below.

Table 3.4 Compression test results

Proof Load, kN	414
Proof Stress, MPa	19
Proof Axial Strain, microns	-1,523
Proof Circumference (Transverse) Strain, microns	452
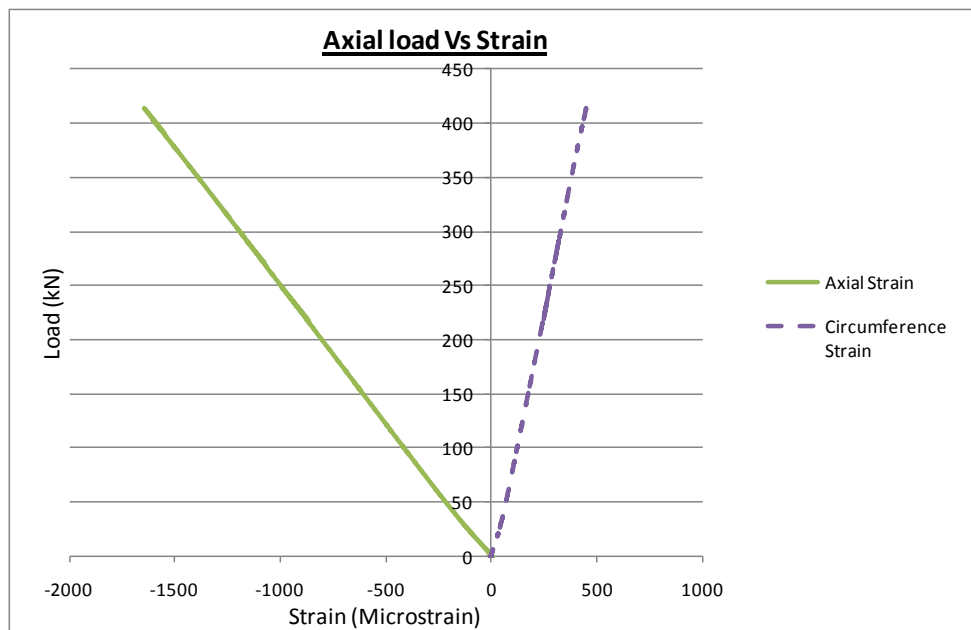
Figure 3.8: Compressive load versus strain (axial and circumference) diagram

Figure 3.8 shows the typical load versus strain relationship of the 300 mm GFRP pile under compressive loading. In both the longitudinal and transverse directions, the 300 mm GFRP pile behaved linear elastic range under pure compressive loading up to 414 kN.

Coupon compression test was undertaken in this study to determine the material properties of a 22 mm thick laminates (i.e. combined effect of fibreglass and Soric XF reinforced laminate) arranged according to Table 3.1. Four test coupons taken directly from the 300 mm external diameter GFRP composite pile were tested according to ISO14126:1999 - Plastic Compression Test. To monitor the deformation, two strain gauges were positioned on the mid height of the specimen. Collections and recordings of data were generated using Systems 5000 data logger

connected to the upper load cell and strain gages. Figure 3.9 shows the set-up and instrumentation of the laminate test.
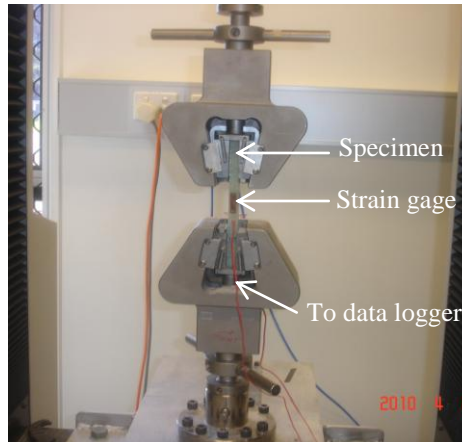
Figure 3.9: Laminate test set-up and instrumentation

Table 3.5 shows the summarised result derived from the coupon compression test obtained from actual pile representing 26 layers as per the Table 3.1. It should be noted that values given are average values at failure. As illustrated in the Table 3.5, the ultimate compressive strength of the laminate is 88 MPa while the strain at failure is 0.00612. Concurrently, the compressive strength of the laminate can be considered as predicted strength of the composite pile assuming no buckling will take place. Apparently, load beyond this value will initiate compression failure on the pile.

Table 3.5: Material properties of overall laminate arrangement (26 layers as per the Table 3.1) at failure.

Properties	Property value	
	Ave:	Std Dev
compressive stress	88 MPa	8.98
Axial deformation	3.46 mm	0.563
Axial strain	0.00612	0.0015
Compressive modulus	14,300 MPa	

Figure 3.8 shows the applied axial load Vs axial and lateral strain behaviour at the mid height of the 230 mm FRP tube. The axial and lateral strain of the composite pile under 414 kN (22.02 MPa equivalent stress) applied load are 1,523 $\mu\varepsilon$ and 452 $\mu\varepsilon$, respectively. The compressive modulus of FRP composite pile using linear regression is estimated to be 14,270 MPa. This value is comparable to the compressive modulus (14,300 MPa) derived from coupon laminate test. Based from

this result, the applied load (i.e. 22.02 MPa) is only 25% of the composite pile's predicted compressive capacity (i.e. 88 MPa). Therefore, compressive failure is not expected to occur at this loading stage.

Predicted ultimate compressive capacity of the pile

= Compressive stress at failure * Area of the pile

= 88*(2*π*139*22)

= 1690.83 ≈ **1690 kN**

Compare to predicted ultimate compressive capacity of the pile (excluding the effect of buckling) 4 times higher than actual Shorncliffe pier loading. Therefore factor of safety of the GFRP pile against Shorncliffe pier under pure compression loading is around 4.

3.4.2 470mm external diameter short GFRP pile

Compression test of a 470 mm external diameter 1000 mm short section of a pile was conducted using a hydraulic jack and a 200-tonne capacity portal frame. The test set up was arranged as shown in Figure 3.10 to determine the behaviour of pile under a serviceability compressive load of 1500kN and the compressive modulus of the pile. Specimen dimensions and strain gauge locations are shown in Figure 3.10 (a). Timber ply was used to protect pile circumference edges from local compressive crushing. Data were recorded using System 5000. Strain gauge locations and the dimension of the short pile are shown in Figure 3.10 (a).

(a)   (b)
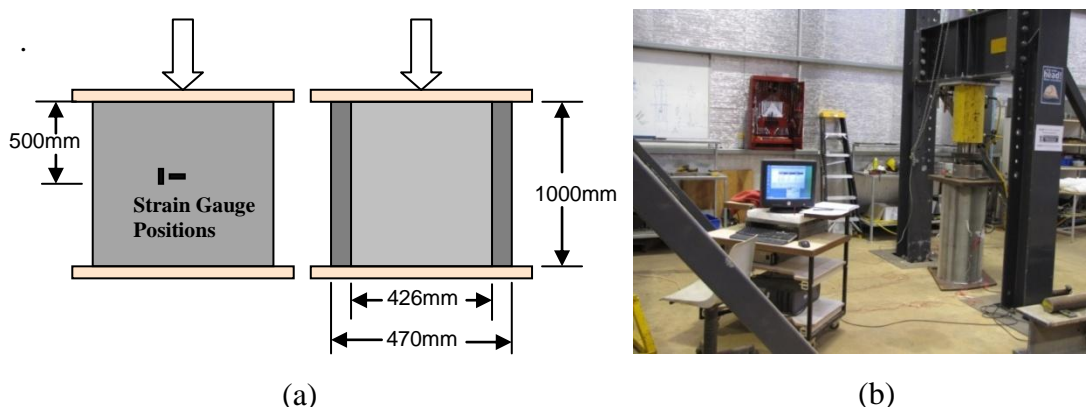
Figure 3.10: Compression test setup arrangements for 470 mm external diameter pile

The maximum compressive serviceability load of 1500 kN was applied to the pile axially starting from 0kN by using hydraulic jack at a rate of approximately 2mm/min. This simulates a sufficient axial load including dead and live loads on a

pile in the actual rural area bridge structure under class 4 road classification according to AS 5100.7-2004. There was no evidence of any damage during loading. Result of compression testing on a 1metre long pile corresponds to 1500kN load is given in Table 3.6 below. A load versus strain diagram of the compression test is shown below in Figure 3.11. Table 3.7 shows the summarised results obtained from the coupon test for the biaxial lamina done in laminate test (Table 3.3).

Table 3.6: Compression test result on short section of pile

Applied Load, kN	1500
Corresponding compressive Stress, MPa	48.44
Corresponding measured Axial Strain, microns	-3231
Corresponding measured Circumference (Transverse) Strain, microns	534

Table 3.7: Material properties of single glass fibre lamina coupon test at failure

Properties	Value
Ultimate compressive stress at failure (MPa)	300
General glass fibre lamina failure strain(µε)	12000
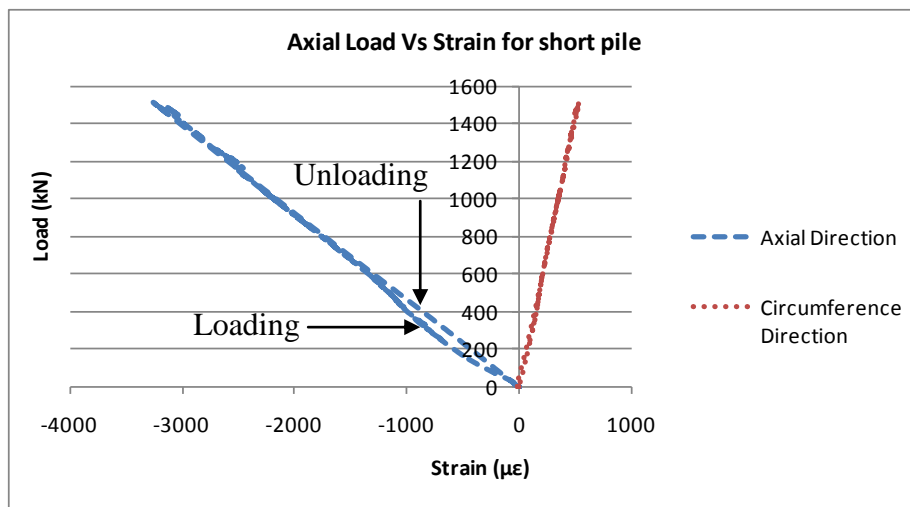
Figure 3.11: Compressive load versus strain (axial and circumference) diagram

Some local compression failure was observed around the top and bottom periphery of the pile due to initial settlement against compression loading. As a result, in Figure 3.11, only loading curve has the disparity linear portion in between strain range of 1000 µε to 0 µε. Using the data from the above tests, a value of 16% of ultimate compressive stress was applied as serviceability compressive stress (48.44MPa) in 1m section of short pile. Poisson's ratio is the ratio of transverse strain

to longitudinal strain in the direction of compressive force and overall Poisson's ratio of the pile is around 0.165 as shown in Figure 3.12. This value is very close to the Poisson's ratio determined from the laminate test for biaxial laminate (Refer Table 3.3).
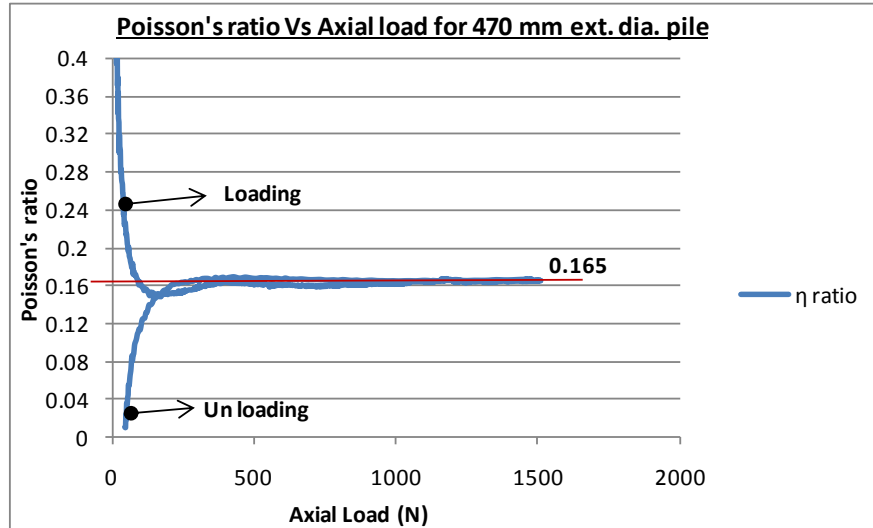
Figure 3.12: Poisson ratio Vs axial load diagram

Overall axial compressive modulus value was obtained by the gradient of the axial stress vs. strain diagram as shown in Figure 3.13. In this graph, axial stresses calculated by using the following equation.

Axial Stress (σ) = Applied axial load (P) / Pile cross section area (A)
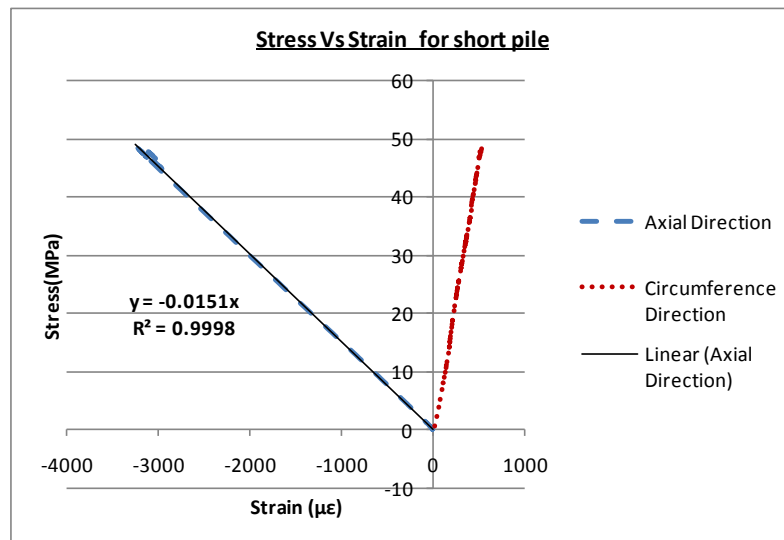
Figure 3.13: Experimental compressive stress Vs strain diagram

Therefore overall axial compressive modulus value = **15100 MPa**

The predicted ultimate compression capacity of the pile can be calculated by using coupon test results at failure (Refer Table3.3). From Table 3.3, biaxial laminate

having around 300 MPa ultimate compression failure capacity, which 37.5 times higher than Soric ultimate compressive failure capacity (8 MPa) given by the manufacturer. Therefore compared with Soric, most of compression capacity withstand by biaxial fibres and assume that, it was proportionate to area of biaxial fibres in the GFRP pile.

Total area percentage of biaxial fibre in the pile $= \dfrac{\text{Thickness of biaxial fibres}}{\text{Total Thickness}}$

$$= 10/22$$
$$= 45.45\%$$

Assuming that the ultimate capacity withstand by biaxial fibres,
Predicted ultimate compressive capacity of the pile = Compressive stress at failure

(Table 2) x Area of the pile x % of

Biaxial fibre in the pile

$$= 300 * (2*\pi*224*22) * 0.4545$$
$$= 4.222\text{E}6 \text{ N}$$
$$\approx \mathbf{4222 \text{ kN}}$$

Theoretical compressive modulus was calculated base on mixture formula per Table 3.8. Individual E value for Biaxial and Soric was considered as 28000 MPa Table (3.3) and 800 MPa (provided by supplier) respectively.

Table 3.8: Theoretical compressive modulus calculation based on mixture formula

Outer Radius (mm)	Inner Radius (mm)	Thicknesses of plies									ΣA
		Biax	soric	Biax	soric	Biax	soric	Biax	soric	Biax	
		2	4	0.5	4	0.5	2	0.5	2	6.5	
235	213	215	219	219.5	223.5	224	226	226.5	228.5	235	
Area-A (mm²)		2689.203	5453.805	688.794	5566.902	702.931	2827.433	710.785	2858.849	9464.833	30963.537
E (MPa)		28000	800	28000	800	28000	800	28000	800	28000	ΣAE
AE		7.530E+07	4.363E+06	1.929E+07	4.454E+06	1.968E+07	2.262E+06	1.990E+07	2.287E+06	2.650E+08	4.125E+08
E$_{\text{effective}}$(Based on ΣAE/ΣA)	13323.70 MPa										

Therefore E Theoretical = 13323.70 MPa. Theoretical axial strain calculated using normal Hooke's law and circumference axial strain calculated based on overall Poisson's ratio. Comparison of theoretical and experimental strain variation is shown in Figure 3.14.

Compare to predicted ultimate capacity of the pile (excluding the effect of buckling) 2.81 times higher than actual Shorncliffe pier loading. Therefore factor of safety of the GFRP pile against actual rural area bridge loadings under class 4 road classification according to AS 5100.7-2004 is around 2.8.
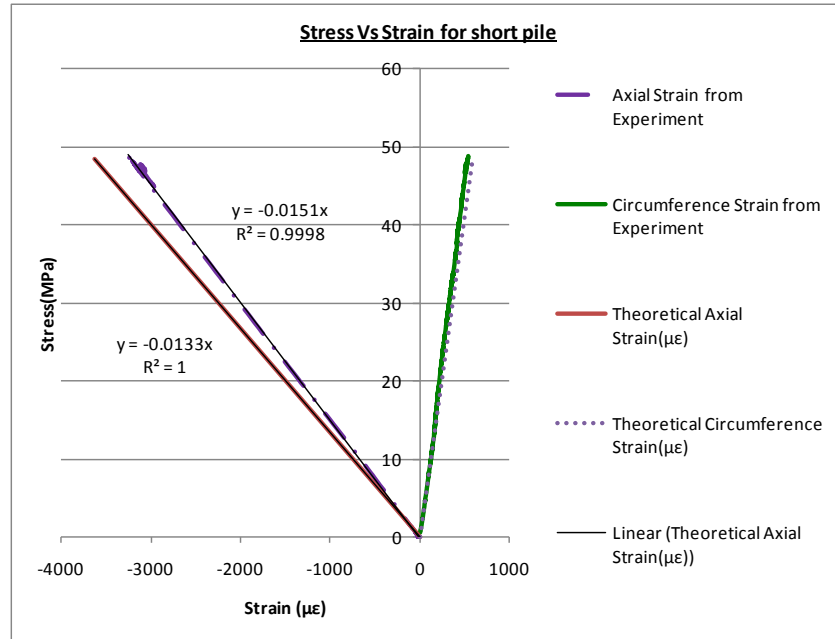
Figure 3.14: Graphical representation for experimental and theoretical results

3.5 Three point bending test on full scale GFRP piles

3.5.1 300 mm external diameter and 3.1 m long GFRP pile

This test was performed to investigate stiffness clarification of 300 mm external diameter GFRP pile. A gradually increased flexural load from 0 kN to 62 kN was applied to the middle of the pile by using hydraulic jack at a rate of approximately 2mm/min and deflections were measured by using wire type displacement transducer. This load represents the lateral loads induced due to flood and debris on a pile in the Shorncliffe jetty. Values were provided by Brisbane City Council. The support span was set to 3 m which approximately 10 times the external diameter of the pile. Also two strain gauges were placed exactly under the load and 500 mm away from the load to measure strain respective to loading. System 5000 was used for data logging.
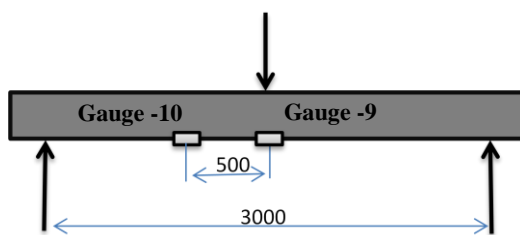
(a)   (b)

(c)   (d)

Figure 3.15: Full scale 300mm external diameter pile testing (Three point bending only)

Measured deflection and stain are given as follows. There was no evidence of damage during loading. From Figure 3.16, deflection over effective span ratio is around $\frac{1}{230}$. Here only lateral deflection was considered, without any axial loadings. But actual situation piles behave against combine axial and lateral loadings which reduce lateral deflection considerably and will be discussed with Section 3.6.
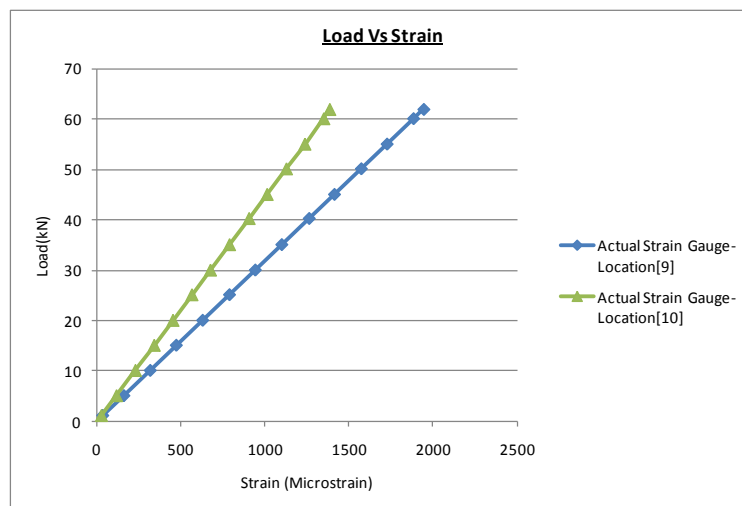
(a)
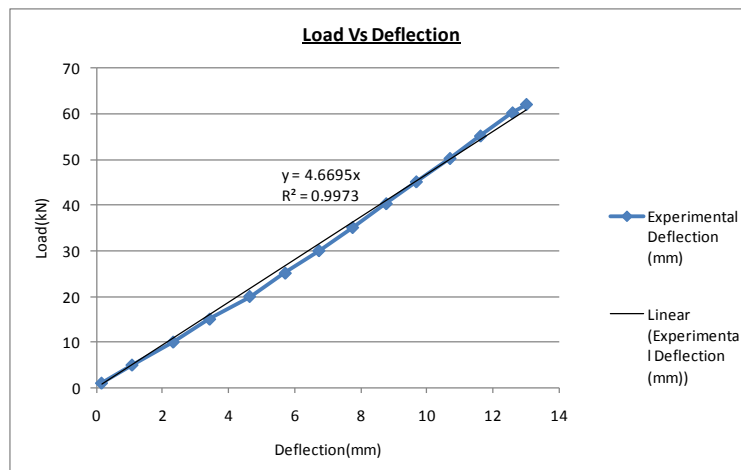
(b)

Figure 3.16: (a) Load Vs Strain diagram, (b) Load Vs Deflection diagram

Flexural stiffness (EI) was calculated by using 3 point deflection formulae. Load/Deflection ( ) were calculated as per the Figure 3.16 (b).

Average Gradient $= 4.6695 \times 10^3$ N/mm

From, 3 point deflection Equation (3.1)

$$EI = \frac{\left(\frac{F}{\delta}\right)}{48} \times L^3 \quad \text{---(3.1)}$$

Where,   L= Support span

F= vertical load at a middle of beam

δ=   Middle deflection

$$EI = (4669.5/48) \times 3000^3$$

$$EI = 2.627E+12 \text{ Nmm}^2$$

Therefore, Flexural stiffness for 300 mm external diameter pile = **2.627 x 10^{12} Nmm^2**

The predicted ultimate bending capacity of the pile can be calculated using the Equation 3.2.

$$\sigma_{Top} \ or \ \sigma_{Bottom} = (M \times y)/I \ \blacktriangleright \ M \le (\sigma_c \times I)/y \quad \text{----------------------------------(3.2)}$$

Where, σ_c= Compressive strength at failure (from coupon test- Table 3.3)

M = Applied moment

y = Distance from neutral axis

E = flexural modulus

I = 2nd moment of inertia of Biaxial fibre in the pile

In this calculation, only biaxial laminates significantly contributed to the 2nd moment of inertia. Because these piles cross sections were comprise of two different materials (Table 3.1) having considerable different E values (biaxial and soric laminates having E of 28000 MPa, 800 MPa respectively). To convert one material, soric thicknesses in pile cross section should multiplied by ratio (E_{soric} / $E_{biaxial}$), which was around 0.028. Therefore, contribution of the soric laminates to the 2nd moment of inertia was negligible.

Table 3.9: Theoretical I calculation for biaxial laminates for 300 mm external diameter pile

Outer Radius (mm)	Inner Radius (mm)	Thicknesses for plies									ΣI
		Biax	soric	Biax	soric	Biax	soric	Biax	soric	Biax	
		2	4	0.5	4	0.5	2	0.5	2	6.5	
150	128	130	134	134.5	138.5	139	141	141.5	143.5	150	
I		1.349E+07	0	3.801E+06	0	4.196E+06	0	4.427E+06	0	6.457E+07	9.048E+07

From Table 3.9,

I $_2{}^{nd}$ $_{\text{moment of inertia of biaxial fibre in the pile}}$ = 9.04E+7 mm^4

$y = (300/2) = 150$ mm

$M_{max} = (300*9.04*10^7) / (300/2) = 1.808*10^8$ Nmm = **180.8 kNm**

Therefore the predicted ultimate flexural load at the middle of pile

$= (2*M_{max}) / (\text{span}/2)$

$= (2*180.8)/(3/2)$

= **241.06 kN**

Theoretical deflection calculated from 3 point deflection Equation 3.1 ($\delta = \frac{F}{48EI} \times L^3$) and theoretical EI value is shown in Table 3.10 based on mixture formula. Here E value of individual materials for biaxial and soric was considered as 28000 MPa (Table 3.3) and 800 MPa (given by supplier) respectively.

Alternatively approximate ultimate capacity of the pile directly can be found using extrapolating three point bending test results. From Figure 3.16 (a), it was assumed that Load Vs Strain variation behave linearly until bending failure. From Table 3.7 ultimate failure strain of the glass fiber laminate is around 12000 με. Therefore ultimate flexural load capacity using experimental approach ≈ (60/2000) x 12000 ≈ **360 kN**. Moment capacity ≈ (360/2) x (3/2) = **270 kNm**.

Table 3.10: Theoretical EI calculation based on lamina properties

Outer Radius (mm)	Inner Radius (mm)	Thicknesses for plies									ΣEI
		Biax	soric	Biax	soric	Biax	soric	Biax	soric	Biax	
		2	4	0.5	4	0.5	2	0.5	2	6.5	
150	128	130	134	134.5	138.5	139	141	141.5	143.5	150	
	E	28000	800	28000	800	28000	800	28000	800	28000	
	I	1.349E+07	2.891E+07	3.801E+06	3.197E+07	4.196E+06	1.724E+07	4.427E+06	1.818E+07	6.457E+07	
	EI	3.777E+11	2.313E+10	1.064E+11	2.557E+10	1.175E+11	1.379E+10	1.239E+11	1.455E+10	1.808E+12	2.610E+12

Comparison of theoretical and experimental strain variation is shown in Figure 3.17.
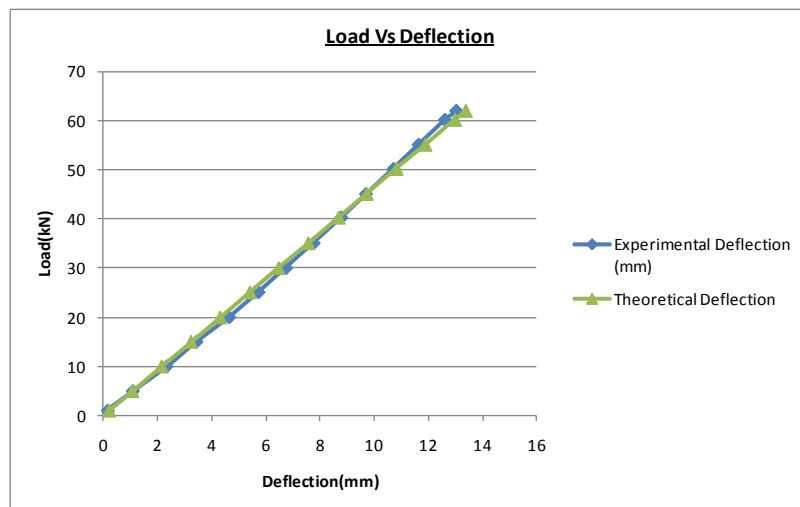
Figure 3.17: Deflection comparison of experimental and theoretical results

3.5.2 470 mm external diameter and 9.2m long pile

Three point bending test was performed to check the flexural stiffness and pure bending capacity at service loads of the 470 mm, 9.2 m long full-scale pile. The support span was set to 8 m which approximately 17 times the external diameter of the pile. In this test, a gradually increased load from 0 kN to 80 kN was applied in the midspan of the pile and deflections were measured by using wire type displacement transducer. This load represents the lateral loads induced due to flood and debris on a pile in the actual bridge structure calculated as per the AS 5100.2-2004. Two strain gauges were placed, one at the midspan the other one at 2000 mm away from the load, to measure strain respective to loading. System 5000 data acquisition software was used for data logging.

(a)

(b)

(c)

(d)
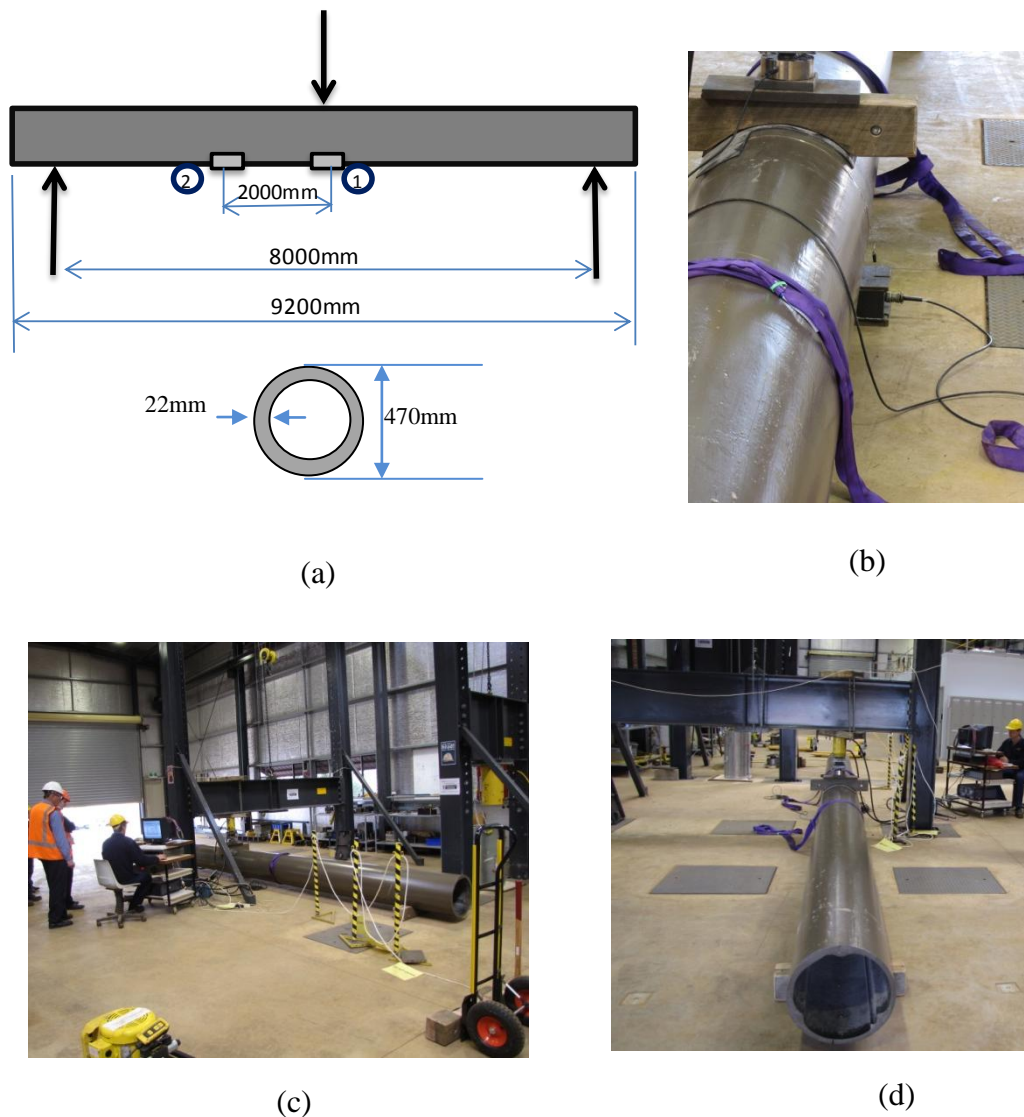
Figure 3.18: Full scale 470 mm external diameter, 9.2 m long pile for bending testing

There was no evidence of damage during loading. Figure 3.19 shows Load Vs Deflection diagram for the three point bending test.
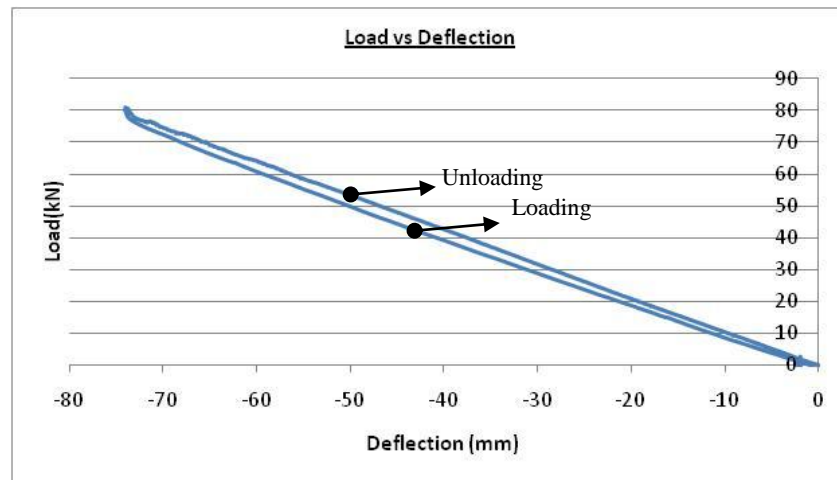
Figure 3.19: Deflection versus Load diagram

Flexural stiffness (EI) was calculated by using 3 point deflection formulae. Load/Deflection ($\frac{F}{\delta}$) for loading and unloading were calculated per the Figure 3.20
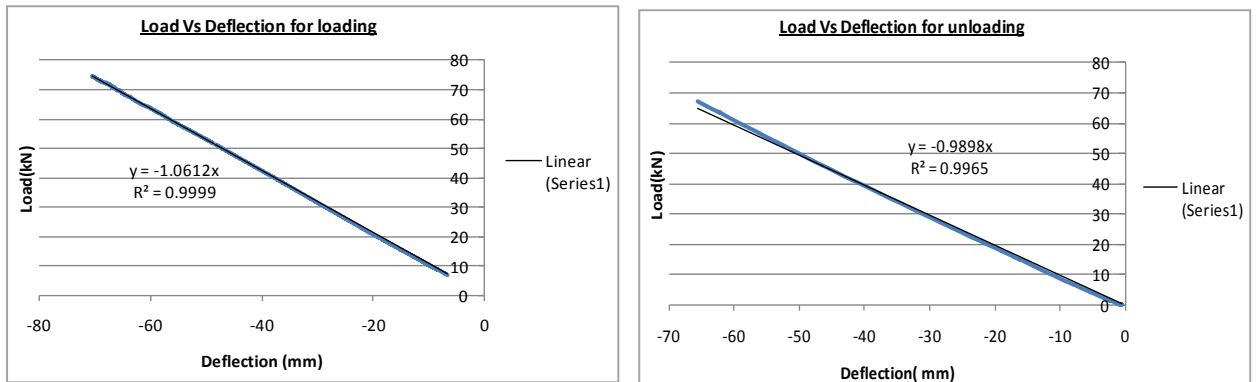
Figure 3.20: Load Vs Deflection for loading and unloading

Average Gradient= $\frac{F}{\delta}$ = (1061.2+989.76)/2 = 1025.48(N/mm)

From 3 point deflection Equation 3.1 ($EI = \frac{\left(\frac{F}{\delta}\right)}{48} \times L^3$),

EI = 1.09385E+13 Nmm^2

Therefore, flexural stiffness for 470mm external diameter long pile = **1.09x10^{13} Nmm^2**.

The predicted ultimate bending capacity of the pile can be calculated using the Equation 3.2 as follow.

$$\sigma_{Top}\ or\ \sigma_{Bottom} = (M \times y)/I \rightarrow M \leq (\sigma_c \times I)/y$$

Here also contribution of the soric laminates to the 2nd moment of inertia was negligible, because same lamina layup arrangements were introduced as 300 mm external diameter pile.

Table 3.11: Theoretical I calculation for biaxial laminates for 470 mm external diameter pile

Outer Radius (mm)	Inner Radius (mm)	Thicknesses for plies									ΣI
		Biax	soric	Biax	soric	Biax	soric	Biax	soric	Biax	
		2	4	0.5	4	0.5	2	0.5	2	6.5	
235	213	215	219	219.5	223.5	224	226	226.5	228.5	235	
	I	6.158E+07	0	1.656E+07	0	1.760E+07	0	1.819E+07	0	2.542E+08	3.681E+08

From Table 3.11,

I 2nd $_{moment\ of\ inertia\ of\ biaxial\ fibre\ in\ the\ pile}$ = 3.68E+8 mm^4

M $_{max}$ = (300*3.68*10^8) / (470/2) = 4.698*10^8 Nmm = **469.8 kNm**

Therefore the predicted ultimate flexural load at the middle of pile = (2*M $_{max}$) / (8/2)

= **234.9 kN**

Theoretical deflection calculated using Equation 3.1 and corresponding theoretical EI value for entire pile based on mixture formula is shown in Table 3.12. Here E value for Biaxial and Soric was considered as 28000 MPa (Table 3.3) and 800 MPa (provided by supplier) respectively. From Table 3.12, corresponding theoretical EI value is around 1.064E+13 Nmm^2. Comparison of experimental and theoretical results for three point bending test is shown in Figure 3.21.

Table 3.12: Theoretical EI calculation based on lamina properties

Outer Radius (mm)	Inner Radius (mm)	Thicknesses for plies									ΣEI
		Biax	soric	Biax	soric	Biax	soric	Biax	soric	Biax	
		2	4	0.5	4	0.5	2	0.5	2	6.5	
235	213	215	219	219.5	223.5	224	226	226.5	228.5	235	
	E	28000	800	28000	800	28000	800	28000	800	28000	
	I	6.158E+07	1.284E+08	1.656E+07	1.366E+08	1.760E+07	7.157E+07	1.819E+07	7.398E+07	2.542E+08	
	EI	1.724E+12	1.027E+11	4.636E+11	1.093E+11	4.927E+11	5.726E+10	5.094E+11	5.919E+10	7.118E+12	1.064E+13
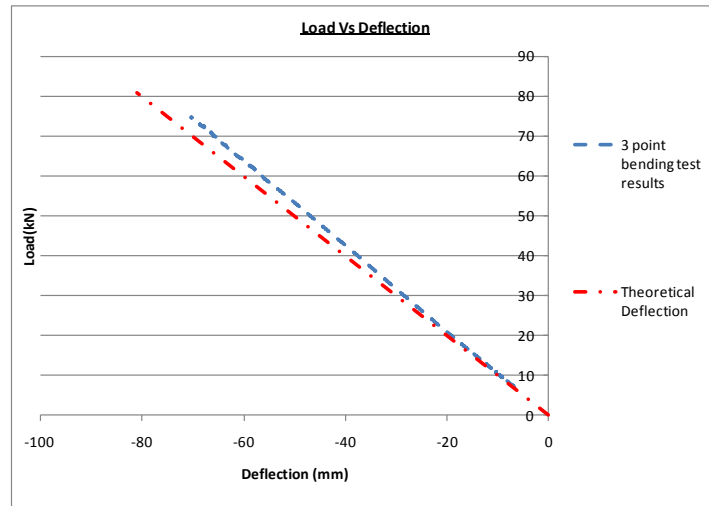
Figure 3.21: Comparison of experimental and theoretical results for three point bending test

Theoretical strain in the location 1 and 2 were calculated using modified version of Equation 3.2.

$$\frac{\sigma_c}{E} = \varepsilon = \frac{M \times y}{EI}$$

Where,

M = Moment at corresponding section

y = Distance from neutral axis

EI= Flexural rigidity

Figure 3.22 shows comparison of experimental and theoretical strains at locations 1 and 2. Anticipated flood load of the middle of the pile is around 80 kN and estimated ultimate capacity around 235 kN, which gave 2.9 safety factor against lateral flood loadings.
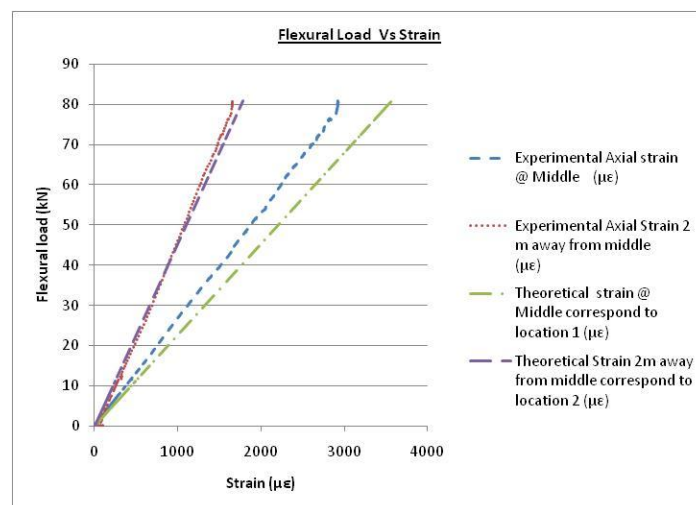
Figure 3.22: Comparison of experimental and theoretical strains at locations 1 and 2

3.6 Combined axial and bending test on 300 mm external diameter, 3.1 m long full scale pile

300 mm external diameter GFRP pile will undergo combined axial and bending loads. The full scale pile (3.1m long) was required to carry the loads under two different load cases mentioned below provided by Brisbane City Council,

- Load case 1: Axial load only = 150 kN

  This load case was represented following load combination including only gravity vertical loads

  $1.2DL+1.5IL = 1.2*26 +1.5 * 78 = 148.2 \text{ kN} \approx 150 \text{ kN}$

  Where,

  DL (Dead Load) =26 (KN)
  IL (Imposed Load) =78 (KN)

- Load case 2: Axial and flexural loads = 62 kN horizontal (axial) + 25 kN vertical (3 point flexure).

  This load case was included both gravity vertical loading and horizontal loading as per according to the following combination

  $1.2DL+0.4IL +1.65WL = 62.4 \text{ KN} + 16.5KN$

  Where,

  DL (Dead Load) =26 (KN)
  IL (Imposed Load) =78 (KN)
  WL (Water Load) =10 (KN)

Test setup was as shown in Figure 3.23. Two hydraulic jacks were used to apply axial and flexural loads. As the pile specimen was too long (3.1 m) to apply axial load vertically using available testing facilities, axial load was applied horizontally and therefore flexural load was applied vertically (Figure 3.23). System 5000 data acquisition software was used for data logging. Wire type displacement transducer was used to measure the deflection. Initially in load case 1, proof axial load of 150kN was applied per the actual Shorncliffe Jetty load of 148.2 kN. Then in load case 2, under 65 kN constant axial load, a flexural load was applied with an increase by 5kN step by step up to 25 kN. Actual requirement in this case was

62.4 kN axial load and 16.5 kN shear load at 2m above the connector. It should be noted that the applied flexural load under constant axial load is equivalent to shear load condition.
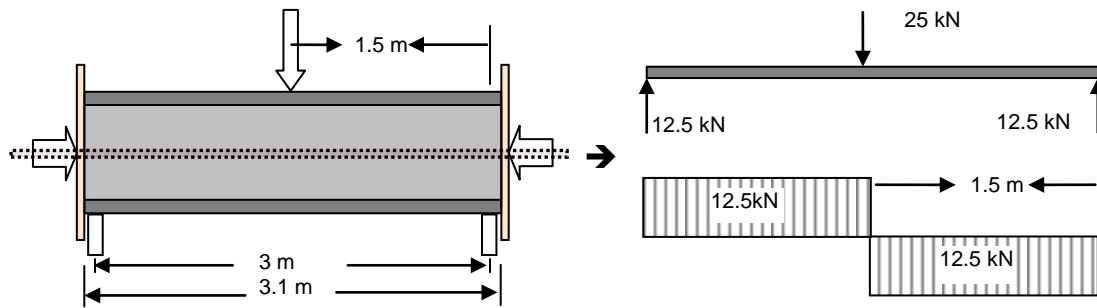
(a)

(b)

(c)

Figure 3.23: (a) free body and shear force diagrams, (b) full scale testing -combined axial and bending, (c) Axial force applied using hydraulic jack

Table 3.13: Full scale pile test result (combined axial and bending)

Load Case 1	
Proof Axial Load, kN	153.00
Load Case 2	
Proof Flexural Load, kN	26.00
Proof (Constant) Axial Load, kN	65.00
Maximum Deflection, mm	7.37

Axial load simulates a vertical axial load including dead and imposed loads on a pile of an actual Shorncliffe Jetty structure while the flexural load simulates the wave load on the pile due to water and debris flow. Result of a full scale pile testing is given in Table 3.13 above. There was no evidence of damage visible during the loadings. Figure 3.24 shows that the pile was given a proof load of 153kN per

load case 1. Figure 3.25 shows that the pile was loaded axially (and kept constant) and transversely per load case 2. From the load case 2, maximum deflection around 7.37 mm and deflection over effective span ratio was around $\frac{1}{407}$. Therefore compared to section 3.5.1, this ratio is getting less when the combination of axial and lateral load was acting against the pile. From AS 5100.2-2004 section 6.11, allowable deflection for the serviceability limit state in the bridge girder lie, in between, $\frac{1}{300}$ and $\frac{1}{600}$ of the span.
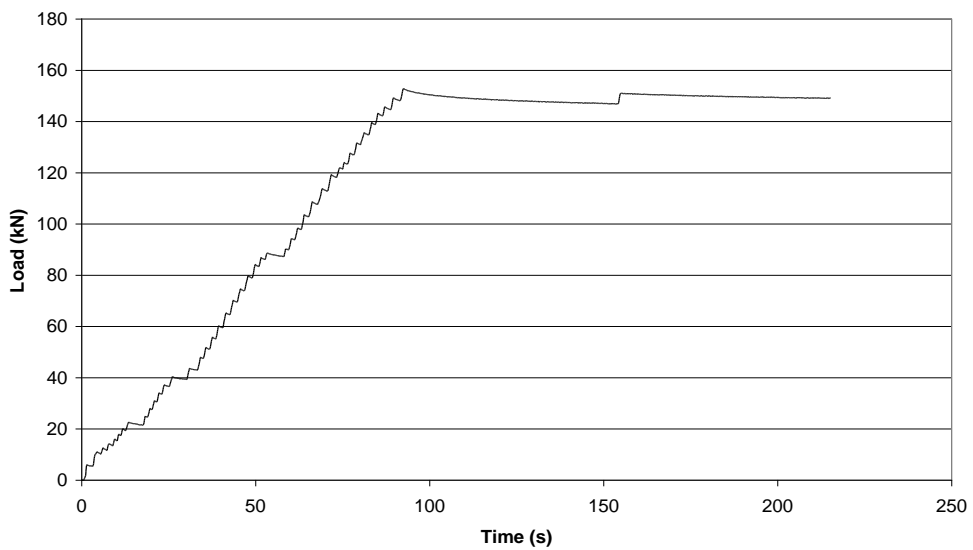
Figure 3.24: Proof axial load (Load case 1)
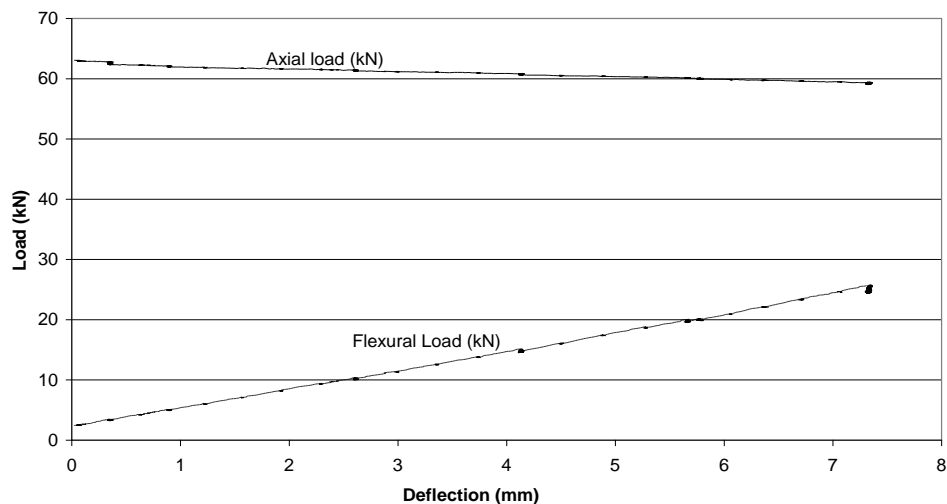
Figure 3.25: Axial and flexural loads versus deflection diagram

Therefore based on above result, 300 mm external diameter GFRP pile is safe against both load cases under serviceability loadings.

3.7 Summary

In this chapter, a detailed experimental investigation was conducted using coupon specimens to characterise the mechanical properties of the glass fibre composite laminates and full scale GFRP pile specimens to identify actual behaviour under serviceability loads. It should be noted that the experiments deals with single pile member. If the pile is connected to other parts of a structure, then entire behaviour is different and appropriate tests are recommended to the connections / joints to verify the capacity of such connections.

There was no evidence of any damage during loading. All the loads applied for the full-scale pile test were proof load to resemble the serviceability loads. It should be noted that the predicted ultimate compressive capacity of the 470 mm external diameter short section of the pile, and the ultimate moment capacity of 9.2 m long pile, were 4222 kN and 469.8 kNm respectively. In addition, the predicted ultimate flexural load at the middle of the pile is approximately 234.9 kN which gave 2.9 safety factor against flood and debris loadings in two lane timber bridge. Therefore at all the times the ultimate capacity of the GFRP pile is higher than the serviceability loads. Based on the theoretical analyses, the compressive elastic modules (E) and flexural stiffness (EI) of the pile are approximately 15100 MPa and 1.09×10^{13} Nmm^2 respectively in serviceability range.

Predicted ultimate compressive capacities of the 300 mm external diameter short section of the pile, and the ultimate moment capacity of 3.1 m long pile, were 1690 kN and 180.8 kNm respectively. Predicted ultimate flexural load at the middle of the pile is approximately 241.06 kN. Here also all the times ultimate capacity of the GFRP pile is higher than the serviceability loads. Based the theoretical analyses, the compressive elastic modules (E) and flexural stiffness (EI) of the pile are approximately 14300 MPa and 2.627×10^{12} Nmm^2 respectively in serviceability range. Combined axial and bending test were done for 300 mm external diameter GFRP pile. Pile was safe against both load cases under serviceability loadings without evidence of any damage during the testing

Moreover, depending on the length of pile, the reduction in capacity due to potential buckling will need to be considered. The appropriate connections between

the pile cap to headstock and the ground fixity will have some influence on the effective length, thus affecting the buckling load.

In Chapter 4, Numerical simulation (finite element analysis) of the experimental results and interpretation of overall behaviour of GFRP pile, followed by connector, is presented.

Chapter 4

NUMERICAL SIMULATIONS OF THE OVERALL BEHAVIOUR OF GFRP PILE SYSTEMS

4.1 Introduction

This chapter presents the numerical simulation of the experiments done in Chapter 3 and overall performance of GFRP pile under different loadings. STRAND 7 (version 2.4.3) Finite Element Analysis (FEA) software package was used for numerical simulation. In this chapter, numerical simulation is divided into three phases to evaluate the behaviour of GFRP tubes under different loading conditions.

In phase I, experiments of 300 mm and 470 mm external diameter hollow GFRP piles were simulated to verify behaviour under axial compression, and pure bending against actual loadings.

In phase II, two case studies were considered to evaluate overall behaviour of the GFRP pile. First case study, a 7.5 m long, by 300 mm external diameter GFRP pile, followed by a connector was simulated to find the behaviour of the Shorncliffe pier loadings, provided by the Brisbane City Council. Two ultimate load cases were considered to evaluate the behaviour of the GFRP connector and the pile. In the second case study, a 7.5 m long, by 470 mm external diameter GFRP bridge pile, was simulated to investigate the behaviour against rural area timber bridge loadings under class 4 classification in AS 5100.7-2004. In addition, a buckling analysis was performed for a 9.2 m long, 470 mm external diameter pile, to evaluate the buckling load capacity.

In phase III, filler material inside the connector was simulated to identify behaviour under bridge loadings.

4.2 Numerical simulation of 300 mm external diameter GFRP pile testings (Phase I)

4.2.1 FEA simulation for 300 mm external diameter short pile

Initially, a short pile FE model was generated using 4 node shell elements. The mesh model comprised of 1280 nodes and 1200 shell elements, with a uniform mesh of

11 mm x 15 mm. In this modelling, laminate properties were adopted as property attributes of shell elements. To do this, lamina stacks made of the composite pile's two component materials (i.e.fibreglass and Soric XF reinforced laminate) were modelled per the Figure 4.1.
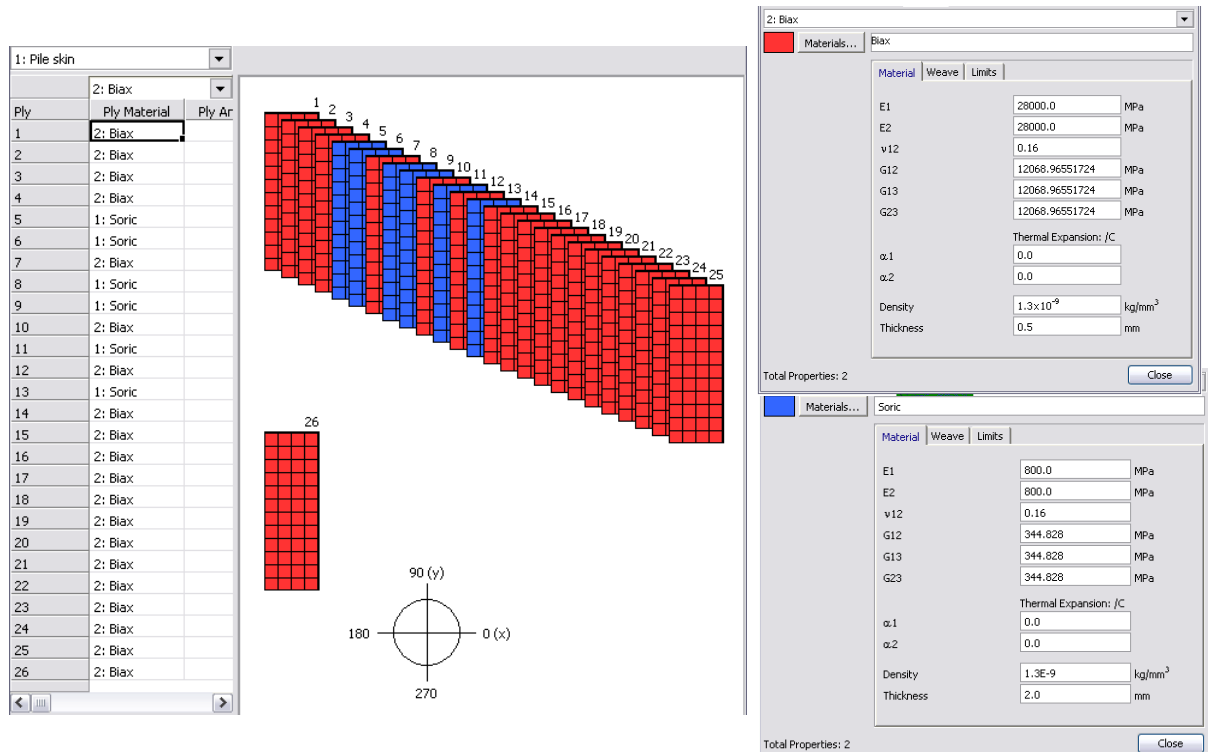
Figure 4.1: Material properties and lamina layup arrangements used in FEA model

Assigned property values of each lamina taken from the coupon tests are shown in Chapter 3, Table 3.3. It should be noted that the mass of each lamina has a small affect on stress formation compared to the applied load, and therefore is neglected in this study.

In the conducted experiment, the composite pile was in contact with stiff loading plates at the two ends. Even if the support condition may emerge to be close to a simply supported condition, previous research conducted showed a much closer value to the experiment results if a "clamped support condition" is adopted (Teng and Hu, 2006). Therefore, the clamped-end condition is more appropriate for this model. To adopt such support conditions, the two ends were fully fixed in all directions, except that the axial displacement of the top end was left unrestrained to allow the application of axial loading.

To properly simulate the loading condition on the specimen, vertical uniformly distributed pressure on the top of the model was applied. A 22.02 MPa uniform

distributed pressure load was applied on the top face of the model. This applied load was identical to that of the load used in experiment (414 kN) to predict the composite pile's behaviour under axial compression.

Figure 4.2 demonstrates the finite element model and deformed mode of the hollow FRP pile generated from the analysis. It is evident from the Figure that both support ends of the pile have undergone a response from the applied load. To visibly compare the stress distribution between the top support face going to the bottom support, the displacement scale was modified, so that a clear deformation at the mid-height is noticed. The difference of the stress distribution in all regions using the finite element method is diminutive so that the strain is almost constant at the ends and at the mid-height of the composite piles in axial direction.

(a)   (b)
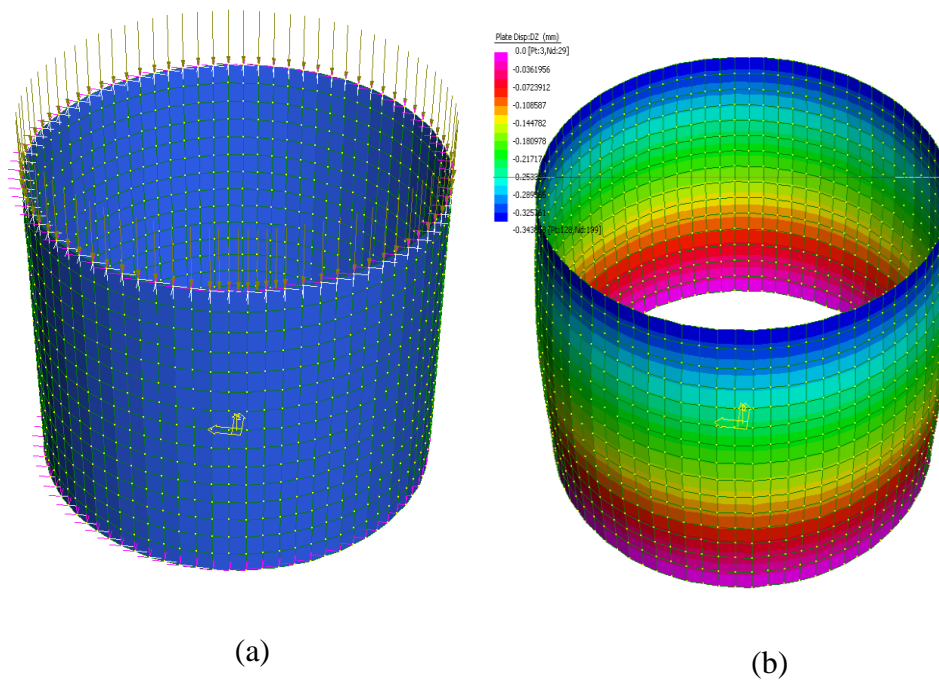
Figure 4.2: (a) Finite element model (b) deformed mode

Table 4.1 summarises the stress, load, and strain results at the mid height section of the FRP composite pile, under a maximum applied load of 22.02 MPa (414 kN). It is noticeable that values in axial direction vary along its thickness with this type of laminate layup. To better understand the behaviour of the composite pile, values of plies were analysed, and are shown in Figures 4.3 (a) and (b).

Table 4.1: Summarized stress, load & strain results of the plies at the mid-height of the pile

		Ply number												
	Unit	1	2	3	4	5	6	7	8	9	10	11	12	13
σ_A	MPa	39.21	39.36	39.51	39.66	1.16	1.18	41.03	1.20	1.22	42.40	1.24	43.17	1.26
P_A	kN	18.11	18.18	18.25	18.32	2.14	2.17	18.95	2.21	2.25	19.58	2.29	19.93	2.33
ε_A	-	1384	1389	1394	1399	1412	1432	1445	1458	1479	1492	1504	1517	1530
ε_L	-	316	316	316	316	316	316	316	316	316	316	316	316	316
		Ply number												
	Unit	14	15	16	17	18	19	20	21	22	23	24	25	26
σ_A	MPa	43.93	44.08	44.23	44.38	44.54	44.68	44.84	44.99	45.15	45.30	45.45	45.60	45.76
P_A	kN	20.29	20.36	20.43	20.50	20.57	20.64	20.71	20.78	20.85	20.92	20.99	21.06	21.13
ε_A	-	1543	1548	1553	1558	1563	1568	1574	1579	1584	1589	1594	1599	1604
ε_L	-	316	316	316	316	316	316	316	316	316	316	316	316	316

σ_A = axial stress, P_A = axial load, ε_A & ε_L = micro-strain in axial and lateral directions, respectively.

Figure 4.3 gives detail of the axial stress and the applied load distribution between the FRP composite pile and the main component materials at the mid-height. The adopted values of the component materials were referred from its individual average stress, load, and strain values. Axial stress of the FRP composite pile remains intermediate, as individual strain increases under this loading condition as shown in Figure 4.3(a). Based from Figure 4.3(b), it was found that glass-reinforced lamina carries 96% of the applied load compared to that of the Soric XF-reinforced lamina. It can be determined from the result that former component material bears most of the load. Moreover, it can be inferred that the total behaviour of the FRP composite pile under axial compression with this kind of laminate layup, depends solely on the response of glass reinforced lamina, and the affects of Soric XF-reinforced lamina, is very minimal.
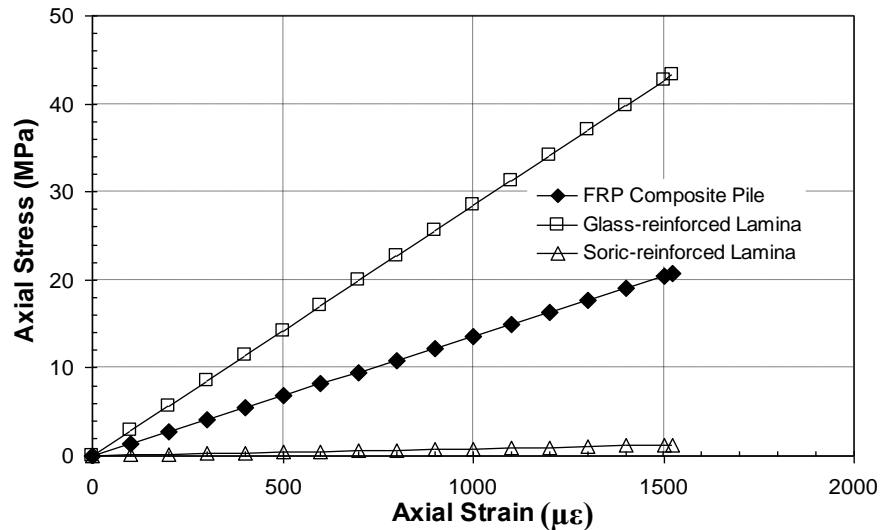
(a)
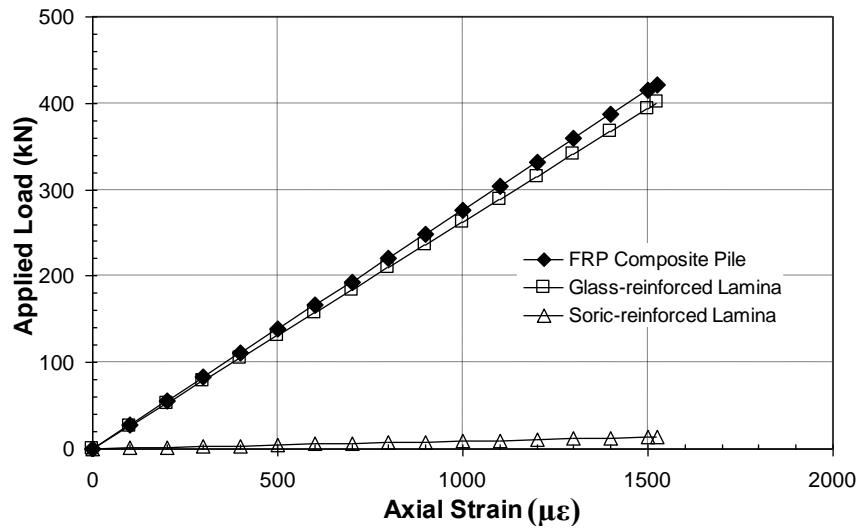
(b)

Figure 4.3: Mid-height axial strain of FRP pile and its component materials versus (a) applied load (b) axial stress.

The relationship of the applied load to the strain of selected representative plies on the mid-height of the model for both axial and lateral direction is given in Figure 4.4 (a) & (b). For clarity, a section of the tube at the mid height is reflected, indicating the labelling number of the plies (i.e. ply 1 and ply 26 at the most inner and outer face of the tube, respectively). It can be observed from the graphs that plies at this section behave differently in axial direction but not laterally if strained under axial compression. From Figure 4.4(a), strain variations of the plies on the axial direction were developed. The strain variations indicate that at increasing load magnitude, section at the mid height starts to undergo wall buckling, although this premature deformation will not cause local failure or sudden collapse to the FRP composite pile as discussed earlier. On the other hand, lateral strain of the plies remains the same across the thickness (i.e. ply 1, ply 2 … ply 26) of the tube irrespective of the loading magnitude as shown in Figure 4.4(b).

The graphical comparison of the applied load-strain and FE analysis results is exposed in Figure 4.4(c). Apparently, the calculated value from the finite element analysis is at par to the experimental value. The use of FE method, thus, proved to be effective in determining the overall compressive modulus of the FRP composite pile in particular, and its compressive behaviour, in general.
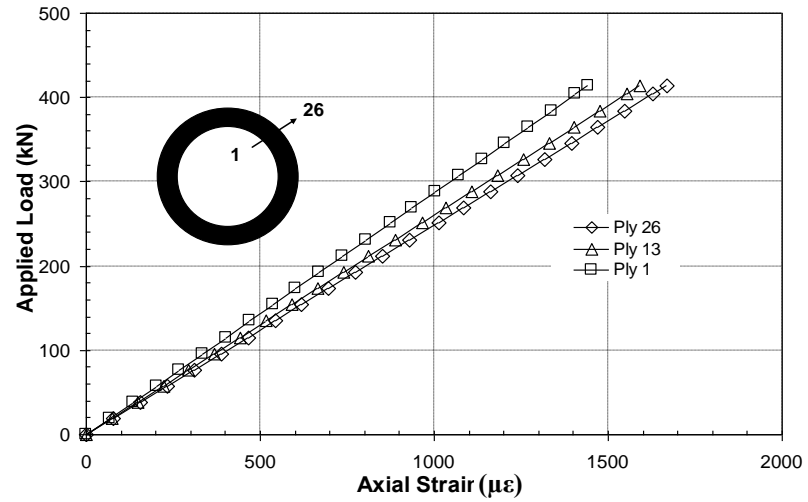
(a)
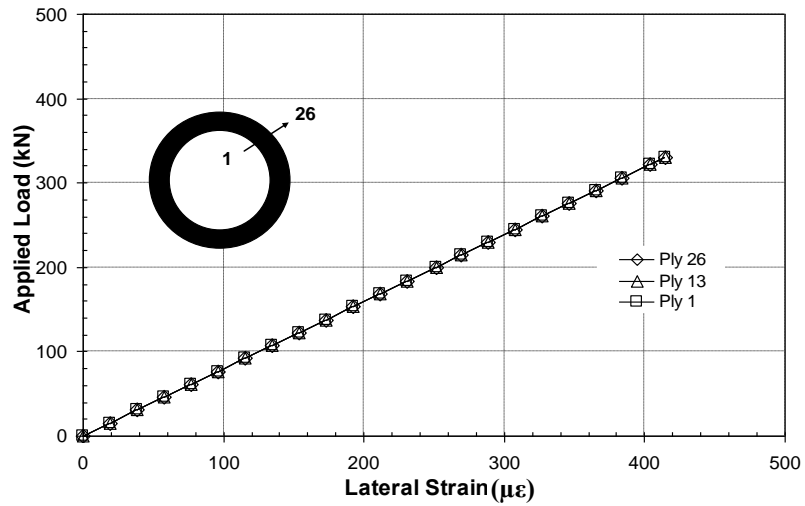
(b)
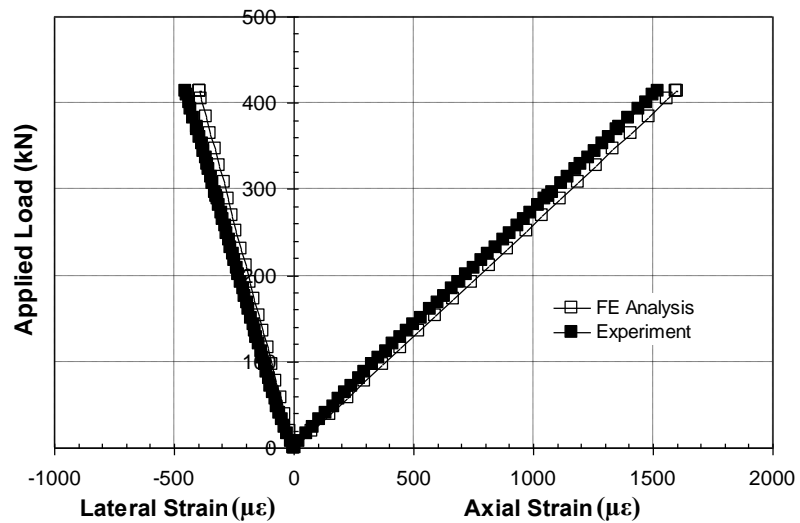
(c)

Figure 4.4: Mid-height applied load-strain relationship of selected plies in (a) axial direction, (b) lateral direction, (c) Comparison of applied load-strain curves of experiment and FE analysis.

4.2.2 FEA simulation for 300 mm external diameter 3.1 m long pile

The same lamina layup shown in Figure 4.1 was used for 3.1 m long pile. The FE model was generated using 8 node shell elements. The mesh model comprised of 4644 nodes and 1692 shell elements with a uniform mesh of 25 mm x 27 mm. In this modelling, laminate properties were adopted as property attributes of shell elements. Assigned property values of each lamina where taken from the coupon tests are shown in Chapter 3, Table 3.3. It should be noted that the mass of each lamina has a small affect on stress formation compared to the applied load, and therefore is neglected in this study. In this test, a 3.1m long pile specimen was placed over flat timber planks and one side pinned and other side roller conditions were given as boundary condition. Figure 4.5 (a) shows deformed shape of the FE model and deflection corresponds to 62kN.Comparison of experimental, theoretical and FEA results were shown in Figure 4.5 (b).

Loading = 62008.97N

Node 203	DX (mm)	0.5514
Quantity	DY (mm)	0.0606
⊙ Displacement	DZ (mm)	13.2505
	RX (deg)	-0.0015
Axis System	RY (deg)	0.6752
⊙ Global	RZ (deg)	-0.2141
○ UCS	D(XY) (mm)	0.5548
	D(YZ) (mm)	13.2507
Find DX	D(ZX) (mm)	13.2620
Min Max	D(XYZ) (mm)	13.2622
☑ Absolute	R(XY) (deg)	0.6752
	R(YZ) (deg)	0.7083
	R(ZX) (deg)	0.2142
	R(XYZ) (deg)	0.7083
	X	0.0000
	Y	1550.0000
	Z	132.5000

(a)

Load Vs Deflection
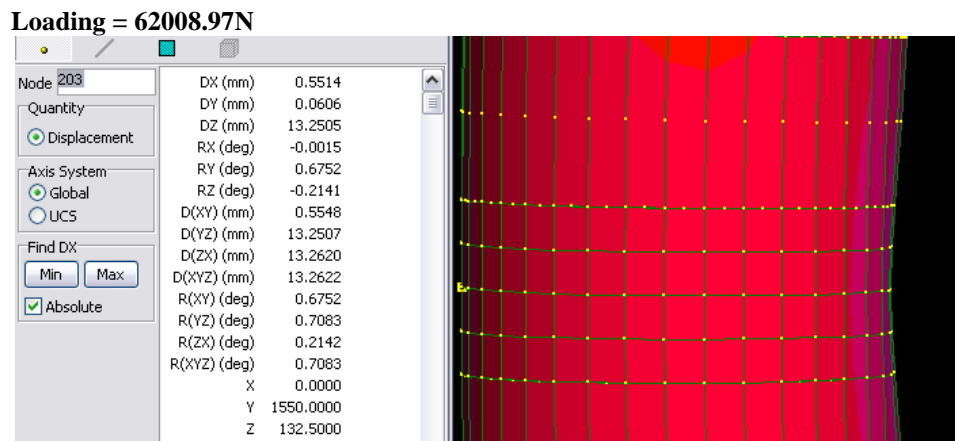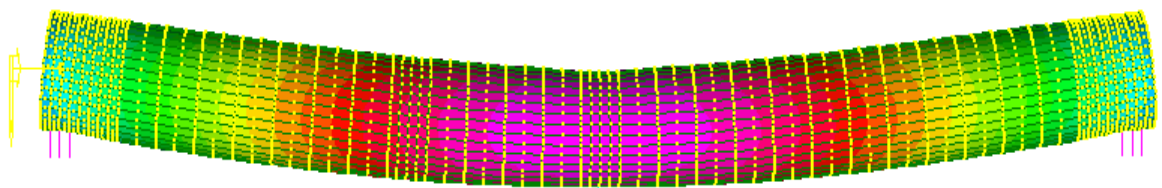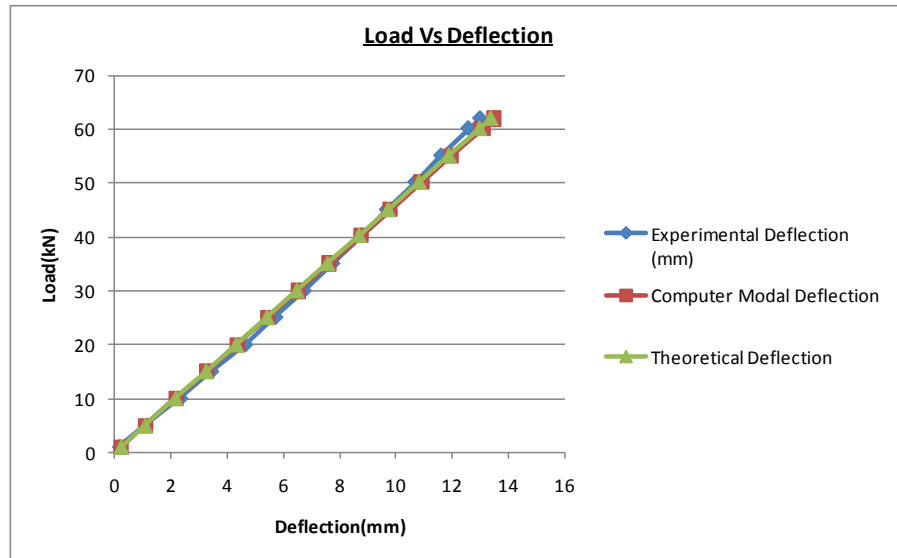
(b)

Figure 4. 5: (a) Deformed shape of the FE model, (b) comparison of experimental, theoretical and FEA results

The deflection value from the finite element analysis followed approximately the same path as theoretical and experimental. The use of the FE method proved to be effective in determining the overall behaviour of GFRP composite pile under flexural loadings.

4.3 Numerical simulation on 470 mm external diameter GFRP pile testings (Phase I)

4.3.1 FEA simulation for 470 mm external diameter short pile

For the FE modelling, E value for biaxial and Soric was considered as 28000 MPa (Chapter 3, Table 3.3), and 800 MPa (provided by the supplier), respectively. For the FEA model, the same lamina layup arrangement and properties were used as shown in Figure 4.1. The FE model was generated using a 8-node shell element. The mesh model comprised of 14259 nodes and 4640 shell elements with a uniform mesh of 18.7 mm x 18.4 mm. In this modelling, laminate properties were adopted as property attributes of shell elements. To do this, lamina stacks made of the composite pile's two component materials (i.e. fibreglass and Soric XF-reinforced laminate),were modelled (Figure 4.1). Assigned property values of each lamina where taken from the coupon tests and are shown in Chapter 3, Table 3.3. It should be noted that the

mass of each lamina has a small affect on stress formation compared to the applied load, and therefore is neglected in this study.
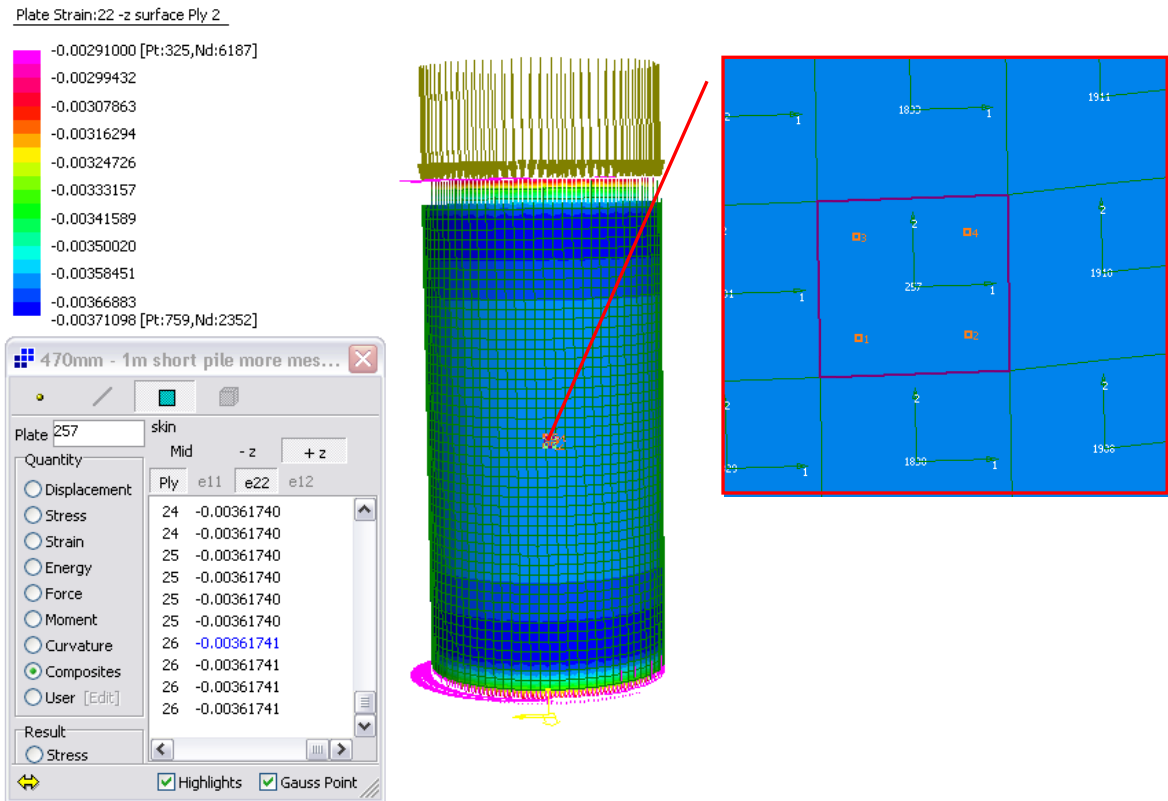
Figure 4.6: FEA axial strain in middle strain gauge position corresponds to compression stress of 48.44 MPa (Corresponding compressive load = 1500kN)

Table 4.2: Results from experimental test and FEA

Load (kN)	Corresponding Stress (MPa)	Experimental		FEA				Theoretical			
		Axial Strain obtained from compression testing (μɛ)	Circumference Strain obtained from compression testing (μɛ)	Axial Strain from FEA– e22 (μɛ)	Error % against experimental data	Circumference Strain from FEA-e11 (μɛ)	Error % against experimental data	Theoretical Axial Strain (μɛ)	Error % against experimental data	Theoretical Circumference Strain (μɛ)	Error % against experimental data
0.00	0.00	0.00	0.00	0.00	0.00	0.00	0.00	0.00	0.00	0.00	0.00
330.84	10.69	-836.36	135.01	-797.93	4.60	127.65	5.45	-801.95	4.11	132.32	1.99
621.61	20.08	-1386.37	222.71	-1499.23	8.14	239.84	7.69	-1506.79	8.69	248.62	11.63
1029.97	33.26	-2248.26	366.75	-2484.09	10.49	397.40	8.36	-2496.60	11.05	411.94	12.32
1500.00	48.44	-3231.26	534.28	-3617.41	11.95	578.70	8.31	-3635.63	12.51	599.88	12.28

In the FE model, the following boundary conditions were considered. Bottom ➔ Fixed both rotation and translation in three directions Top ➔ Only axial translation allowed. The two ends were fully fixed in all direction except that the axial displacement of

the top end was left unrestrained to allow the application of axial loading. 8-Node quadrilateral elements (Quad8) were used in the FE 1 m short pile modelling. Based on Table 4.2 and Figure 4.7, the Quad 8 elements were given good results for the short pile compression test.
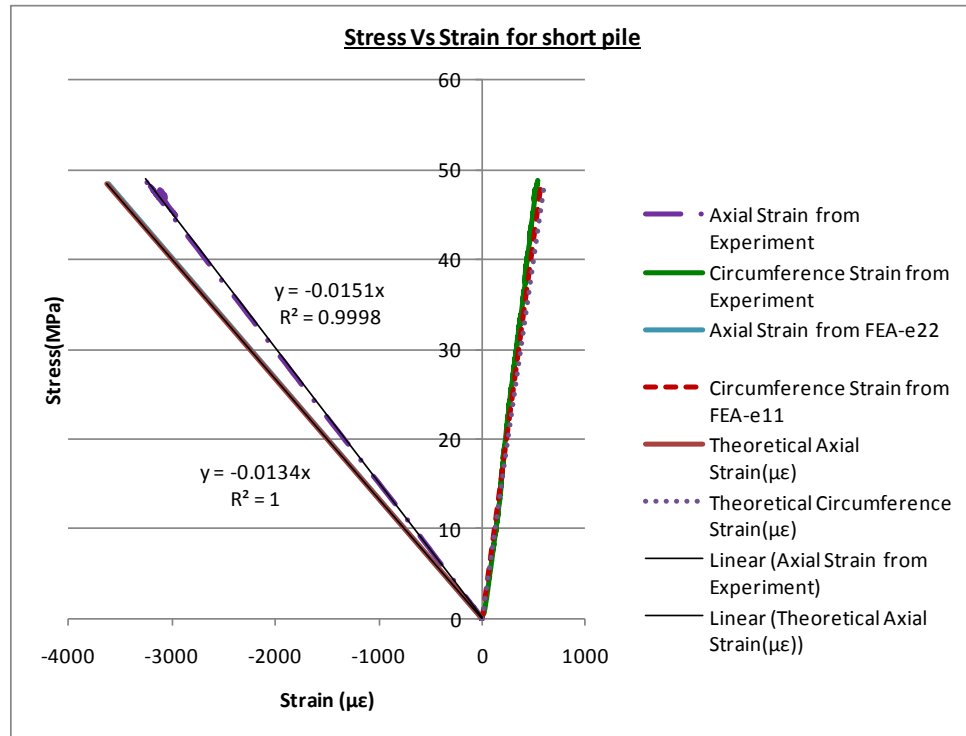
Figure 4.7: Graphical representation for experimental and FEA results

From Figure 4.7 and Table 4.2, circumferential strain in the FEA model followed approximately the same path as in the experimental results, but the axial strain showed a deviation of 11.25% compared to the test results. The FEA results and theoretical calculations show nearly the same results. However, the ideal boundary conditions do not exist in experimental conditions, attributing to this difference of 11.25%, which is considered reasonable. Therefore, the short column compressive modulus value can be considered as **15100 MPa**.

4.3.2 FEA simulation for 9.2 m long 470 mm external diameter full scale pile

For the FEA simulation of 9.2 m long pile, the E value of individual materials for biaxial and Soric was considered as 28000 MPa (Table 3.2) and 800 MPa (provided by the supplier), respectively. The same lamina layup shown in Figure 4.1 was used for 9.2 m long pile.

Identifying the appropriate boundary conditions in the FE model, proved a little difficult. In the actual experiment, two timber planks were used as supports, and are shown in Figure 4.8.

Figure 4.8: Support condition in bending test.

The following trial boundary conditions were considered for FEA modelling.

1. Both sides pinned connections ➔

(a)

Both Sections X-X & Y-Y
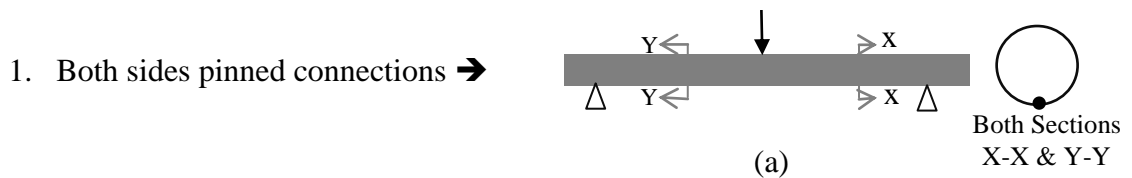
One node was selected in either side to assign boundary conditions.

2. One side pinned and other side roller ➔

(b)

Section X-X roller support

Section Y-Y pinned support
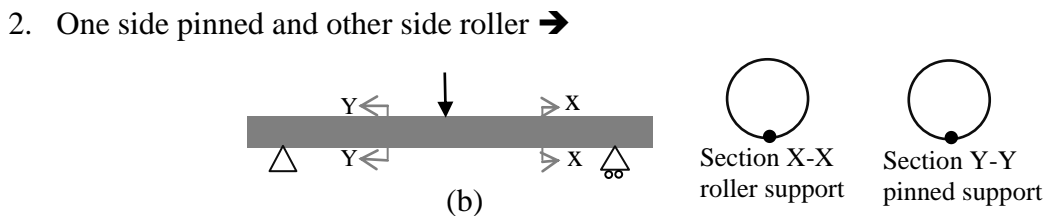
One node was selected in both sides to assign boundary condition as pinned and roller.

3. One side pinned and other side roller, to cover the angle of nodes 30^0, 90^0, 120^0 and 180^0.

(c)

Section X-X roller support to cover 30^0 angle of nodes

Section Y-Y pinned support to cover 30^0 angle of nodes

(d)

Section X-X roller support to cover 90^0 angle of nodes

Section Y-Y pinned support to cover 30^0 angle of nodes

(e)

Section X-X roller support to cover 120^0 angle of nodes

Section Y-Y pinned support to cover 120^0 angle of nodes

(f)

Section X-X roller support to cover 180^0 angle of nodes

Section Y-Y pinned support to cover 180^0 angle of nodes

Figure 4.9: (a), (b), (c), (d), (e) & (f) line diagrams for boundary conditions in three point bending FE model

Table 4.3 shows FEA results for different boundary conditions. Based on the results, 120^0 angle of nodes covered by one side pinned and other side roller condition was given more reliable solutions, close to actual experiment results. Here, middle strain value and deflection value were deviated 9.2% and 10.2% respectively from the experimental values. To this FE model, flexural load was applied on one node at the middle of the pile, as shown in Figure 4.11. Because of that, the middle area around the pile model was locally distorted, and the results deviated from the actual experimental results. 2 m away from the middle, strain value was of the same order as experimental, because local distortion occurs in the vicinity of the middle load section. If flexural load in the middle was distributed among the middle nodes (as boundary condition identification approach), then, the middle strain and deflection values could become close to actual experimental results. Figure 4.10 shows the comparison of strain between the FEA model, and the experiment.

Table 4.3: Comparison of different FEA model with results

Experimental flexural load = 80818 kN	Different FEA models					
	Both side pinned	One side pinned other side roller	Angle covered by one side pinned and other side roller			
			180	120	90	30
Middle Deflection	Middle Deflection	Middle Deflection	Middle Deflection	Middle Deflection	Middle Deflection	Middle Deflection
-74.07	-68.41	-106.7	-64.54	**-81.675**	-92.145	-103.4
Middle Strain	Middle Strain	Middle Strain	Middle Strain	Middle Strain	Middle Strain	Middle Strain
e22	e22	e22	e22	e22	e22	e22
2927.52	1705.84	3200.69	2194.78	**2655.52**	2930.46	3195.65
2m away from middle strain	Strain at 2m away from middle	Strain at 2m away from middle	Strain at 2m away from middle	Strain at 2m away from middle	Strain at 2m away from middle	Strain at 2m away from middle
e22	e22	e22	e22	e22	e22	e22
1658.84	427.84	1978.89	482.54	**1688.08**	1834.67	1976.14
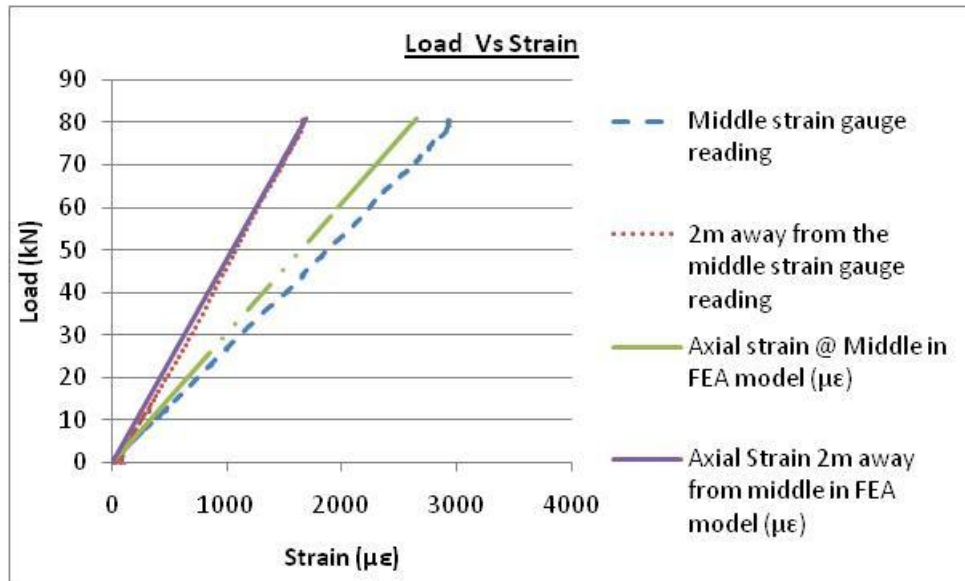
Figure 4.10: Comparison of strain between FEA model and experiment
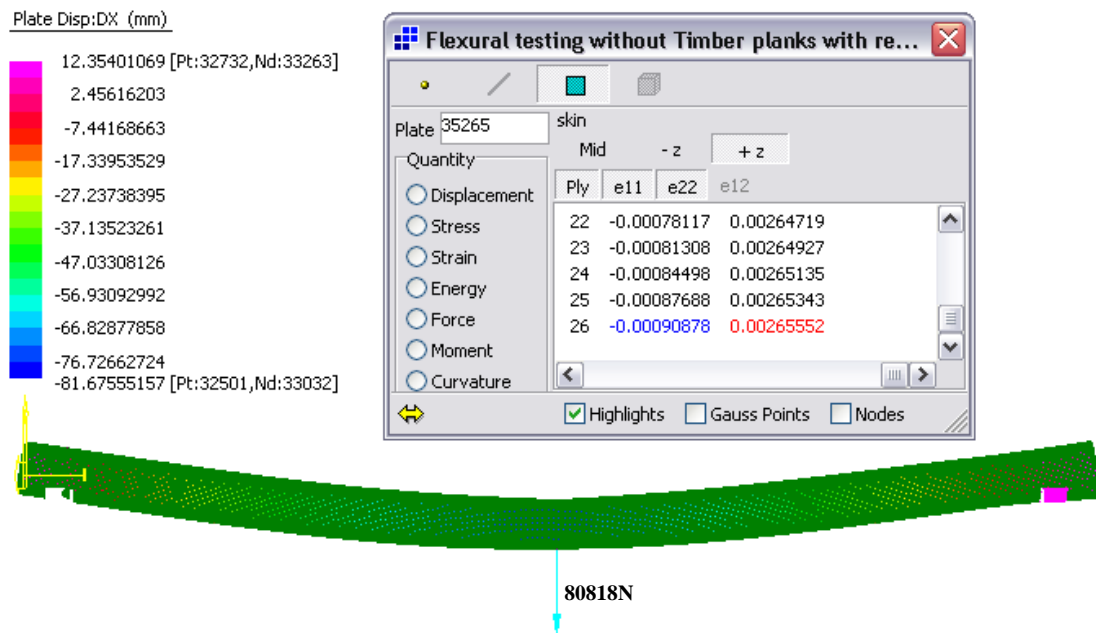
Figure 4.11: Deflection and corresponding axial (e_{22}) strain in the middle according to 80.8kN load in FEA model

Table 4.4: Results from experimental test and FEA

Load(N)	From 3 Point Bending Test			From Theoretical Analysis						From FEM analysis					
	Middle Deflection (mm)	Experimental Axial strain @ Middle(µm)	Experimental Axial Strain 2 m away from middle (µm)	Middle Deflection (mm)	Error % against experimental data	Theoretical Axial strain @ Middle (µm)	Error % against experimental data	Theoretical Axial Strain 2 m away from middle (µm)	Error % against experimental data	Middle Deflection (mm)	Error % against experimental data	Axial strain @ Middle in FEA model (µm)	Error % against experimental data	Axial Strain 2m away from middle in FEA model (µm)	Error % against experimental data
0	0	0	0	0	0	0	0	0	0	0	0	0	0	0	0
20000	-19.31	758	479.67	-20.06	3.87	883.76	16.59	441.88	7.88	-20.21	4.67	657.16	13.30	417.75	12.91
60000	-56.54	2249.3	1273.38	-60.17	6.42	2651.28	17.87	1325.64	4.10	-60.63	7.24	1971.48	12.35	1253.25	1.58
80818	-74.07	2927.5	1658.84	-81.05	9.42	3571.18	21.99	1785.59	7.64	-81.67	10.26	2655.52	9.29	1688.08	1.76

The FEA model used for the flexural simulation is shown in Figure 4.11. Comparison among the three point bending test, theoretical analysis, and FEA model is shown in Table 4.4 and Figure 4.12. According to the Table 4.4, FEM strain values are comparable with the theoretical prediction, with only 6.7% deviation from experimental deflection values.
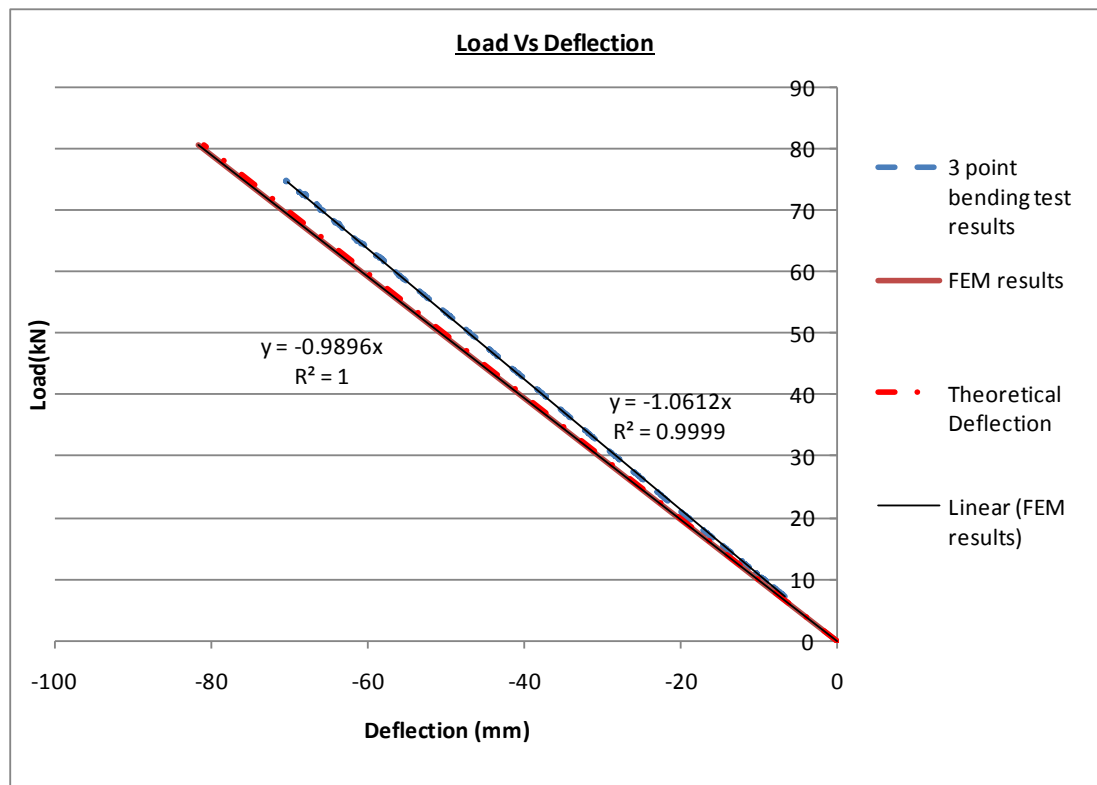
Figure 4.12: Comparison of experimental, theoretical and FEA results for three point bending test

From the FEA, $\frac{F}{\delta} = 989.6$.

From the 3 point deflection Equation (4.1)

$EI = 1.0555E+13$ Nmm^2 $(EI = \frac{\left(\frac{F}{\delta}\right)}{48} \times L^3)$

The flexural stiffness for the 9.2 m long pile, using FEA simulation, $= \mathbf{1.055 \times 10^{13}}$ **Nmm**^{2}.

The Flexural stiffness (EI) value obtained from the FEA was 3.3% lesser than experimental value.

4.4   Finite element simulation of overall behaviour of GFRP piles (Phase II)

In this section, the overall behaviour of the 300 mm external diameter GFRP pile followed by the connector against the Shorncliffe pier loading will be evaluated using the FEA model. In addition 470 mm external diameter GFRP pile performance will be assessed against a two lane timber bridge loadings under class 4 road classification in AS 5100.7-2004. FEA modelling, STRAND 7, (version 2.4.3) was used. Both 300 mm and 470 mm external diameter GFRP piles consisted of the same lamina layup arrangement as Table 4.5 and Figure 4.1. A total of 20 layers of 600 g/m2 Biaxial glass fibre, and 6 layers of XF Soric were used, based on the following layup arrangements, and having an overall thickness of 22 mm (from the inside to outside of the pile wall).

Table 4.5: Layup arrangements of both 300mm and 470mm external diameter GFRP piles models

Number of Layers	4	2	1	2	1	1	1	1	13	Total tickness (mm)
Type	Biaxial	Soric	Biaxial	Soric	Biaxial	Soric	Biaxial	Soric	Biaxial	
Thickness (mm)	2	4	0.5	4	0.5	2	0.5	2	6.5	22

00 Biaxial fibres were aligned to the pile axis

Material properties and allowable stresses were used based on coupon tests results as shown in Chapter 3, Table 3.3.

4.4.1 Behaviour of 300 mm external diameter GFRP pile followed by connector FE model against Shorncliffe pier

In this FE model, checks regarding suitability and performance of the 300 mm external diameter GFRP pile, followed by the connector under the Shorncliffe pier loadings, provided by Brisbane City Council. According to the Brisbane City Council information, clear timber pile height in the Shorncliffe pier varies from 3 m to 7.3 m, from sea bed level. Therefore this FE modelling, 7.5 m height, 300 mm external diameter GFRP pile, followed by the connector was selected for the analysis to obtain a worse-case scenario. Figure 4.13 shows the line diagram, and the FE model. Minor dimensions of the pile connector were shown in Chapter 3 Figure 3.3 (a). For the connecter, effective length of the bottom part was selected by adding external diameters of lower and upper section. Therefore effective length of lower section = 300 (diameter of top pile) + 440 (diameter of bottom pile) ≈750 mm. Filler material thickness depends on amount of the lift of the connector and top pile,

until attached to the head stock. Here for the simplicity, only angle portion of the connector was filled with the filler.
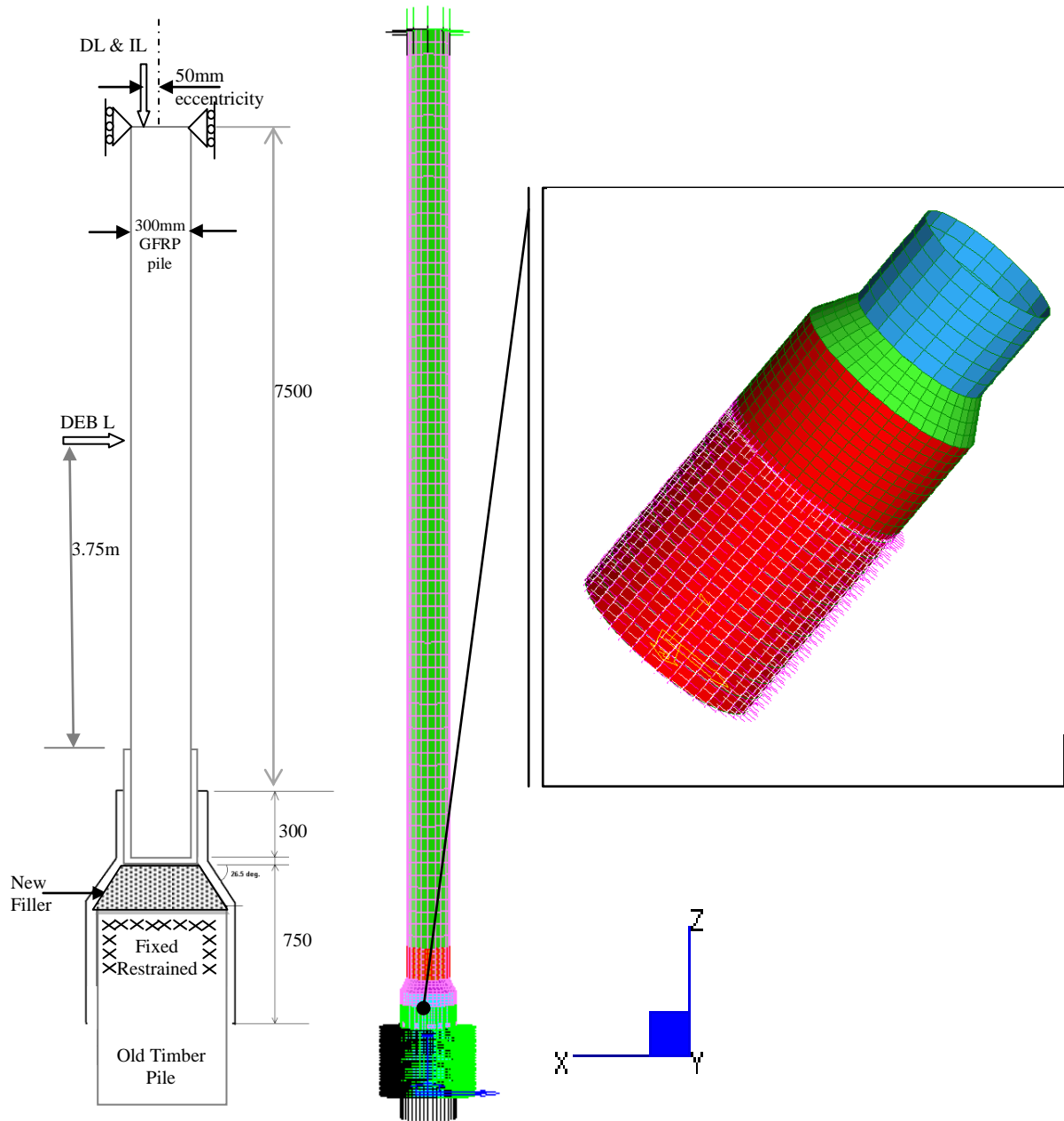
Figure 4.13: Schematic diagram and FE model in STRAND 7

·   Table 4.6: Loadings per pile and appropriate safety factors from the Brisbane City Council

Load category	Value (kN)	Ultimate Safety factor
Dead Load (DL)	26	1.2
Imposed Load (IL)	78	1.5
Water Load (W L)	10	1.65

All loadings, ultimate load factors and load cases were provided by the Brisbane City Council, and are shown in Table 4.6. The following two load cases were considered for the FE model.

Load Case 1:

1.2DL+1.5IL -- (4.1)

(Vertical force with 0.050 m offset)

Load Case 2:

1.2DL+0.4IL +1.65WL -- (4.2)

(Vertical force with 0.050 m offset and debris load acting on mid height of the pile)

It is suggested that the top of the pile is connected to deck platform, where the displacement is not significant due to the platform being supported by many other piles. Pinned joints (axial displacement allowed), were applied on the top of the pile for both load cases 4.1 and 4.2. It was assumed that the joint in between the GFRP pile, the GFRP connector, and the existing intact timber stump are fully bonded. A fixed support was applied on the base of the existing intact timber pile.

The following lamina layup arrangements were introduced to the FE model and are shown in Chapter 3, Figure 3.3(b and c).

1. 8 layers 600 / 225 g/m^2 Biax / CSM glass (inner top)
2. 8 layers 600 / 225 g/m^2 Biax / CSM glass (inner bottom)
3. 12 layers 600 / 225 g/m^2 Biax / CSM glass (outer)

Biax fibres were aligned at 0 degrees to the cylinder axis.

The potential composite laminate failure was calculated and measured in this model by Reserve Factor (Safety Factor). The Reserve Factor is computed as the failure load divided by the applied load.

$$Max\ stress\ reserve\ factor = \frac{Allowable\ stress}{Applied\ stress} \text{---------------------------- (4.3)}$$

Thus, a failure index of 1 or above indicates structure is safe. The Direction of the local axis in the FE model is given in Figure 4.14.
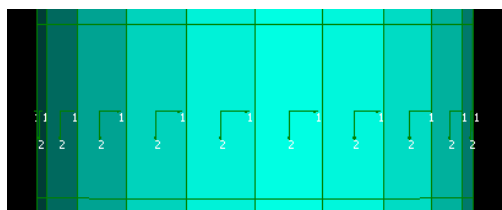
1-1: GFRP pile circumference direction, 2-2: GFRP pile axial direction
Figure 4.14: Local axis system for the whole system

4.4.1.1 Load case 1: 1.2DL+1.5IL

Figure 4.15: Outer ply stresses in local axis 1-1
(a) 300 mm GFRP pile,
(b) pile connector,
(c) in side stress variation in 26.5^{0} angle portion,
(d) inner bottom laminates
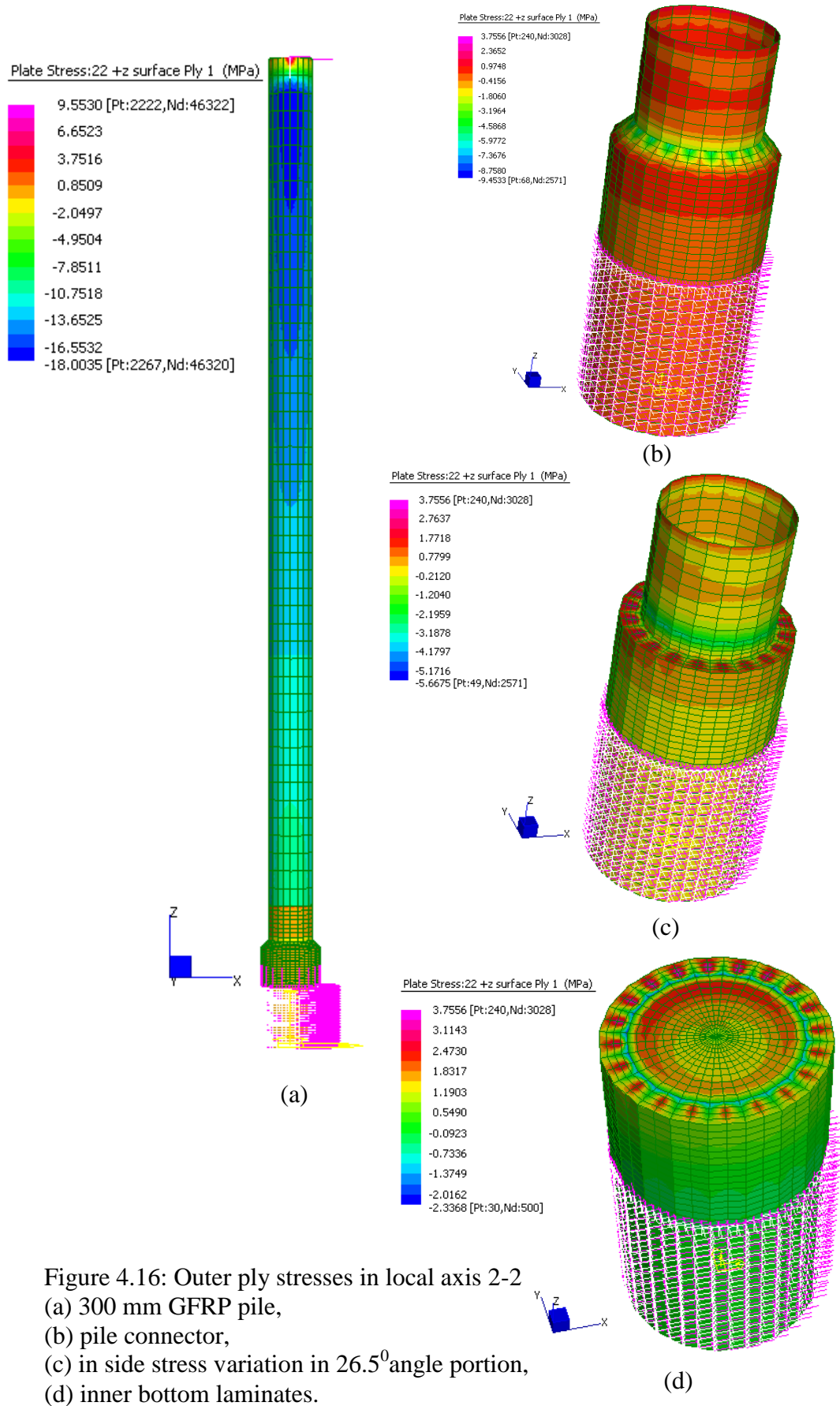
Figure 4.16: Outer ply stresses in local axis 2-2
(a) 300 mm GFRP pile,
(b) pile connector,
(c) in side stress variation in 26.5^0 angle portion,
(d) inner bottom laminates.
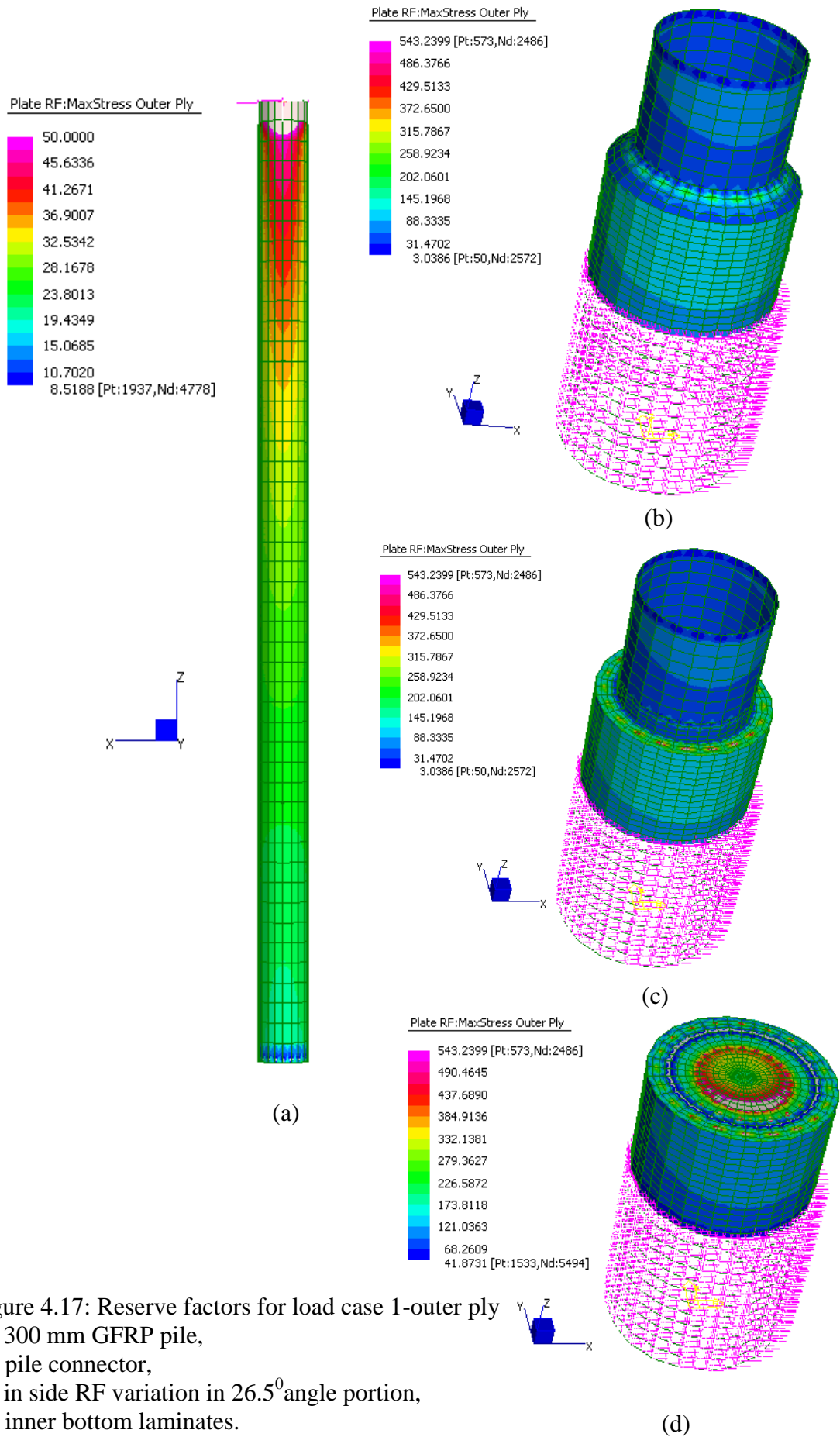
Figure 4.17: Reserve factors for load case 1-outer ply
(a) 300 mm GFRP pile,
(b) pile connector,
(c) in side RF variation in 26.5^0 angle portion,
(d) inner bottom laminates.
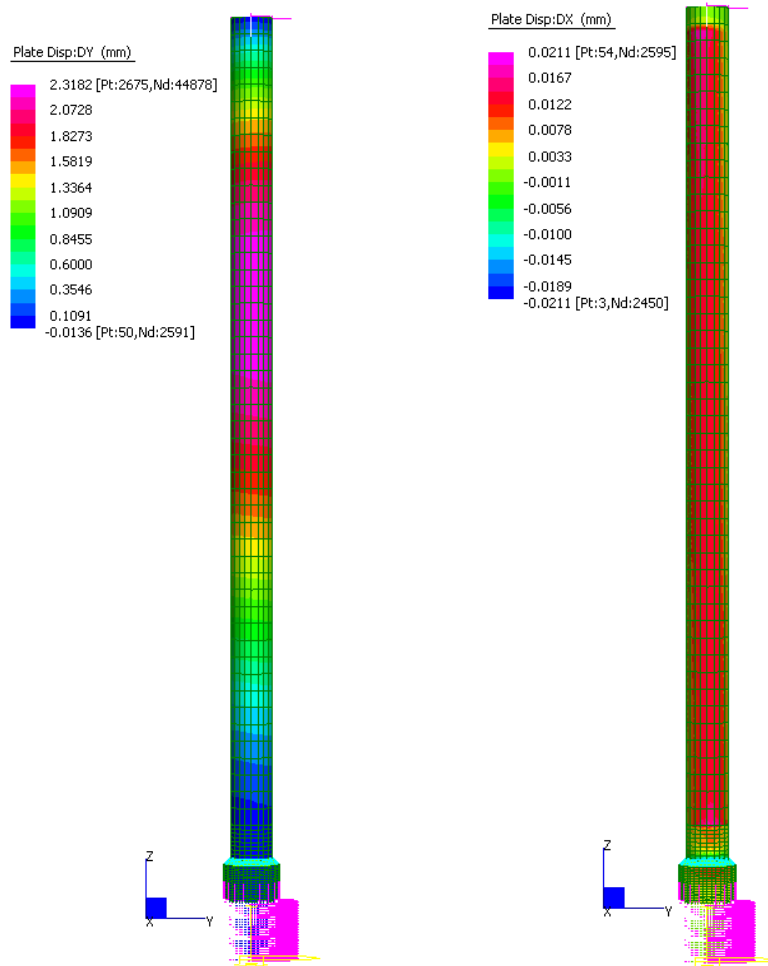
Figure 4.18: Deflection for load case 1

According to Figure 4.15, outer ply stress variations along circumference direction were between 7.0937 (tension) and -23.8064 (compression) both GFRP connector and pile. From Figure 4.16, outer ply stress variations along axial direction were between 9.553 (tension) and -18.003 (compression) for GFRP pile, and 3.755 (tension) and -9.453 (compression) for GFRP adaptor. Therefore for the load case one, outer ply stress variation within allowable limits compared to coupon lamina failure stresses under compression and tension (Chapter 3, Table 3.3). From Figure 4.17, outer most ply reserve factors were greater than 8.5 for GFRP pile and 3.03 for GFRP connector. For the GFRP pile model, maximum reserve factor was limited to 50 to get good contour variation. This implies that no potential lamina failure occurs in this outer most layer of pile and connector. Inner most ply reserve factors were checked in the same manner and the reserve factor was greater than 2.45 for both GFRP pile and connector. Therefore the pile and connector are safe against the load case 1 (Equation 4.1). To take the maximum deflection, 50 mm eccentricity was placed to vertical loads (DL and IL). As a result, the maximum deflection was less than 3 mm along y-y direction, where 50 mm eccentricity was placed.
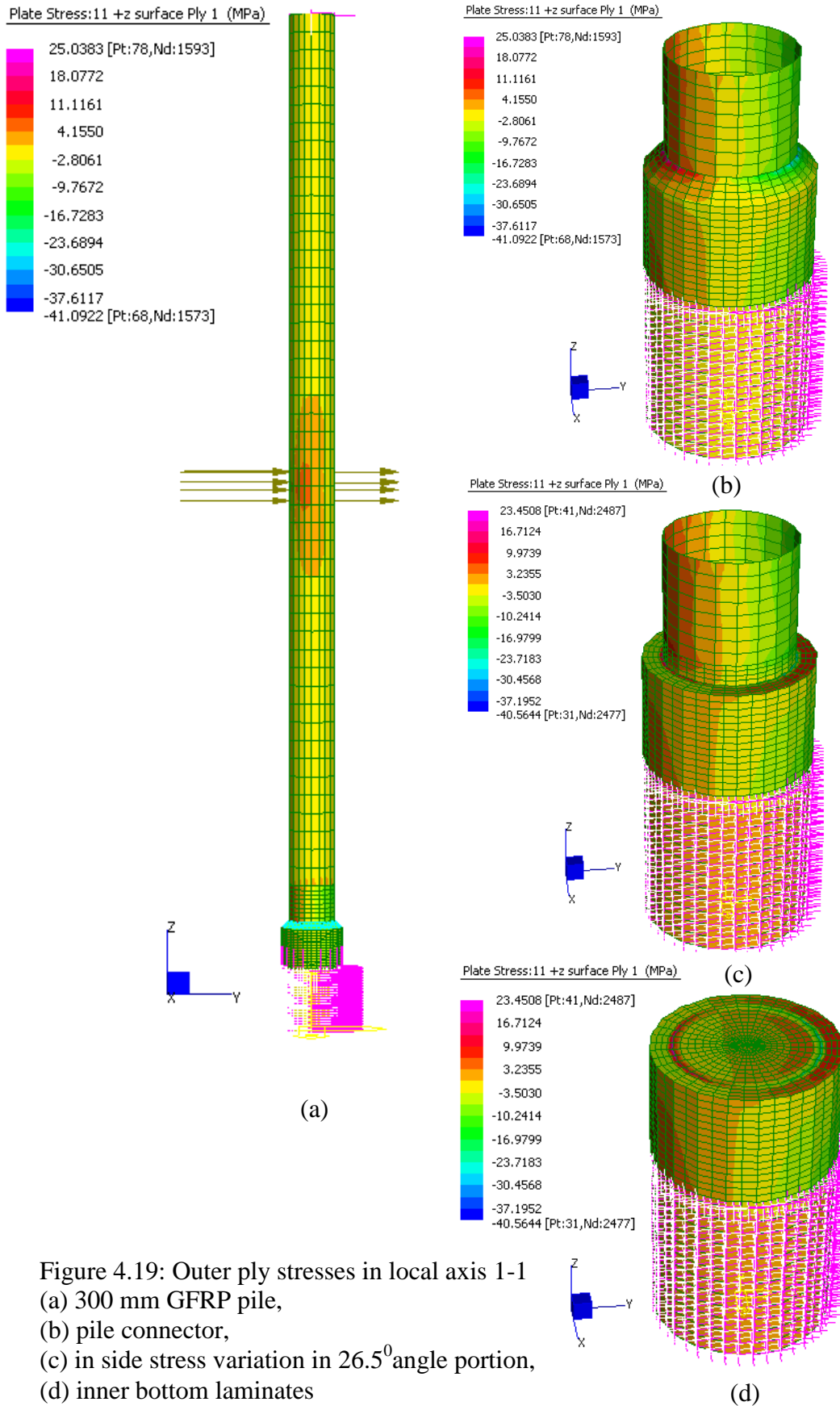
Figure 4.19: Outer ply stresses in local axis 1-1
(a) 300 mm GFRP pile,
(b) pile connector,
(c) in side stress variation in 26.5^{0}angle portion,
(d) inner bottom laminates
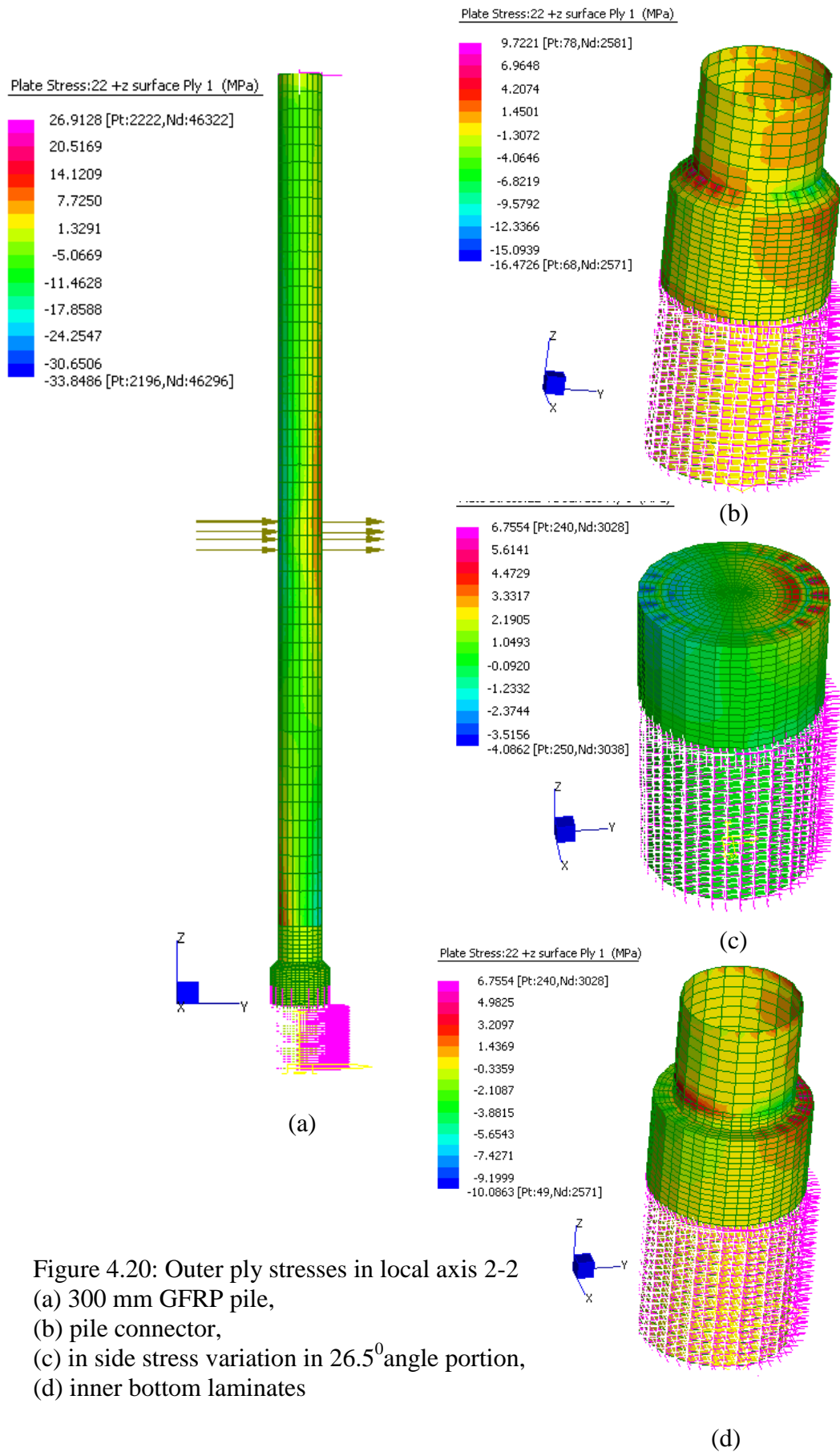
Figure 4.20: Outer ply stresses in local axis 2-2
(a) 300 mm GFRP pile,
(b) pile connector,
(c) in side stress variation in 26.5^0 angle portion,
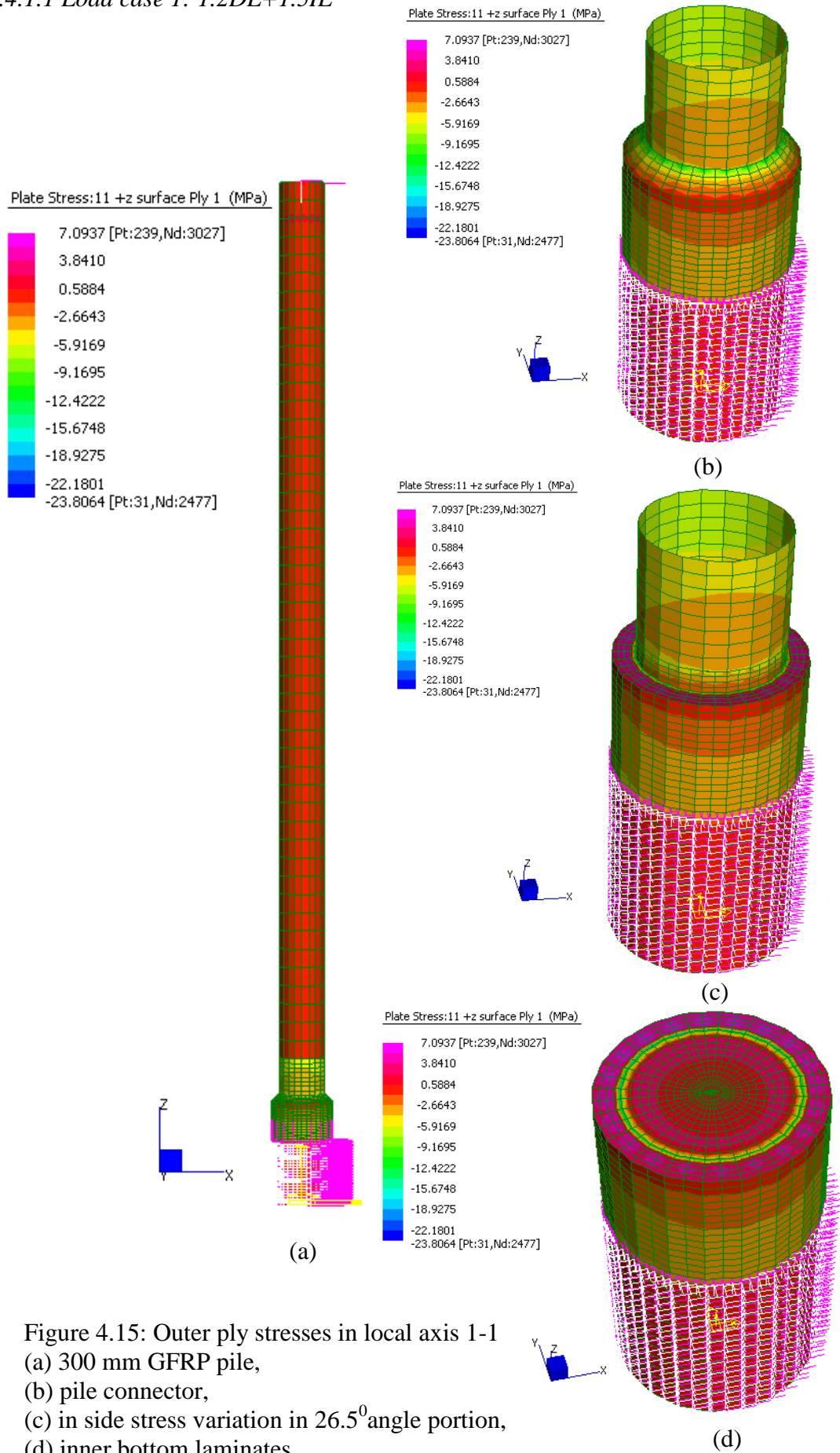(d) inner bottom laminates
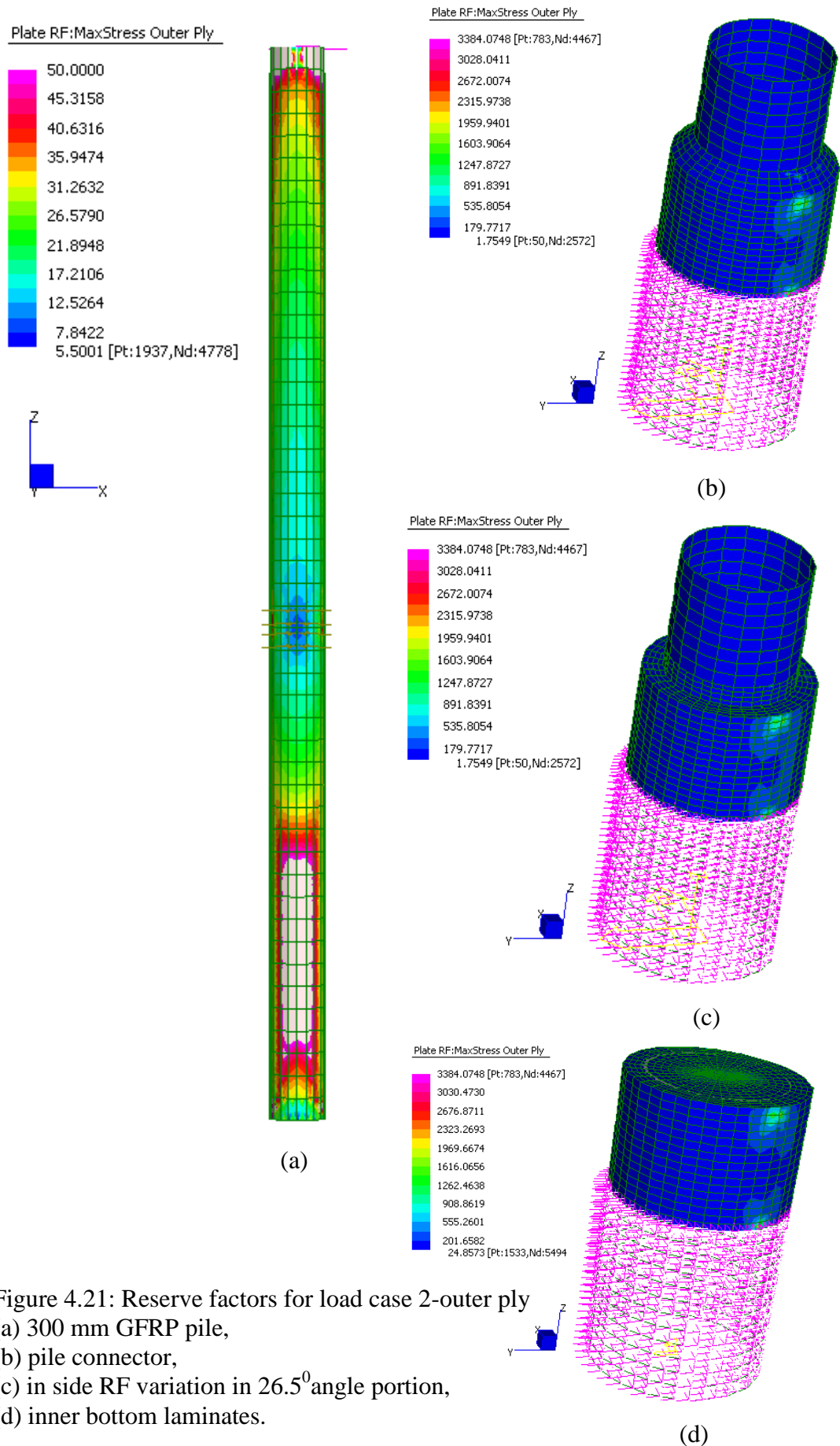
Figure 4.21: Reserve factors for load case 2-outer ply
(a) 300 mm GFRP pile,
(b) pile connector,
(c) in side RF variation in 26.5^0 angle portion,
(d) inner bottom laminates.
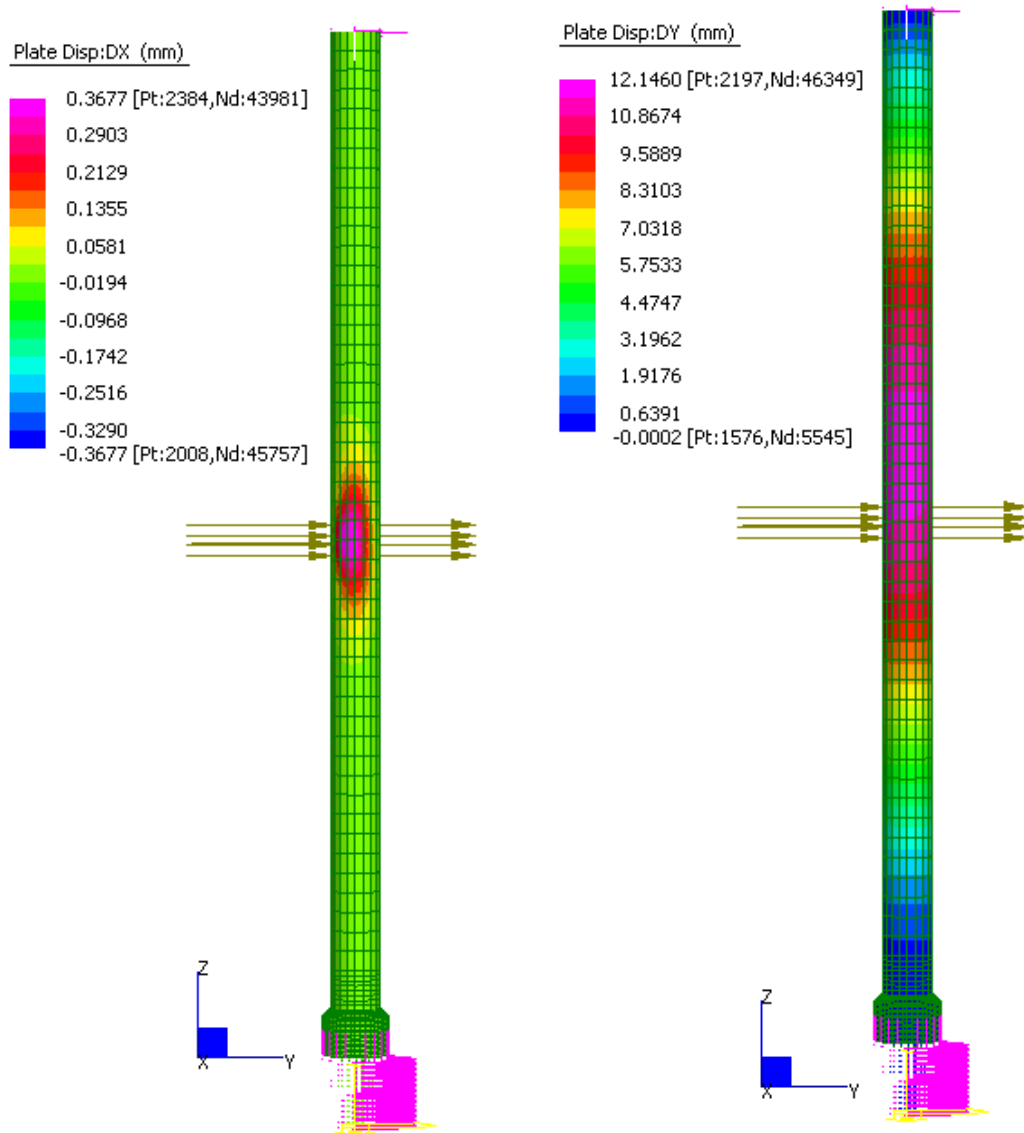
Figure 4. 22: Deflection for load case 2

According to the Figure 4.19 and 4.20 results, outer ply stress variation along circumference e and axial directions were within allowable limits compared to Chapter 3, Table 3.3. From Figure 4.21, RF was greater than 5.5 for GFRP pile and 1.75 for GFRP connector. This implies that no potential lamina failure occurs in this outer-most layer. Therefore pile and connector are safe against load case 2 (Equation 4.2). To take maximum deflection, 50 mm eccentricity was placed to vertical load (DL and IL), as additional moment to WL direction. In addition, maximum deflection was less than 13 mm along y-y direction, where 50 mm eccentricity was placed.

By considering the above analysis, worst load case was 1.2DL+0.4IL +1.65WL. The lower margin safety factor of pile and connector were

5.5, 1.75 respectively. Also, deflection appears not to be critical and for both load cases it is less than 13 mm. The maximum allowable displacement of the pile at the top is limited to 25 mm due to the support from other existing piles. Therefore against the above mentioned loadings, this GFRP pile and the connector behave in the safest possible way.

In this FE analysis, connection between the GFRP connector to existing intact timber stump, and the GFRP pile to head stock or deck platform is not considered. Only overall behaviour of the pile, followed by the connecter was investigated. Unlike steel, GFRP behaviour in connection is unpredictable, and further research is needed. It should be noted that this section deals with FE modelling of a hollow pile section and connector. In case a higher capacity is required, or buckling needs to be prevented, the capacity and stiffness could be improved by filling such piles with appropriate filler material. While this would increase the capacity of the pile, the bond between the composite skins and long-term durability issues of the filler material on the fibre composites skins needs to be considered. In the next section, behaviour of GFRP pile filled with polymer base filler material against a two lane timber bridge loading will be investigated.

4.4.2 Behaviour of 470 mm external diameter GFRP pile FE model (completely filled with polymer based filler material) against actual two lane timber bridge loadings

In this FE model, checks regarding the suitability and performance of 470 mm external diameter GFRP pile under a rural area timber bridge loadings (class 4 road classification) according to AS 5100.1-2004. Therefore calculating loads, a typical two lane timber bridge was used and attached in Appendix 2. According to AS 5100.1-2004, A160 axial load class was considered for traffic loadings. Also calculating debris load, it was assumed that a 10 m x 1.2 m debris mat and flood level sitting just above the middle of the pile would receive the worst bending affect.

Most two lane timber bridges in Queensland Australia, clear pile height (from ground to head stock), ranging from 2.5 m to 7.5 m (Timber bridges maintenance manual, February 2005). Therefore in this FE simulation, 7.5 m height GFRP pile was selected as a replacement section. Table 4.7 shows, all the loadings and safety factors were taken into the FE model as per AS 5100.1-2004.

Table 4.7: Loadings per pile and appropriate safety factors from AS5100.1-2004

Load category	Value (kN)	Ultimate Safety factor (AS5100.1-2004)
Dead Load (DL)	120	1.2
Traffic Load (TL)	160	1.8
Debris Load (DEB L)	80	1.65

Two load cases were considered.

Load Case 1:

1.2DL+1.8TL --- (4.4)

(Vertical force with 0.050 m offset)

Load Case 2:

1.2DL+1.8TL +1.65DEB L --- (4.5)

(Vertical force with 0.050 m offset and debris load acting on mid height of the pile)

Figure 4.23 shows line diagram of the pile model. To take maximum deflection, 50 mm eccentricity was placed to TL and DL as additional moment. For this analysis, the pile connector was not considered, and fixed support was applied on the base and pin condition (axial displacement allowed) applied on the top of the pile. It was considered that the top of the pile is connected to the deck via the pile cap of the bridge, where the displacement is negligible due to the deck, which is supported by many other piles. Therefore, top of the pile was considered as pin connection. To cater for higher loadings (Two Lane timber bridge loading as per Table 4.7), compared to the Shorncliffe pier, it was assumed that the GFRP pile filled with appropriate filler material (will discuss with Chapter 5) would increase stiffness and reduce deflection due to lateral loadings. It was assumed that a perfect bond was formed in between GFRP pile and filler material. In practical it is unfair to consider perfect bond. In case of imperfect bond, bearing capacity of the pile will reduce and some local buckling failure can be happen in GFRP skin.

Based on shrinkage, workability, and pumping ability requirements, Methacrylates polymer concrete was selected as a trial for FE modelling, and material properties were shown in Table 4.8, which extracted from Chapter 2, Table 2.1.

The potential composite laminate failure was calculated and measured in this model by Reserve Factor (Safety Factor). The direction of the local axis in the FE model is given in Figure 4.24.

Table 4.8: Strength properties in Methacrylates polymer concrete (Source: CBD-242, ACI 548.5R-94)

Filler properties	Methacrylates polymer concrete
Average compressive strength	40 MPa
Average modulus of elasticity	5000 MPa
Average tensile strength	10.5 MPa
Average Poisson's Ratio	0.275
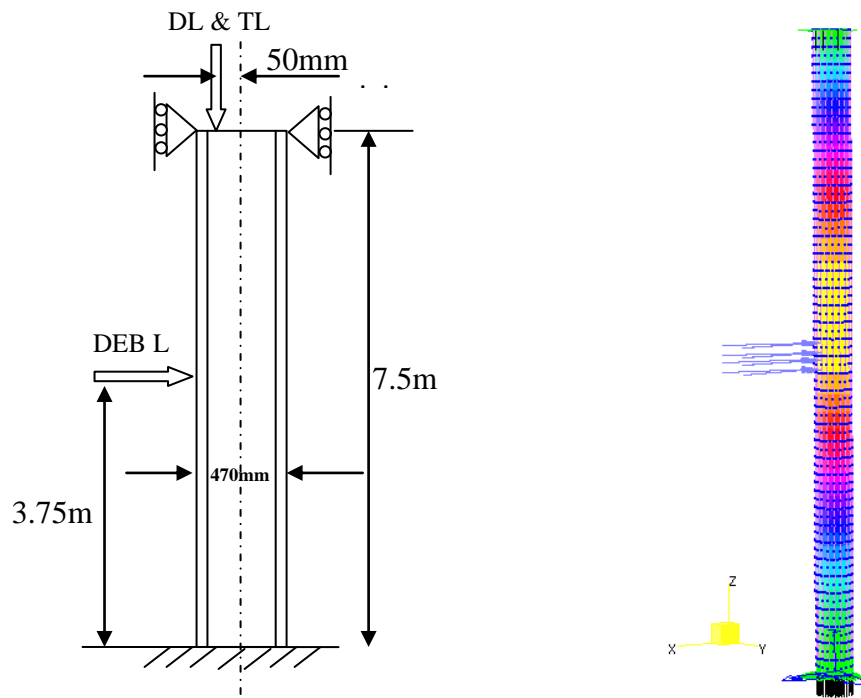
Figure 4.23: Composite bridge pile model
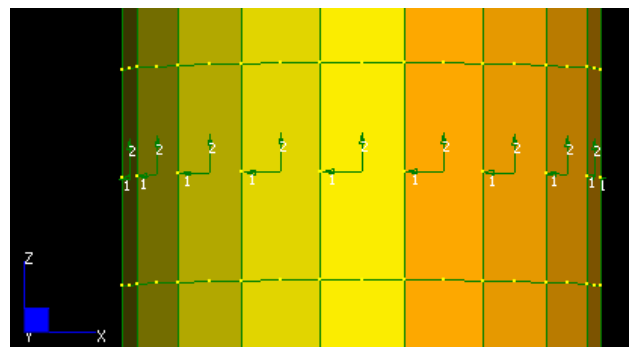
1-1: GFRP pile circumference direction, 2-2: GFRP pile axial direction
Figure 4.24: Local axis system for the 470 mm external diameter pile

4.4.2.1 Load case 1: 1.2DL+1.8TL
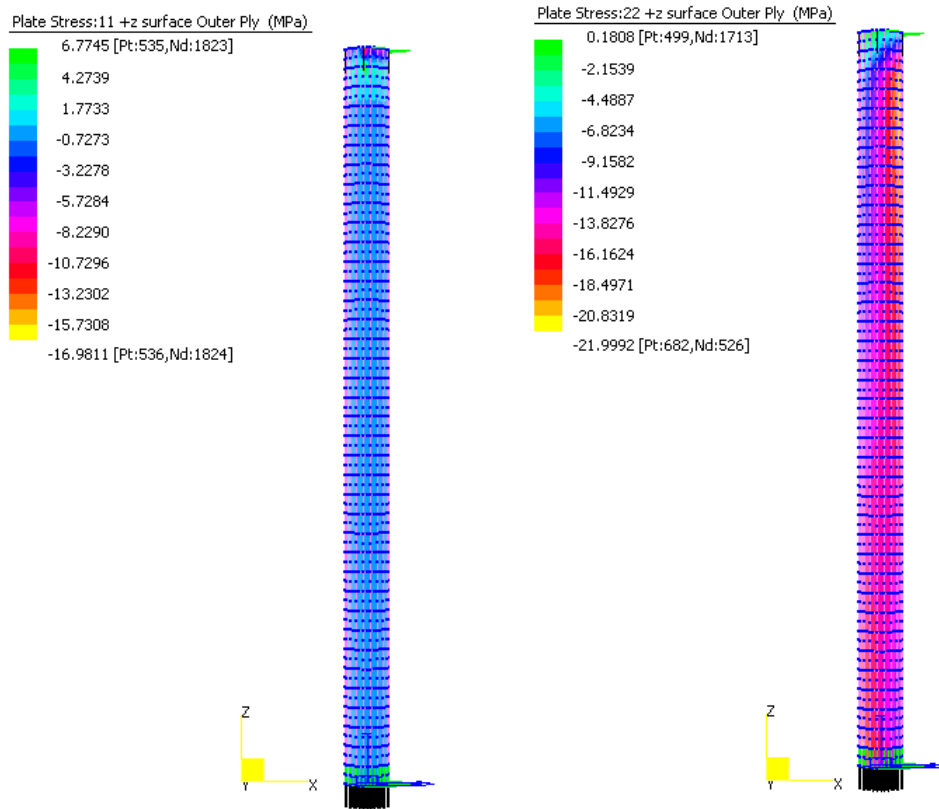
Figure 4.25: Outer ply stresses in local axis 1-1 and 2-2 directions
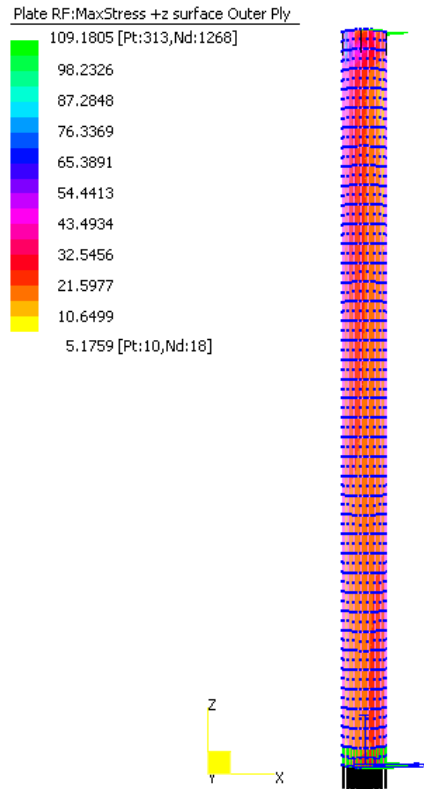
Figure 4.26: Reserve factors for load case 1- Outer Ply

In load case 1, outer ply stress variations in direction 1-1 and 2-2 is shown in Figure 4.25. According to Figure 4.26 minimum safety factor (RF) in outer ply is around 5 and no failure occurred.
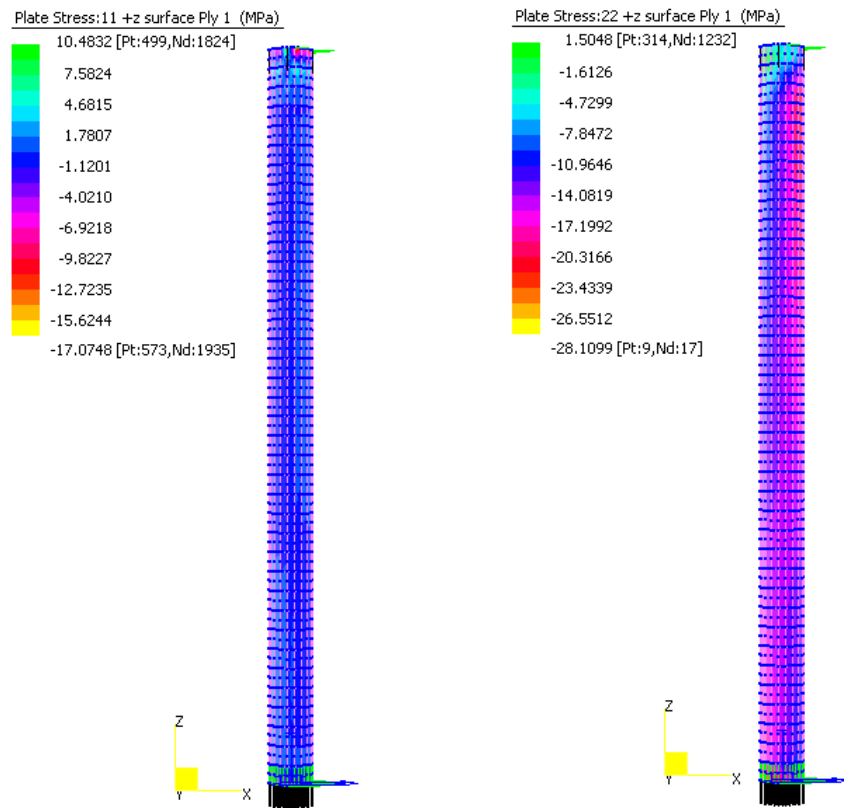
Figure 4.27: Inner most ply stresses in local axis 1 and 2 directions
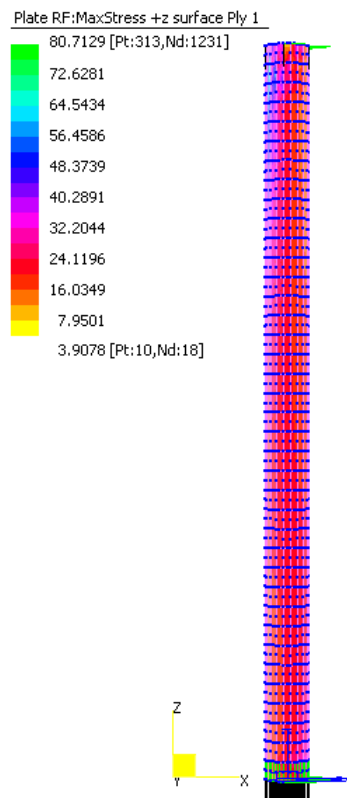
Figure 4.28: Reserve Factors for load case 1- innermost ply

Innermost ply (ply 1) stress variations in direction 1-1 and 2-2 are shown in Figure 4.27. Reserve factors for the innermost ply are given in Figure 4.28 and the minimum safety factor is over 3. This implies no potential lamina failure occurs in this inner most layer. Therefore, all other layers should be safe against load case 1. In addition, according to Figure 4.29, maximum deflection was less than 5 mm along x direction, where 50 mm eccentricity was placed.
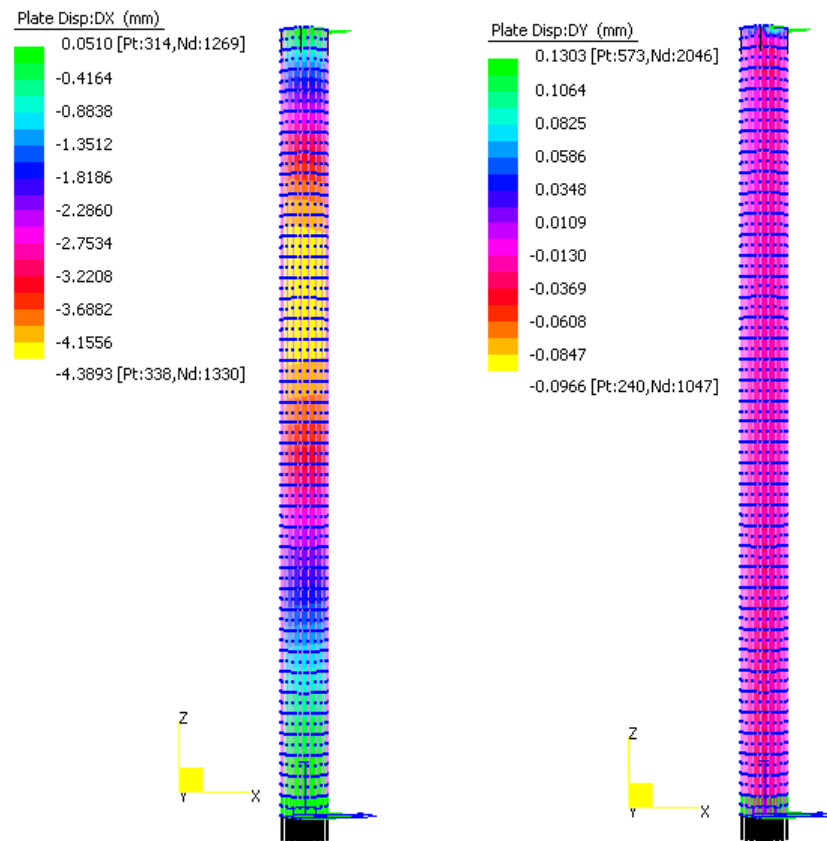
Figure 4.29: Deflection for load case 1

Figure 4.30 shows stress strain behaviour in the filler material along longitudinal section X-X for the load case 1 (Equation 4.4). In Z-Z direction along the longitudinal section, filler material was under pure compression. Just below the loading point local compression failure is visible in the axial direction because, in the FE model, all the DL and TL were applied to the individual node, which is 50 mm away from the pile centre to make eccentricity loadings. But, in a real situation, these dead and traffic loads are not acting as a point load, and should transfer to the pile through the pile cap as distributed load with appropriate eccentricity. From Figure 4.3, brick compressive stresses along Z-Z direction for load case 1 (Equation 4.4) are in between -10.55 and 10.63 MPa. Corresponding strains are within the reasonable

limits of between -0.0023 and 0.0045, except local strain failure, below the loading point. Any materials which have f'$_c$ greater than 10.55 MPa can be used as filler. However, it should also have at least 10.63 MPa tensile capacity to satisfy load case 1. Alternatively strain wise, this filler material must have 0.0045 for tension and 0.0023 for compression. It should be obvious that we cannot use concrete as filler because concrete is inherently weak in tension and having around 0.003 strain at tensile failure. Therefore, there is a need to develop a new filler material to cater for above loadings and corresponding strains.
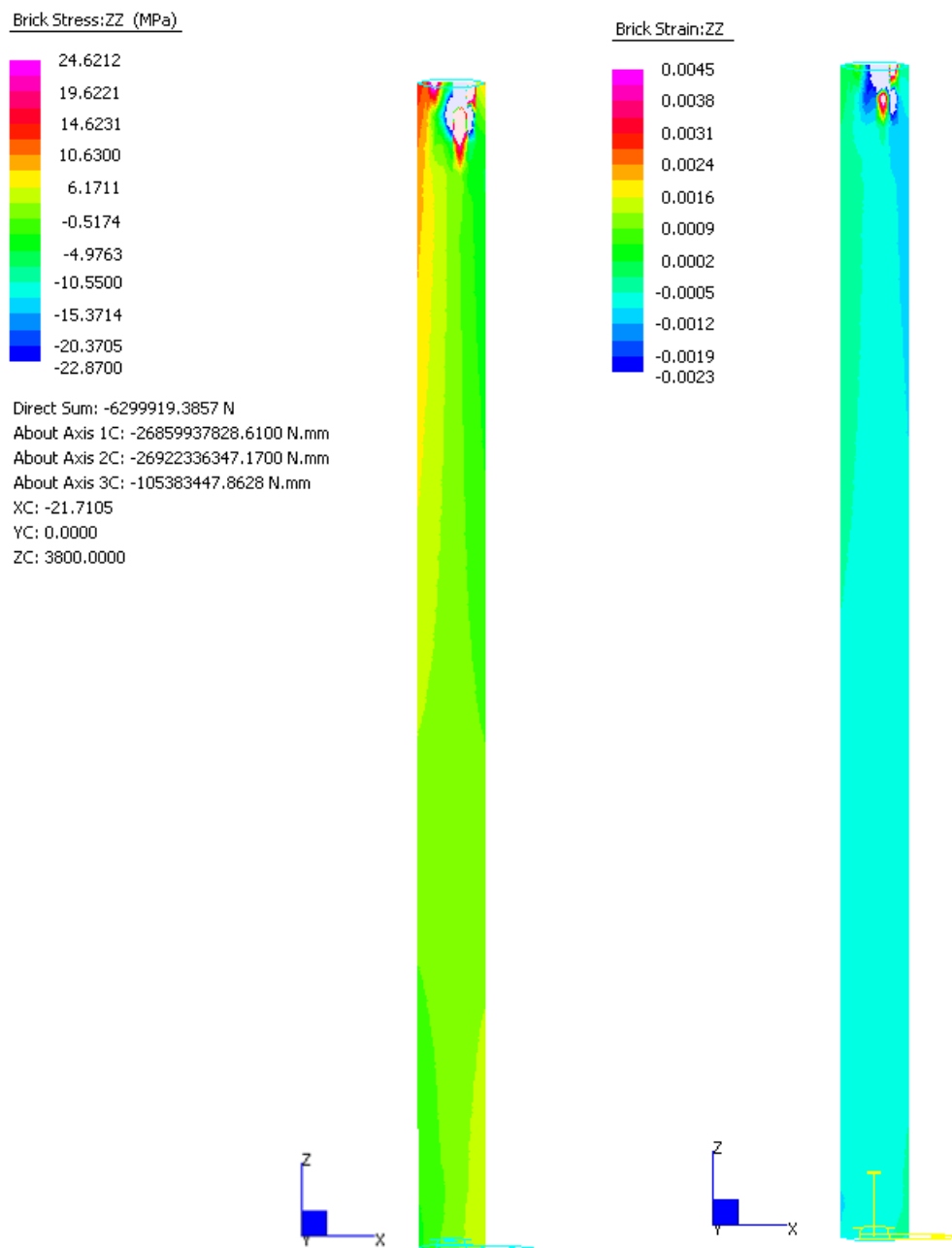
Figure 4.30: Stress and strain variation in filler material along longitudinal section X-X for load case 1

4.4.2.2 Load case 2: 1.2DL+1.8TL +1.65DEB L
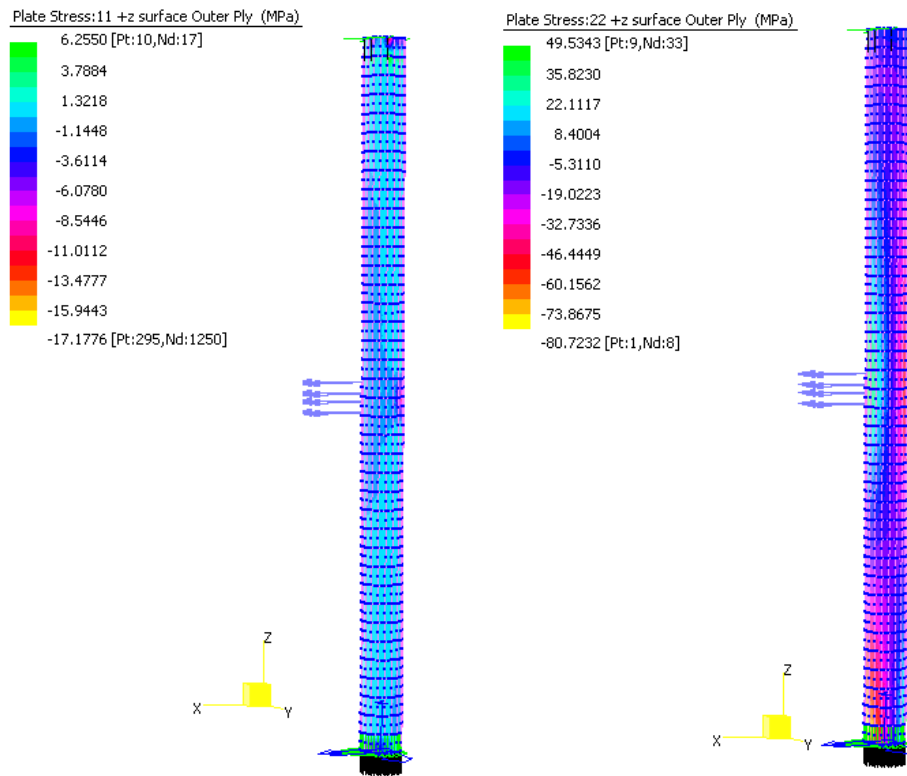
Figure 4.31: Outer ply stresses in local axis 1 and 2 directions
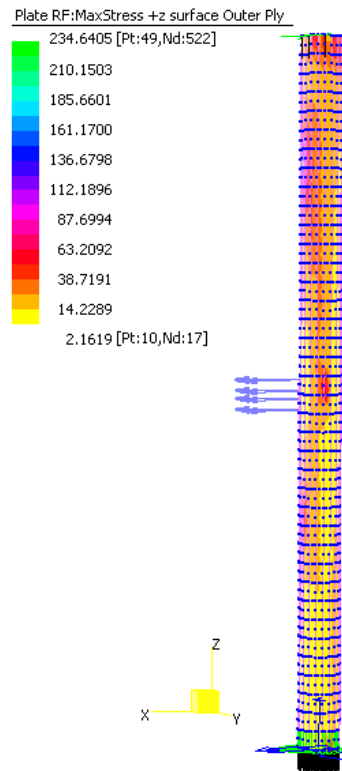
Figure 4.32: Reserve factors load case 2- outer ply

Figure 4.31 shows in load case 2, outer ply stresses in direction 1-1 and 2-2. Reserve factors for the outer ply are given in Figure 4.32 and minimum safety factor is over 2.
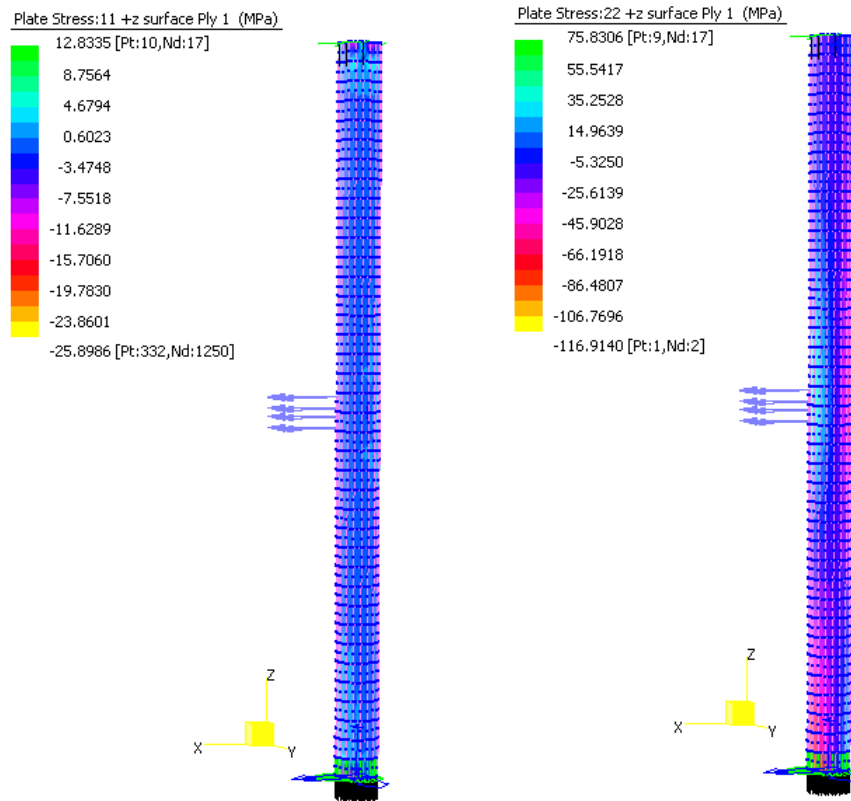
Figure 4.33: Inner ply (ply 1) stresses in local axis 1 and 2 directions
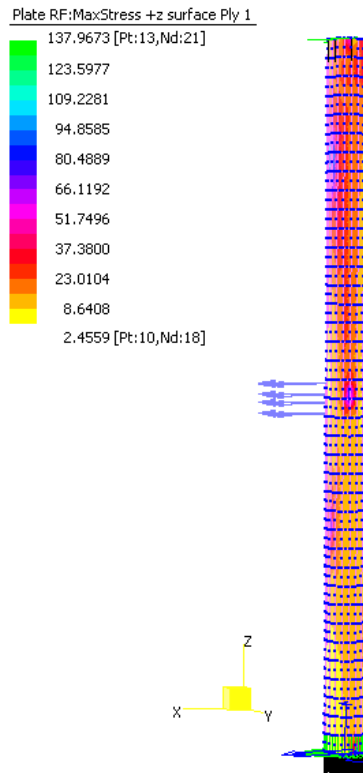
Figure 4.34: Reserve factors load case 2- Inner ply

Figure 4.33 shows inner ply stresses in 1-1 and 2-2 directions for load case 2. Reserve Factors for the inner ply given in Figure 4.44 and minimum safety factor is over 2. Maximum deflections are less than 43 mm in both X and Y direction.
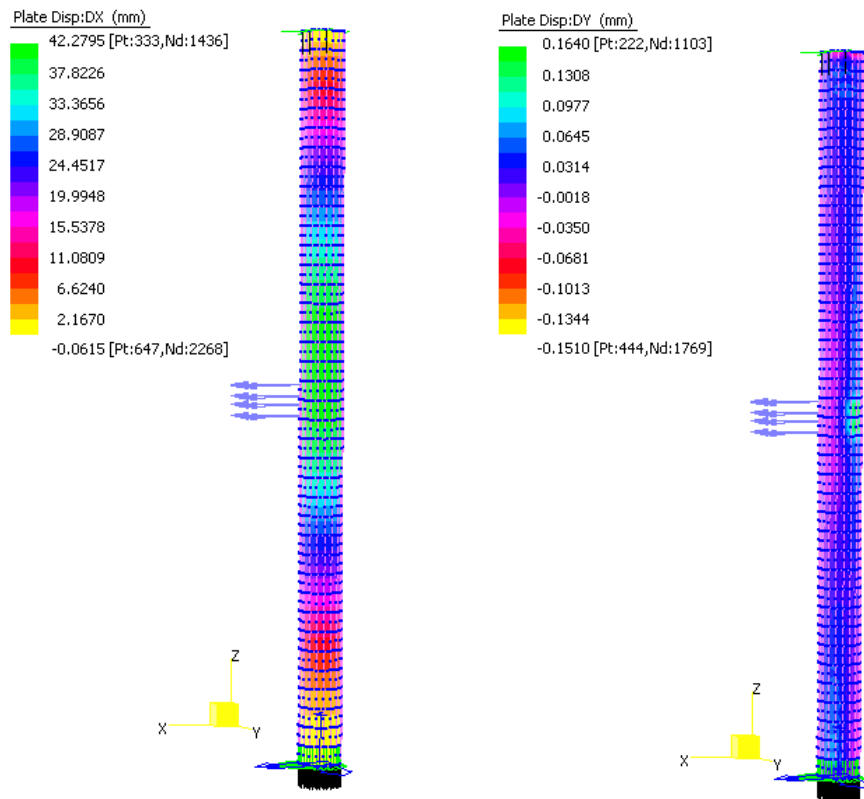
Figure 4.35: Deflection for Load case 2
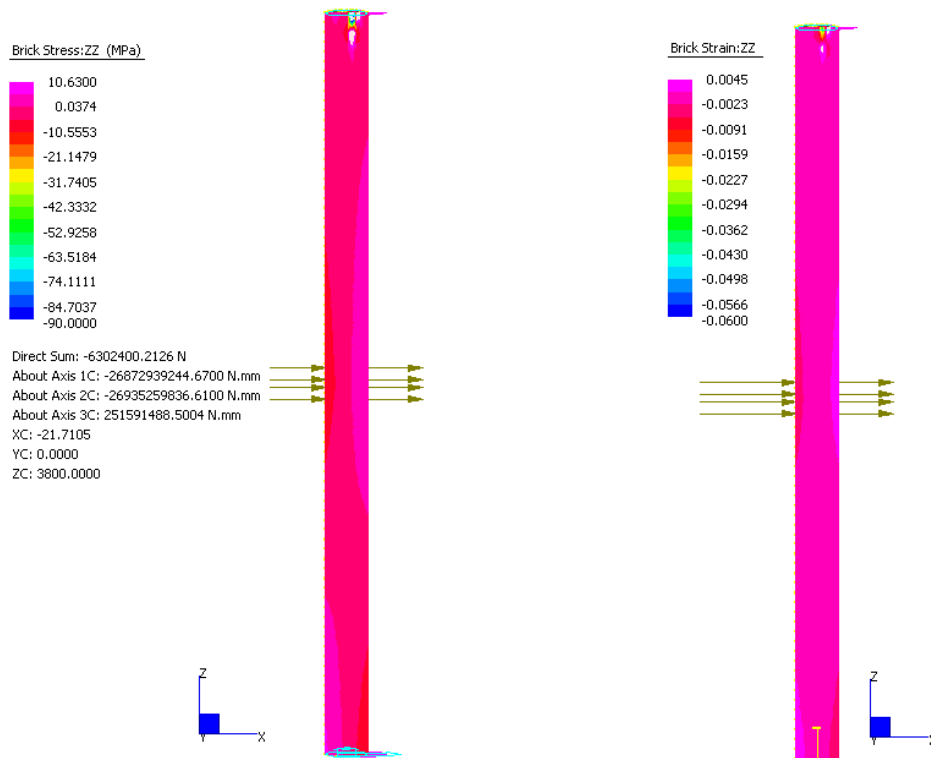
Figure 4.36: Stress and strain variation in filler material along longitudinal section X-X for load case 2

Figure 4.36 shows stress strain behaviour in filler material along longitudinal section for the load case 2. In Z-Z along the longitudinal section, filler material was under the combination of compression and tension, and denoted by the colour difference.

Z-Z direction stresses vary from 10.55 MPa (compression) to 10.63 MPa (tension). Corresponding strains change from 0.0023 (compression) to 0.0045 (tension). Here also, just below the loading point, local compression failure is visible because, in the FE model all the DL and TL were applied to the individual node, which is 50 mm away from the pile centre. For the load case 2 also, concrete cannot be used in tension regions, and it is therefore required to develop new filler material.

By considering the above analysis, the worst load case was 1.2DL+1.8TL +1.65DEB L. The lower margin safety factor of this pile was 2. Also, deflection appears not to be critical, and for both load cases it is less than 43 mm. Therefore, against the above mentioned loadings, this pile behaves in the safest possible way if the appropriate filler material is used. It is also recommended that this pile is suitable for remote areas only, which are receiving 2, A160 axial load vehicular traffic. Further development and analysis is required for GFRP piles, which are placed on a bridge having M1600 and S1600 vehicular traffic loads.

4.4.3 Buckling analysis for 9.2 m long 470 mm external diameter full scale pile

Two analyses were done using a theoretical approach and FEA simulations.

4.4.3.1 Theoretical analysis

The critical buckling load (elastic stability limit) is given by Euler's formula

$$F = \frac{\pi^2 EI}{(KL)^2}$$ ------------------------------------- (4.5)

Where,

F = maximum or critical force (vertical load on column),

E = modulus of elasticity,

I = Second moment of inertia,

L = unsupported length of column,

K = column effective length factor, whose value depends on the conditions of end support of the column, as follows.

For both ends pinned (hinged, free to rotate), K = 1.0.

For both ends fixed, K = 0.50.

For one end fixed and the other end pinned, K = 0.699....

For one end fixed and the other end free to move laterally, K = 2.0.

KL is the effective length of the column.
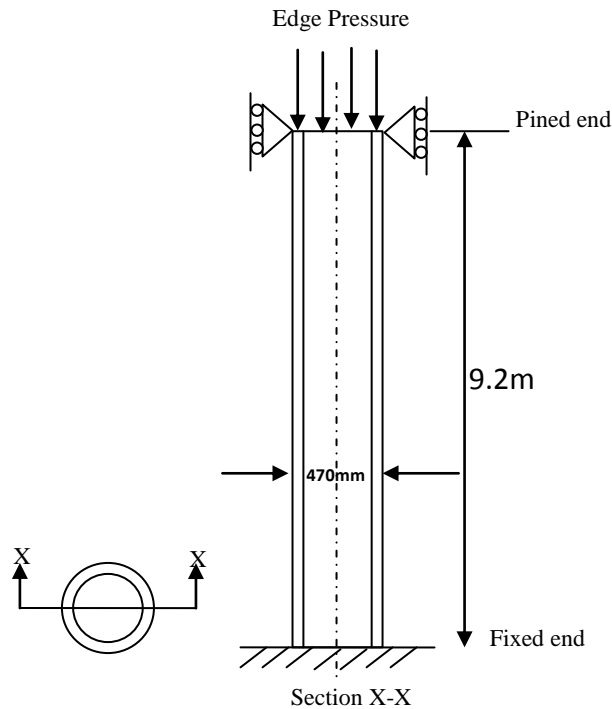
Figure 4.37: Bridge pile model

Therefore for this 9.2m pile,

EI = 1.093×10^{13} Nmm^2

K=0.7

L=9200 mm

F= $\pi^2 * 1.09 * 10^{13} / (0.7*9200)^2$ = **2594.64 kN**

4.4.3.2 Using FEA Simulation

Applied plate edge pressure @ top = 48.44MPa (Correspond to 1500 kN axial load)

Equivalent force $= 48.44 * 2 * \pi * 224 * 22 = 1500$ kN

From linear buckling analysing using STRAND7, 3 major buckling modes were identified.

```
FINAL BUCKLING RESULTS
CALCULATED BUCKLING LOAD FACTORS
   1      1.68157759E+00
```

```
2      1.68190244E+00
3      2.26713176E+00
```

From these three modes, mode 1 occurred early and giving the anticipated failure
load   = 1500.00*1.6815

     = 2522.15 kN

Therefore, comparing 4.5.1 and 4.5.2, the pure buckling capacity of the pile is
approximately **2500 kN**.

(a)   (b)   (c)
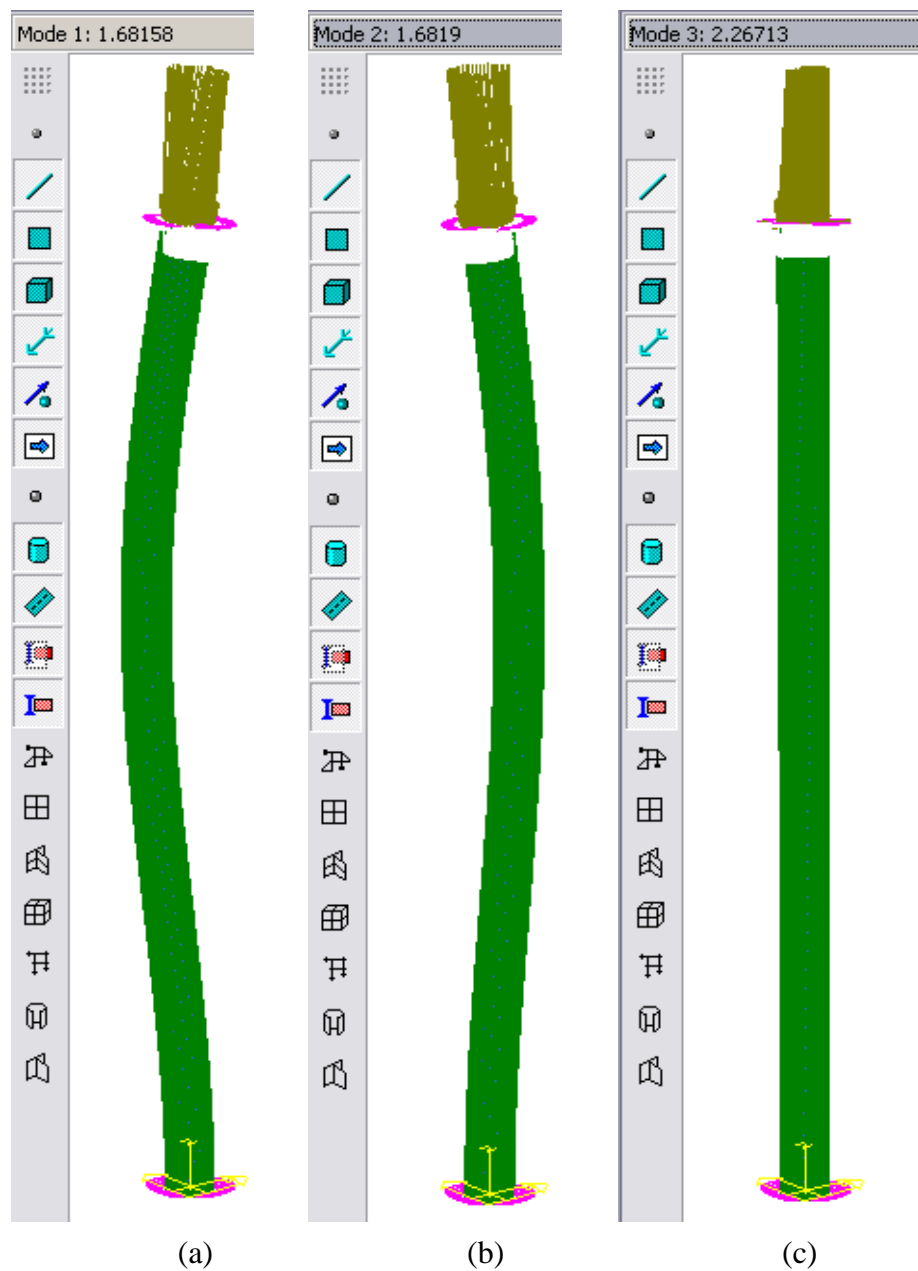
Figure 4.38: Buckling modes correspond to load factor (a) 1.6815, (b) 1.6819 and
(c) 2.267

4.5   Finite element modelling for the filler (Phase III)

For the understanding of the stress strain behaviour of the new polymer filler in pile connector, STRAND 7 modelling was done. To obtain the maximum effect on the filler inside connector, rural area timber bridge loadings under class 4 classification in AS 5100.7-2004 were considered. All loads and ultimate load factors were according to the Table 4.7. For simplicity, a 7.5 m height 350 mm external diameter timber pile was introduced to the top part of the connector as a replacement pile to withstand the two-lane timber bridge loadings.
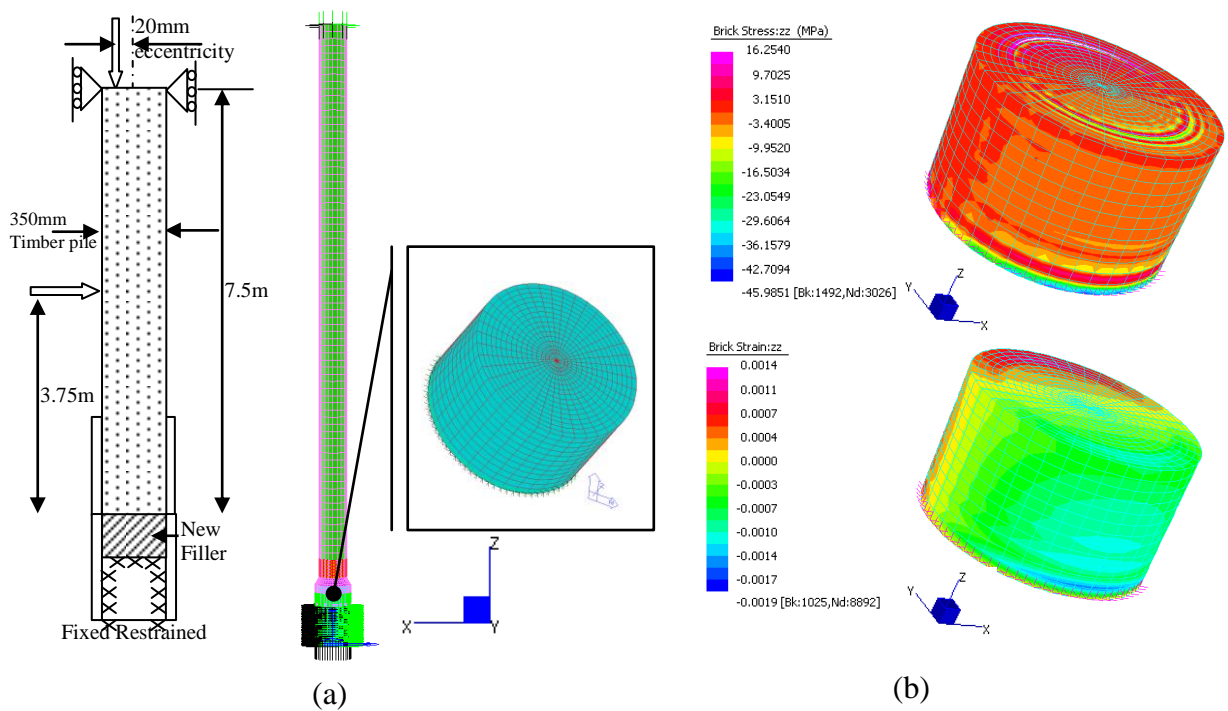
Figure 4.39: (a) schematic diagram and FE model in STRAND 7, (b) Stress strain behavior of the filler in zz direction under critical load combination 2

For all vertical loading 20 mm eccentricity was introduced as additional moment to take maximum stress strain behaviour in the filler (Figure 4.39 (a)). Load combinations per the AS 5100.2-2004 following ultimate load combinations were considered.

Load combination 1

1.2DL+1.8 TL--- (4.6)

Load combination 2

1.2DL + 1.8TL+ 1.65 DEB L--- (4.7)

Load combination 3

1.2DL + 1.65DEB L--- (4.8)

For the FE modelling, it was assumed that the bottom of the pile connector behaves as fixed and restrained, and the top of the timber pile as pinned support with rollers. 20-node hexahedral brick elements were used to create the filler portion in FE modelling.

The laminate layup for the connector is

1.8 layers 600 / 225 g/m2 Biax / CSM glass (inner top)

2.8 layers 600 / 225 g/m2 Biax / CSM glass (inner bottom)

3.12 layers 600 / 225 g/m2 Biax / CSM glass (outer)

Biax fibres were aligned at 0 degrees to the cylinder axis.

After analysing all three combinations, Load combination 2 was identified as critical. Table 4.9 shows stress and strain variation in brick elements in load combination 2. This connector and pile model acted as a combination of the three point bending test, with end moment and axial force. Therefore, according to Figure 4.39 (b) one side of the filler undergoes maximum compression due to the components of pure compression and flexural. Result outputs came from STRAND7 is shown in Table 4.9.

Table 4.9: Brick stress in the filler after analysing FE model (load case 2)

	Brick Stress (MPa)			Corresponding Brick Strain		
	zz*	xx*	yy*	zz*	xx*	yy*
Maximum compression	45.9851	45.9832	45.9853	0.0019	0.0005	0.0014
Maximum Tension	16.2540	16.2518	16.2523	0.0014	0.0004	0.0011

*- zz, xx & yy – local coordinate system

Regarding Table 4.9, strains were in three local axes less than 0.01 for both compression and tension. Hence, based on this trial loading configuration, any suitable polyester filler material having more than 46 MPa compressive strength, and 0.002 failure strain can be recommended as filler for the connector. Also other properties such as low cost, less shrinkage, gel time, pumping ability, and workability, need to be considered.

4.6   Conclusions

Numerical simulations were performed using the finite element analysis approach to verify experiments and study behaviour of overall pile rehabilitation systems, followed by the connector. Generally most of the calculated mechanical property values from the finite element models are approximately the same order as the experimental investigation values. The use of FE method, thus, proved to be effective in determining the overall compressive modulus and flexural modulus of the GFRP composite piles under serviceability loadings. From FEA, it was found that glass-reinforced lamina bears 96% of the applied load while 4% was carried by Soric XF-reinforced lamina for particular lamina arrangement introduced to the GFRP pile. Lateral strain of the plies remains the same across the thickness, irrespective of the loading magnitude, while strain variations of the plies on the axial direction were developed and more pronounced at the maximum applied load.

Overall performance of the pile rehabilitation system was evaluated by considering two FE models, which represented two types of load scenarios. First scenario: behaviour of 300 mm external diameter 7.5 m long pile, followed by the connector against the Shorncliffe pier loadings was evaluated. Here 1.2DL+0.4IL +1.65WL load case was identified as worst and lower margin safety factor of combine pile, and connector were around 5.5, 1.75 respectively. Therefore, against the Shorncliffe pier loadings given by the Brisbane City Council, this GFRP pile and the connector behave in the safest possible way. Second scenario: behaviour of 470 mm external diameter 7.5 m long pile filled with polyester based filler against rural area bridge loadings was evaluated. Here, 1.2DL+1.8TL +1.65DEB L load case was identified as worst, and the lower margin safety factor of pile was around 2. It was also recommended that this pile be considered as being suitable for only remote areas which only experience 2, A160 axial loads vehicular traffic. Further development and analysis is required for GFRP piles, which are placed on bridges having M1600 and S1600 vehicular traffic loads.

Both finite element simulations against actual Shorncliffe pier loadings and two-lane timber bridge loadings performed well, with reasonable safety factors. Therefore this pile rehabilitation and replacement concept can be applied to Shorncliffe pier, and will be extended to rural two-lane timber bridges. Unlike steel,

GFRP behaviour in connection and joints remains unpredictable and further research will be needed in this area.

FE modelling for polymer based filler was done against to the two-lane timber bridge loadings, per AS 5100 bridge code. From the FEA results any suitable polyester filler material having more than 46 MPa compressive strength and 0.002 failure strain can be recommended as filler for the connector. Therefore considering other factors such as gel time, pumping ability, workability and durability requirements, further development of this polyester based filler material is important and will be duly discussed in Chapter 5

Chapter 5

DEVELOPMENT OF POLYMER BASED FILLER MATERIAL

5.1 Introduction

The objective of this section is the preliminary development of polymer based filler materials for the FRP tubular connectors in timber pile rehabilitation. This research investigates the structural properties of polymer based filler materials with different proportions of resin, sand, and fly ash. This ongoing research aims to rehabilitate a portion of a deteriorated timber pile, by using a glass fibre reinforced polymer (GFRP) pile and GFRP connector. Due to good compressive strength, pump ability, and workability, the new polymer based filler material is applied in between the GFRP connector, and existing timber pile as shown in Figure 5.1. A research program has been initiated to improve the fundamental understanding of this material, and to provide the knowledge required for its broad utilisation.
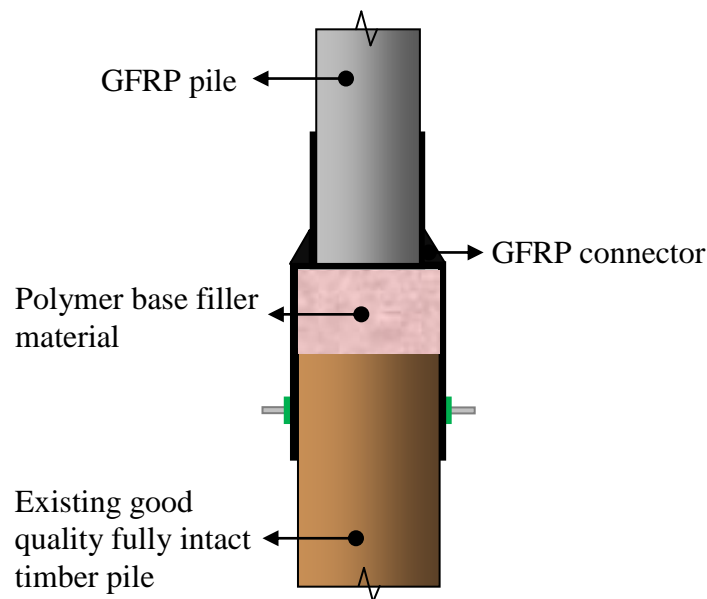
Figure 5.1: Position of the filler material

5.2 Background

In the past decade most research programs were conducted to study the behaviour of concrete, wrapped with GFRP confinement. When FRP systems are used with concrete, whether internal or external reinforcing, the fibres and matrix will be exposed to the high alkaline environment present in the concrete. This environment

is known to attack some glass in FRP composites (Christensen 1996). Katsuki and Uomoto (1995), tested glass, aramid, and carbon FRP exposed to NaOH solution. Circular AFRP, CFRP and GFRP rods with 6 mm in diameter and 40 mm long, were immersed in a solution of NaOH, and then tested until a tensile failure occurred. The GFRP rods were subjected to a solution with half the concentration of NaOH because of poor resistance of glass fibres to alkali. The NaOH solutions were kept at a temperature of 40°C. The rods were tested at 20°C after exposure times of 7–120 days. It was found that the alkali penetrated the GFRP rods radially with time, while the CFRP and AFRP rods had no penetration of alkali. In addition, tensile tests showed that only the GFRP rods lost strength with time after exposure to alkali. The area of the GFRP rods penetrated by alkali failed at a lower load than the areas not penetrated by the solution (Hamilton 2000).

The proposed novel timber pile rehabilitation method GFRP connector will act as a confinement for the filler material. Due to durability considerations, concrete is not a suitable material to be confined by GFRP. Therefore this chapter focuses on developing an innovative polymer based filler material instead of traditional concrete.

5.2.1 Polymer concrete

Polymers are being increasingly used in civil-engineering applications as adhesives, modifiers, and matrix materials in concrete. As structural and repair materials, polymers and their composites must be able to withstand high stresses under extreme service conditions. Polymer Concrete (PC) is a composite material, formed by combining a mineral aggregate, such as sand and gravel, with a polymerising monomer (Vipulanandan 1993).

In most applications, the polyester binder is a general purpose, unsaturated polyester prepolymer formulation. These formulations are available in the form of 60 to 80 percent solutions of the prepolymer in copolymerizable monomers, such as styrene and styrene-methyl methacrylate. During the hardening process, the polyester prepolymer and the monomer react through their unsaturated groups (double bonds). The chemical reaction is called cross-linking, the production process associated with it is referred to as curing, and the resulting polymer binder is a thermosetting polymer.

Polyester PC has good mechanical strength, relatively good adhesion to other materials, and good chemical and freeze-thaw resistance. It has, however large setting and post-setting shrinkage (up to ten times greater than Portland cement concrete, a serious disadvantage in certain applications).

Because of low cost, the most widely used polymer-binders are based on unsaturated polyester polymer. Therefore in this preliminary filler material development, polyester was used as a resin. To reduce setting and post setting shrinkage, sand and fly ash were used as additives. The potential filler material must have good workability, reasonable curing time to allow for workmanship, and fair compressive capacity to transfer superstructure load, plus reasonable pump ability qualities.

5.3 Materials used for polyester based filler development

The following constituent materials were used in the production of the polymer based filler.

5.3.1 Polyester Resin

Medium reactivity, rigid orthophthalic polyester resin was used. Typical properties in liquid and cured states are shown in Table 5.1 and Table 5.2 respectively. Compared with other polyester families, orthophthalic polyester has good chemical resistance and processing ability (Dudgeon, 1987).

Table 5.1: Typical properties in pure neat resin - liquid state at 25°C (Source: FGI brochure - www.fgi.com.au)

Viscosity	
Brookfield LVT sp.2/12 rpm	1500 -1900 cP
Cone and Plate	180 - 230 cP
Density	1.10 gcm^{-3}
Gel Time (1% MEKP Interox NR20)	40 – 45 minutes

Table 5.2: Typical Mechanical properties in pure neat resin - cured state (Source: FGI brochure - www.fgi.com.au)

		Test Method
Density	1.19 gcm^{-3}	ISO/R 1183-1970
Tensile Strength	60 MPa	ISO/R 527-1966
Tensile Elongation	2.0%	ISO/R 527-1966
Flexural Strength	100 MPa	ISO 178-1975
Flexural Modulus	4000 MPa	ISO 178-1975
Volume Shrinkage	7-8%	ISO 3521-1976

5.3.2 Initiator

Methyl ethyl ketone peroxide(MEK) in dimethyl phthalate (DMP) was used as the initiator. Chemical lattice structure and composition are given below.

Peroxide content: 30%

Balance   : 63% DMP, 4% MEK + Water
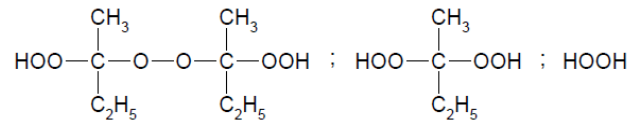
Figure 5.2: Chemical lattice structure of initiator

5.3.3 Fly ash

Unprocessed Concrete grade fly ash with d50 of approximately 15µm was obtained from Wagners in Queensland, Australia. The chemical composition provided by the supplier is provided in Table 5.3.

Table 5.3: Chemical composition of fly ash (by mass%)
(Source: www.wagner.com.au/Divisions/CementandFlyash)

Element	Percentage
SiO_2	51.8
Al_2O_3	24.4
Fe_2O_3	9.62
CaO	4.37
MgO	1.5
Na_2O	0.34
K_2O	1.41
SO_3	0.26
LOI(Loss of Ignition)	---

5.3.4 Sand

Fine dry sand was obtained from Wagners in Queensland, Australia with a bulk density of 1494 kg/m^3 and particle size smaller than 425 µm.

5.4   Experimental program

An experimental program was conducted to characterise the behaviour of polyester based filler material by assessing their behaviour in:

- Compression,
- Flexural,

- Shrinkage, and
- Gel time.

5.4.1 Compression Testing

Compressive load capacity and modulus behaviour were investigated using the un - axial compression method. Testing was done in accordance to ASTM D 695 M-91 standard. Testing was undertaken using cylindrical specimens with a diameter of 50 mm and a height of 100 mm. The load was applied uniformly on the loading surface of the specimen through an AVERY testing machine, with 500kN loading capacity at a constant cross head speed of 1mm/min. The compressive strength was calculated by dividing the load to the cross sectional area of the specimen. Typical compressive failure patterns are shown in figure 5.3.
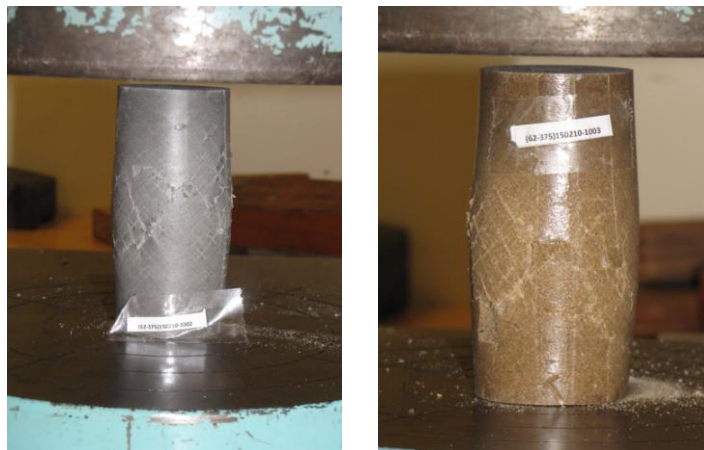
Figure 5.3: Typical compressive failure pattern for test cylinders

5.4.2 Flexural Testing

Flexural behaviour was assessed using a three point bending test performed according to ISO 178:1993. The specimen was simply supported and tested under the 3-point loading, with the span set at approximately 16 times the thickness of the core. The load was applied at midspan of the specimen at a constant rate of 1 mm / min using a 10 kN MTS testing machine. The load and midspan deflection were recorded up to failure to determine the strength and elastic properties of the polyester based filler materials. Specimens dimensions were l = 160 mm, b = 16 mm and h = 9 mm. The support span was set at L= 144 mm (9x16). Test setup arrangement is shown in figure 5.4.

(a)   (b)   (c)
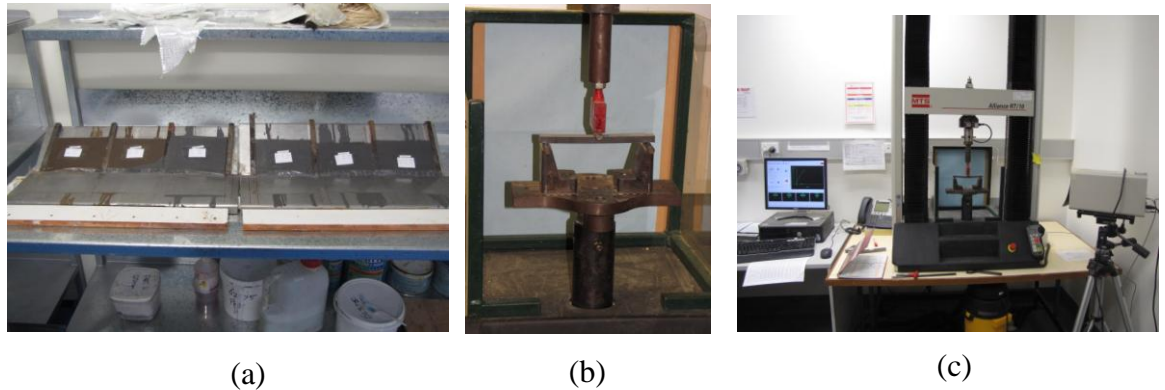
Figure 5.4: Flexural Test: (a) samples preparation, (b) & (c) three point bending testing apparatus

5.4.3 Shrinkage Testing

A linear method was selected to assess the shrinkage, in accordance with the ASTM standard D6289–98. This test method provides for the measurement of shrinkage of thermosetting plastics from their moulds both initially, and after post-cure. A multiple cavity steel mould (figure 5.5) was fabricated with cavities to the dimensions specified for bars of:

    Length = 127 mm,

    Width = 12.7 mm, and

    Depth = 12.7 mm.

    The pre-calculated masses of resin and filler for each volume fraction were combined manually and blended to ensure all the filler was wet out, and distributed evenly throughout the mix. The initiator was added and thoroughly mixed. Specimens were cast for filler volume fractions and allowed to cure at room temperature. The specimens were measured within 16 - 72 hours of casting to determine both linear and volumetric shrinkage.

Figure 5.5: Shrinkage testing mould

5.4.4 Gel Time

Trial mixes were prepared and temperatures recorded, with respect to time. The interval of time required for a colloidal solution to become semisolid jelly, or gel was measured. This time is known as gel time, and higher gel time allows for mixing and pumping operations.

5.5   Design of a polyester based filler material

Two approaches were considered to design an appropriate polyester based filler material. Initially sample trial mixes were selected based on suitable weigh percentages of aggregates covering 40-60% (w/w) resin range. In the second method mix, proportions were selected using volumetric analysis of sand.

5.5.1 Preliminary approach based on weight percentage

Sample trial mixes were considered based on several weight percentages of polyester resin, fly ash, and sand given in Table 5.4. Initially 40 - 60% (w/w) polyester resin content was used to achieve the required good pump ability and workability.

Table 5.4: Mixing proportions by total weight

Sample Number	(Resin+Initiator)% -By total weight -(R)	Filler (%)		Initiator(%)- Weight % of resin
		Sand -(S)	Fly ash -(F)	
1000(R-50%, S-25%, F-25%)	50	25	25	2.5
1001(R-50%, S-20%, F-30%)	50	20	30	2.5
1002(R-50%, S-30%, F-20%)	50	30	20	2.5
1003(R-50%, S-50%)	50	50	-	2.5
1004(R-60%, S-40%)	60	40	-	2.5
1005(R-40%, S-60%)	40	60	-	2.5
1006(R-56%, F-44%)	56	-	44	2.5
1007(R-65%, F-35%)	65	-	35	2.5
1008(R-45%, F-55%)	45	-	55	2.5

5.5.1.1 Mechanical properties

All the samples achieved high mean compressive strength of more than 40 MPa. More than 60 MPa compressive strength can be achieved easily in the filler material development when polyester resin content varied from 40 - 60% (w/w) with fly ash and sand. Polyester based filler materials have considerably lower density than Ordinary Portland Cement (OPC) concrete. The percentage of fine material used in the mix directly affected the gel time. Table 5.5 shows filler material properties for the selected mix proportions.

Table 5.5: Test results from compression test, shrinkage test and gel time test

Sample Number	Gel time (min)	Compressive Capacity (MPa)	Compressive modulus (MPa)	Linear Shrinkage (%)	Volumetric Shrinkage (%)	Density (kg/m^3)
1000(R-50%, S-25%, F-25%)	65	68	3869.23	0.98	8	1451.83
1001(R-50%, S-20%, F-30%)	80	67	3357.14	0.73	6	1410.00
1002(R-50%, S-30%, F-20%)	60	68	3300.00	0.78	7	1443.85
1003(R-50%, S-50%)	75	63	3304.35	0.74	7	1514.06
1004(R-60%, S-40%)	40	45	1642.00	1.2	5	1468.69
1005(R-40%, S-60%)	180	50	2866.67	0.36	5	1660.88
1006(R-56%, F-44%)	40	58	2800.00	0.56	7	1288.05
1007(R-65%, F-35%)	20	43	2058.82	0.70	7	-
1008(R-45%, F-55%)	Difficult to mix – low percentage of resin					

These tested specimens were observed to be shrunk when they hardened. This phenomenon is similar to OPC concrete that shrinks as it hardens. The volumetric shrinkage of the trial mixes were between 5% to 8%, depending on the mix proportions. Comparing samples 1003 to 1005, and 1006 to1007, it is obvious that the higher the polymer content, the higher the linear shrinkage. This shrinkage property is important in this filler as it may lead to develop some cracking due to confinement in the FRP connector. In addition this crack lead to penetrate water and durability issues can be predominating. Therefore less volumetric shrinkage mix proportions are more desirable for this nature of applications.

In this initial filler development, all the samples were mixed with 2.5% (weight % of resin) of initiator. In all three categories of mixes (1000 to1002, 1003 to1005 and 1000 to 1007), gel times were proportions to the percentage of the fine material used. For example, (samples 1002 and 1001), when the fly ash amount was changed

from 20% to 30%, gel time increased from 60 to 80 minutes. Therefore the amount of fine material directly affected the gel time of the mix.

All the samples achieved a high mean compressive strength of more than 40MPa. Figure 5.6(a) shows that sample numbers 1000, 1001 and 1002 have more than 60MPa compressive strengths, with considerable uniform plastic region and more than 10% strain. The same trial mixes have comparatively higher compressive modulus values of more than 3000MPa. All of these samples used 50% resin by weight (resin: materials = 1:1). However figure 5.6(b) and 5.6(c) illustrate that trial samples do not have uniform plastic regions except sample number 1005. Sample 1005 also used 50% resin by weight (resin: material = 1:1). Therefore by comparing Figure 5.6(a), 5.6(b) and 5.6(c), it can be concluded that nearly 50% resin (Resin: material =1:1 trial mixes) gives more uniform plastic region.
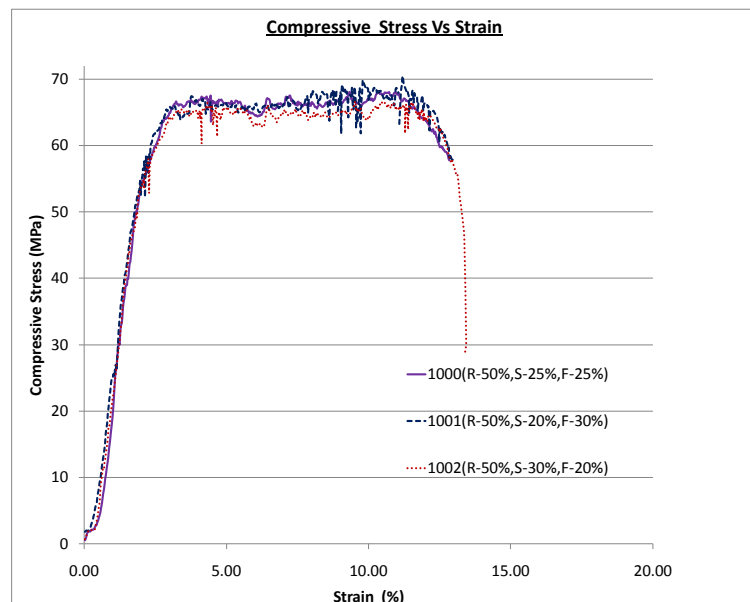
(a)
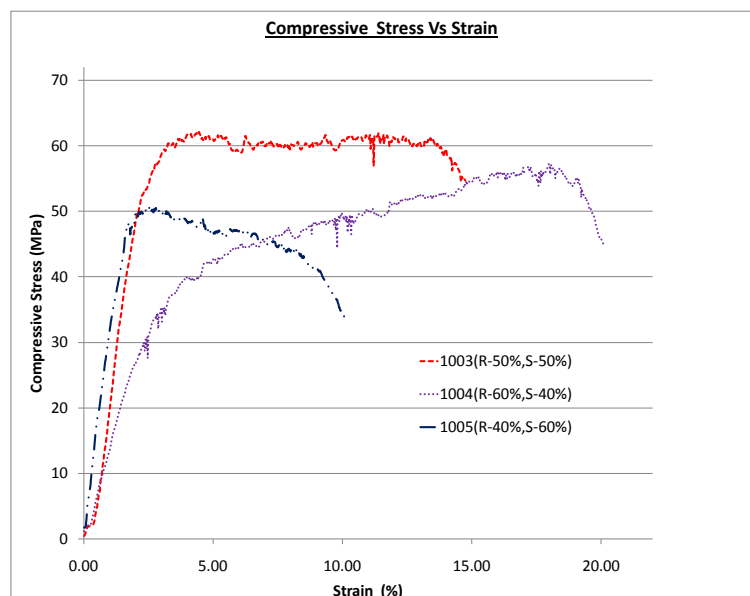
(b)
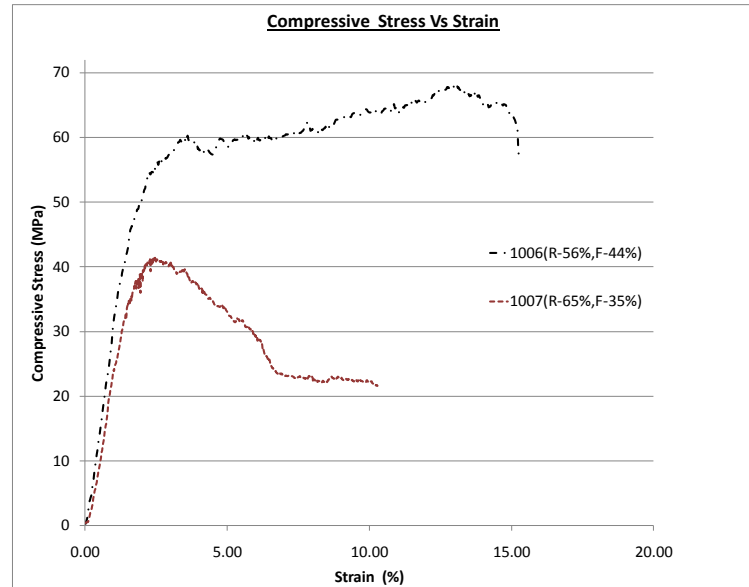
(c)

Figure 5.6: Compressive stress Vs strain graphs for trial mixes made out from (a) resin, sand and fly ash, (b) resin and sand, (c) resin and fly ash.

Flexural test samples were selected based on compressive strength and modulus values. Sample numbers 1004 and 1007 were not considered for flexural test because of low compressive modulus and strength. Table 5.6 and Figure 5.7 show the flexural test results.

Table 5.6: Flexural modulus and modulus of rupture

Sample Number	Flexural modulus (MPa)	Modulus of rupture (MPa)
1000(R-50%, S-25%, F-25%)	2828.37	21.19
1001(R-50%, S-20%, F-30%)	2550.31	20.61
1002(R-50%, S-30%, F-20%)	2558.85	20.30
1003(R-50%, S-50%)	2343.05	20.07
1005(R-40%, S-60%)	2818.91	15.19
1006(R-56%, F-44%)	1902.70	19.57

According to Figure 5.7, all the samples except 1005 show good modulus of rupture with more than 0.01 strains at failure in tension side, which is 3.3 times compared with that of reinforced concrete (0.003).
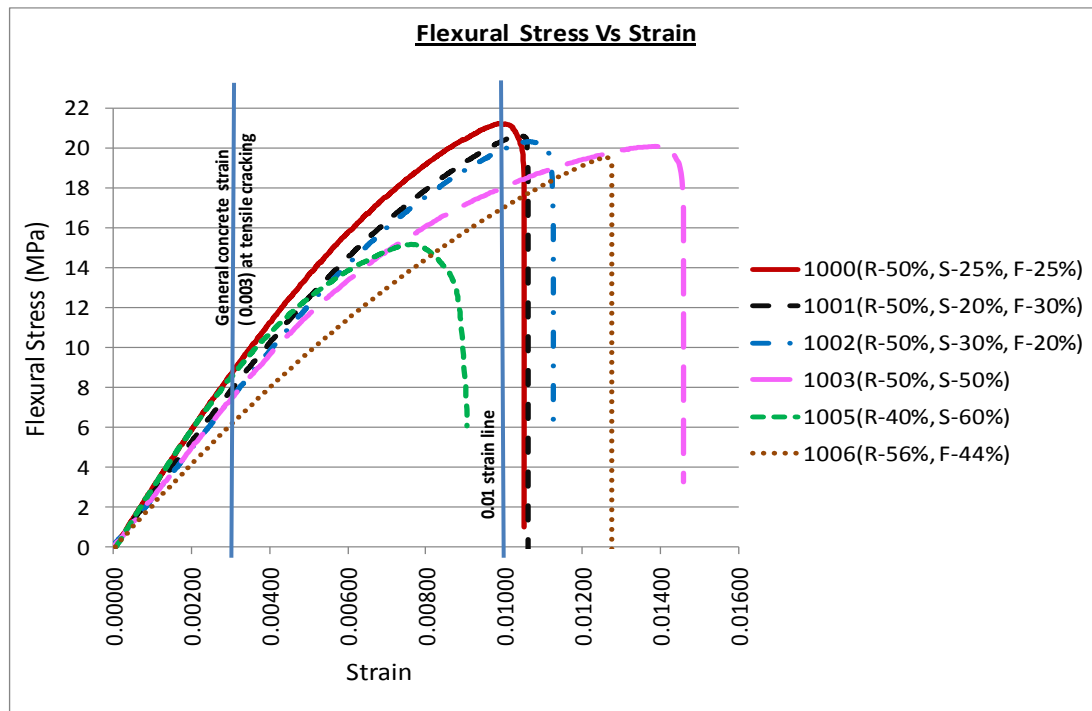
Figure 5.7: Flexural stress Vs strain graphs

Based on the compressive and flexural strengths, stress-strain relationships, most of the initially tested trial polyester filler materials can be used in the connector for bridge pile rehabilitation. However when an appropriate mix design is to be selected, shrinkage and gel time play an important role. Hence, as a result of this preliminary study, sample1001(R-50%, S-20%, F-30%) is recommended as filler material, based on less volumetric shrinkage and considerably higher gel time.

5.5.2 Approach based on volumetric analysis.

This approach was based on measuring the air voids in sand and trying to fill the air voids using appropriate proportions of resin and fly ash. Specific gravity approach was used to find air voids in sand. Test method ASTM C128 covers the determination of bulk specific gravity, Saturated Surface Dry (SSD) specific gravity, apparent specific gravity and absorption of fine aggregate. To comply with the above standards following definitions were taken in to account.

- *Specific Gravity (SG)* - The ratio of the mass (or weight) in air of a unit volume of material to the mass of the same volume of water at a specified temperature. Specific gravity is a dimensionless term.

- *Apparent Specific Gravity (ASG)* - The ratio of the weight in air of a unit volume of the impermeable portion of aggregate to the weight in air of an equal volume of gas-free distilled water at specified temperature.

- *Bulk Specific Gravity (BSG)* - The ratio of the weight in air of a unit volume of aggregate (including the permeable and impermeable voids in the particles, but not including the voids between particles) to the weight in air of an equal volume of gas-free distilled water at specified temperature.

- *Bulk Specific Gravity (SSD)* - The ratio of the weight in air of a unit volume of aggregate, including the weight of water within the voids filled to the extent achieved by submersion in water for 24 hour (but not including the voids between particles) to the weight in air of an equal volume of gas-free distilled water at specified temperature.

The ASTM C128, SSD condition of the sand was verified by using the cone test. As shown in Figure 5.8 (c), when the moulded shape slightly slumps, a saturated-surface-dry condition has been reached.

(a)

(b)

(c)
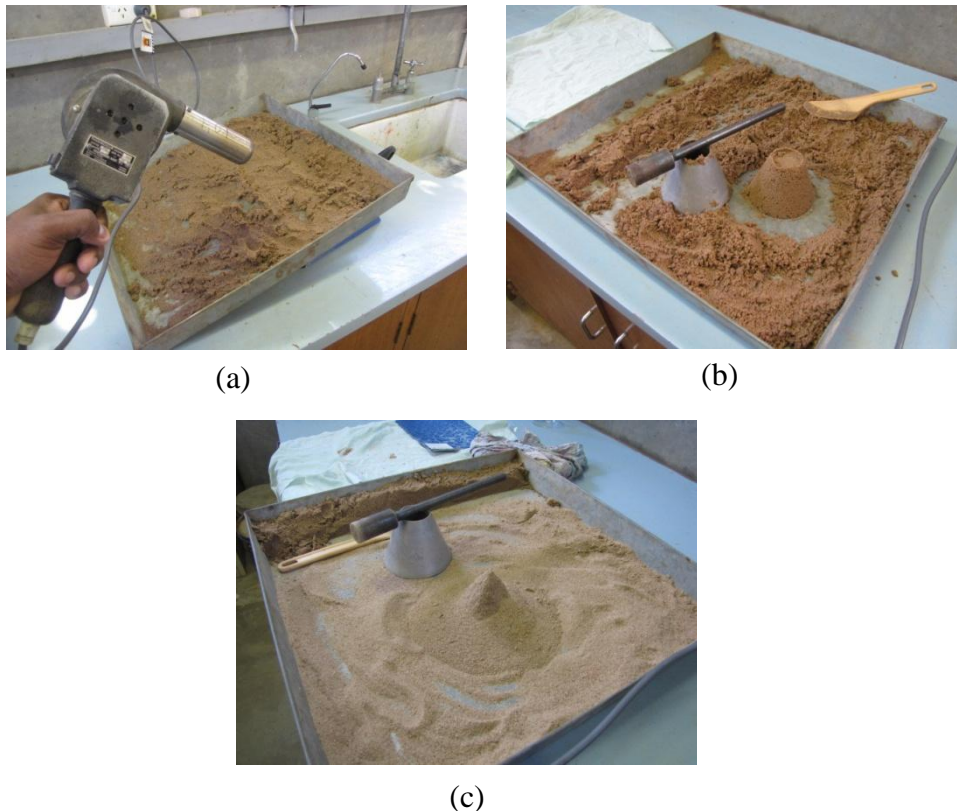
Figure 5.8: Achieving SSD condition of industrial sand (a) Sample drying using drier, (b) SSD condition not achieved, (c) SSD condition achieved (slightly slump indication)

5.5.2.1 Determination of voids in sand mix

According to Figure 5.9 total volume of sand comprises of, air voids and volume of sand.

Therefore, $\qquad V = v_a + v_m$ -- (5.1)
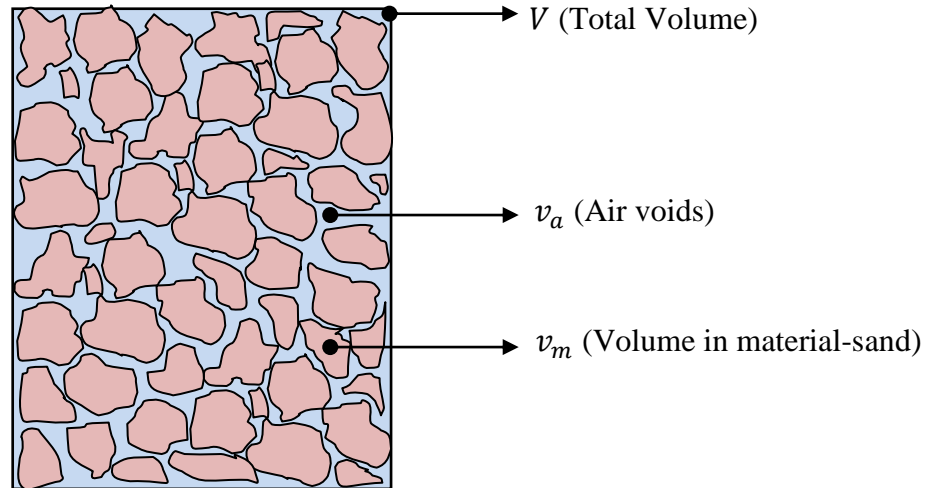
Figure 5.9: Volumetric components of normal industrial sand mix

Bulk density of sand was obtained according to the ASTM D-1556 standard. Therefore mass of the sand can be found using the following equation.

$$m_m = V\rho \text{ -- (5.2)}$$

From Bulk Specific Gravity (BSG) definition:

$$BSG = \frac{\textit{Weight in air of a unit volume of aggregate (including permiable and impermiable voids in particles, not voids between particales)}}{\textit{Weight in air of an equal volume of water at specific temperature}}$$

$$BSG = \frac{m_m}{m_s + m_b - m_c} \text{ -- (5.3)}$$

$$\rho_m = BSG * \rho_w \text{ -- (5.4)}$$

From normal density definition;

$$v_m = \frac{m_m}{\rho_m} \text{ --- (5.5)}$$

Therefore air voids in sand sample;

$$v_a = V - v_m \text{ --- (5.6)}$$

Where,

V = Total Volume

v_a = Air voids in sand mix

v_m = Volume in material (sand)

m_m = Mass of oven dry sand sample ➔

m_s = Mass of Saturated surface dry Sand sample ➔

m_b = Mass of flask fills with water ➔

m_c = Mass of flask with sand sample + water ➔

ρ = Bulk density of sand

ρ_m = Material density of sand

ρ_w = Density of water at specific temperature

Table 5.7 shows specific gravity test results for industrial sand obtained from Wagners, in Queensland, Australia.

Table 5.7: Specific Gravity test results

	Trials		
	1	2	3
Weight of Picnometer (kg)	0.097	0.096	0.095
Weight of Picnometer + SSD Specimen(kg)	0.249	0.27	0.179
Weight of Picnometer + SSD Specimen + Water(kg) **(C)**	0.438	0.452	0.395
Weight of Picnometer filled with water (kg)**(B)**	0.345	0.344	0.343
Weight of oven dry sample in air (kg)**(A)**	0.15	0.174	0.084
Weight of SSD specimen (kg)**(S)**	0.152	0.174	0.084
Water Temperature (^{0}C)	25	25	25
Bulk Sp. Gr.= A/(B+S-C)	2.542	2.636	2.625
Bulk Sp. Gr. (SSD) =S/(B+S-C)	2.576	2.636	2.625
Apparent Sp. Gr. =A/(B+A-C)	2.632	2.636	2.625

From the above three trials, trial 1 shows good variation among BSG, BSG-SSD and ASG except trial 2 & 3 results. This implies that trials 2 and 3 are away from the SSD condition. Therefore, results of trial 1 were selected. In this laboratory

testing, fine sand was placed in a pan, dried in the oven to constant mass at a temperature of 110°C, per the ASTM C128 and permitted to stand for 24 hours. It is then allowed to cool to a comfortable handling temperature (approximately 30 °C). This dry sand was used to make laboratory filler material specimens. Apparent Sp. Gr. was selected for the calculation of bulk density, because it was free from water filled with permeable voids. Natural air dry sand is used for mass production of fillers in proposed pile rehabilitation method. For this Bulk Sp. Gr. is to be used for calculating bulk density of sand, because its content of water particles is filled with permeable voids.

(a)   (b)

Figure 5.10: Three samples (a) Picnometer + SSD Specimens + Distilled Water, (b) Oven dry samples

From Table 5.7,

Apparent Sp. Gr. (the ratio of the weight in air of a unit volume of the impermeable portion of aggregate to the weight in air of an equal volume of gas-free distilled water at specified temperature) = 2.632

From equation 5.4, Apparent Density = 2.632*995.6502 (Water Density 25°C)

$$= 2620.55$$

Bulk density of the sand accordance with ASTM D1556

$$= 1493.68 \text{ kg/m}^3$$

Consider 1m^3 of bulk sand material,

Weight of 1m3 of material = 1493.68kg

Volume of pure material without voids (Including impermeable voids inside particle)

$$= 1493.68/2620.55$$

$$= 0.5699 \text{m3}$$

Therefore free air voids between sand particles

$$= 1 - 0.5699$$

$$= 0.43\text{m}^3$$

Percentage of free air voids in industrial sand obtained from Wagners, Queensland, Australia   = **43%**

Sand percentage   = 100-43 = **57%**

The aim of this approach is to fill this 43% air voids with appropriate proportions of resin and fly ash.

5.5.2.2 Determination of mixing proportions

Initially, several mixing proportions propionates were considered according to the percentage of total volume per the table 5.8. Then based on their mixing ability and gel time, final proportions were chosen.

Table 5.8: Mixing proportions by volume

Sample identification	Sand percentage by volume	(Resin + Initiator) percentage by volume	Fly ash percentage by volume	Gel Time -Min	Remarks
S57R43	57	43	-	52	
S57R40F3	57	40	3	53	
S57R30F13	57	30	13	58	
S57R22F21	57	22	21	60	
S57R20F23	57	20	23	65	
S57R15F28	57	15	28	-	Resin % not enough to mixing
S57R10F33	57	10	33	-	Resin % not enough to mixing

Samples S57R15F28 and S57R10F33 could not be mixed properly, because of low percentage of resin by volume (figure 5.11).

(a)   (b)

Figure 5.11: (a) S57R15F28, (b) S57R10F33

Marginally, mixing of S57R20F23 can be achieved, but liquefy formation was not enough to make a good workability flow, to allow pumping action. Therefore S57R43, S57R40F3, S57R30F13 and S57R22F21 were selected for further investigation. These four samples had a good gel time, ranging from 52Min to 60Min with 2.5% initiator by weight of resin.

5.5.2.3 Determination of mixing formula

In this method proportions of the ingredients were selected based on the percentage of total volume. To make the laboratory samples, these volume proportions should be converted to weight proportions. The following formula was used for the conversion. It was assumed that no volume reduction or expansion would occur after mixing.

V	= Total Volume of Mixture ➔ Known
ρ_{Sa}	= Density of Sand ➔ Known
ρ_{Re}	= Density of Resin ➔ Known
ρ_{In}	= Density of Initiator ➔ Known
ρ_{FA}	= Density of Fly ash ➔ Known
Sand: (Resin + Initiator): Fly ash By volume	= α: β: γ ➔ known
V_{Sa}	= Volume of Sand ➔ Known
V_{Re}	= Volume of Resin ➔ Known
V_{In}	= Volume of Initiator ➔ Known
V_{FA}	= Volume of Fly ash ➔ Known
W_{Sa}	=Weight of Sand ➔ Unknown
W_{Re}	=Weight of Resin ➔ Unknown
W_{In}	=Weight of Initiator ➔ Unknown
W_{FA}	=Weight of Fly ash ➔ Unknown
W_{In}	= μ x W_{Re} ➔ (This case μ =0.025; 2.5% initiator by weight of resin)
W	= Total weight of samples ➔ Unknown

$W = W_{Sa} + W_{Re} + W_{In} + W_{FA}$ -- (5.7)

From definition of density,

$W_{Sa} = \rho_{Sa}\,\alpha\,V$ --- (5.8)

$W_{FA} = \rho_{FA}\,\gamma\,V$ -- (5.9)

$V_{Re} = W_{Re} / \rho_{Re}$

$V_{In} = W_{In} / \rho_{In}$

But $W_{In} = \mu \times W_{Re}$

Therefore, $V_{Re} + V_{In} = \beta\,V = W_{Re}\left(\dfrac{1}{\rho_{Re}} + \dfrac{\mu}{\rho_{In}}\right)$

$W_{Re} = \dfrac{\beta\,V}{\left(\dfrac{1}{\rho_{Re}} + \dfrac{\mu}{\rho_{In}}\right)}$ -- (5.10)

Substituting these values to equation 5.7,

$$W = V\left[\ \rho_{Sa}\,\alpha + \rho_{FA}\,\gamma + \dfrac{\beta\,(1+\mu)}{\left(\dfrac{1}{\rho_{Re}} + \dfrac{\mu}{\rho_{In}}\right)}\ \right]$$ -- (5.11)

Using equations 5.8, 5.9, 5.10 and 5.11 weights of individual components corresponding to various volume proportions can be calculated. Table 5.9 shows corresponding weight percentages.

Table 5.9: Comparison of mixing proportions by weight and volume

| Sample identification	Volume percentages			Corresponding volume percentages based on equation 5.11		
	Sand percentage by volume	(Resin + Initiator) percentage by volume	Fly ash percentage by volume	Sand percentage by weight	(Resin + Initiator) percentage by weight	Fly ash percentage by weight
S57R43	57	43	-	65.1	34.9	-
S57R40F3	57	40	3	64.3	33.2	2.5
S57R30F13	57	30	13	64.3	24.9	10.8
S57R22F21	57	22	21	64.3	19.3	17.4
S57R20F23	57	20	23	64.3	16.6	19.1

In this approach, resin + initiator percentages were between 16.5-35% (w/w) which is more economical than the previous approach. Table 5.10 shows common resin percentages used by other researchers. Considering economic aspects and shrinkage issues, most researchers prefer to work on lower percentage ranges (w/w).

Table 5.10: Common resin percentages use for different researches

| Type of Resin	Percentage range	Reference
Polyester Resin	15.5-21.5	(Kallol Sett et al ,2004)
Furan Resin	7.5- 15	(M. Muthukuma et al,2004)
Epoxy Resin	12.4-16.4	(Marinela Barbuța et al, 2010)
Polyester Resin	13-14	(Jane et al , 2004)

5.5.2.4 Mechanical properties

Compressive testing was performed according to the ASTM D 695 M-91 standard as described in the section 5.3. 3, 7, 14, 21 and 28 days strengths were checked to investigate the behaviour of compressive strength, with respect to the age. Figure 5.11 shows compressive stress Vs strain graphs for different proportions with age. All the samples achieved high mean compressive strength of more than 60 MPa. More than 60 MPa compressive strength can be achieved easily in the filler material development, when polyester resin content varied from 16.5 - 35% (w/w) with fly ash and sand. It is observed that plastic region of each mix proportion has a correlation with the amount of fly ash percentage. For example, generally S57R43 had 5.5% strain plastic region with 0% fly ash. When fly ash percentage was increased up to 13%, S57R30F13 had around 2% strain plastic region. Further increase in fly ash amount up to 21%, further decreased the plastic region (S57R22F21 had around 1% strain plastic region). Therefore by introducing fly ash, mixes were transformed from ductile to brittle behaviour with less plastic region.
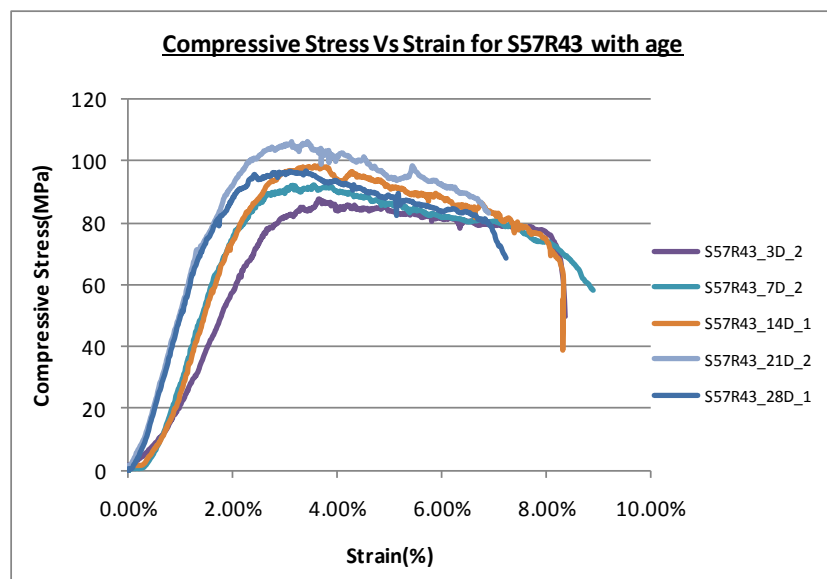
(a)
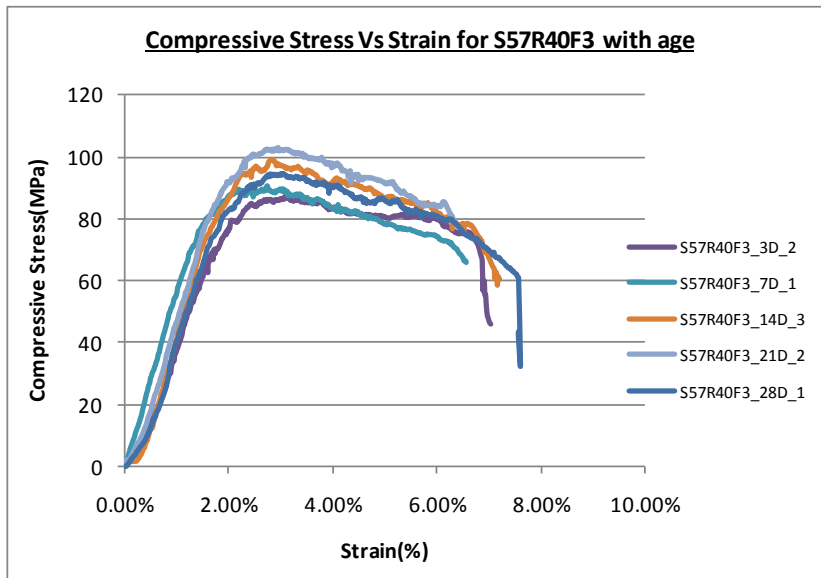
(b)
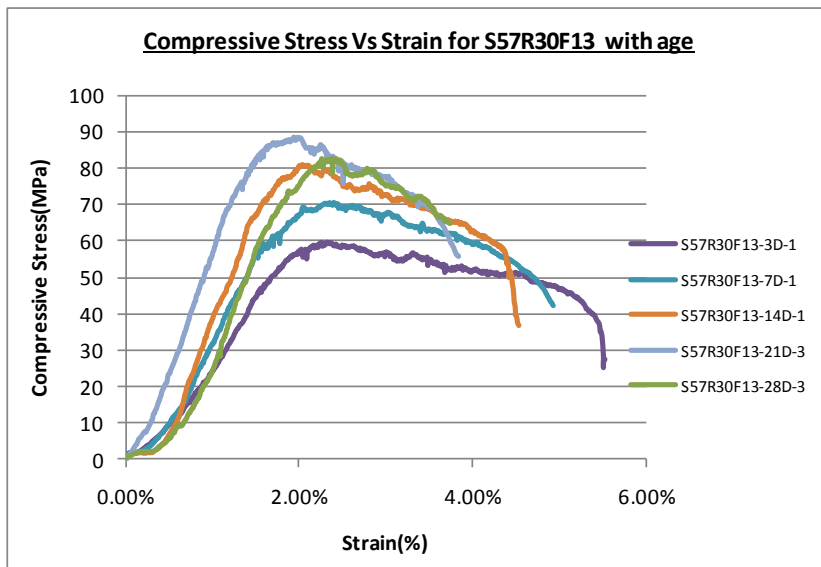
(c)
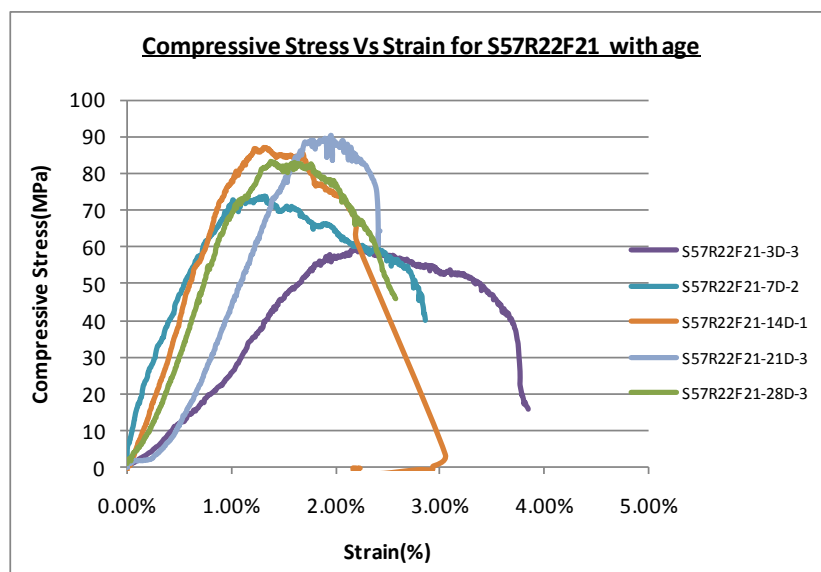
(d)

Figure 5.12: Compressive stress Vs strain graph with ages (a) S57R43, (b) S57R40F3, (c) S57R30F13 and (d) S57R22F21

Table 5.11: Variation of compressive strength and modulus with time

Sample Identification	3 Days		7 Days		14 Days		21Days		28Days	
	Compressive Value (MPa)	Compressive E value (MPa)	Compressive Value (MPa)	Compressive E value (MPa)	Compressive Value (MPa)	Compressive E value (MPa)	Compressive Value (MPa)	Compressive E value (MPa)	Compressive Value (MPa)	Compressive E value (MPa)
S57R43	85	3933	91.25	5500	98.5	5750	103.75	5625	96.25	5700
S57R40F3	86	4350	90	6150	97.5	6000	102.5	6000	95	5950
S57R30F13	60	4042	71.25	5440	77.5	6000	87	6500	82.5	6550
S57R22F21	60	3714	73.12	7125	87.5	7200	90	7000	80	7150
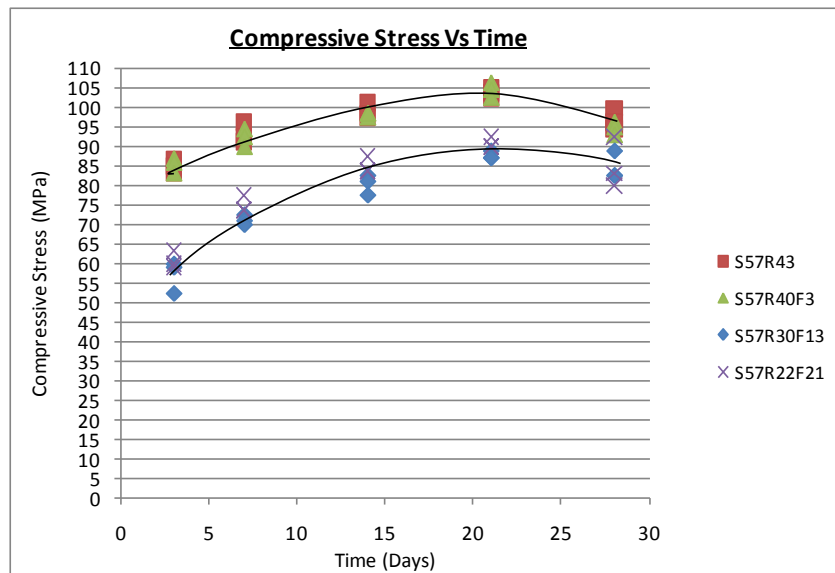
(a)
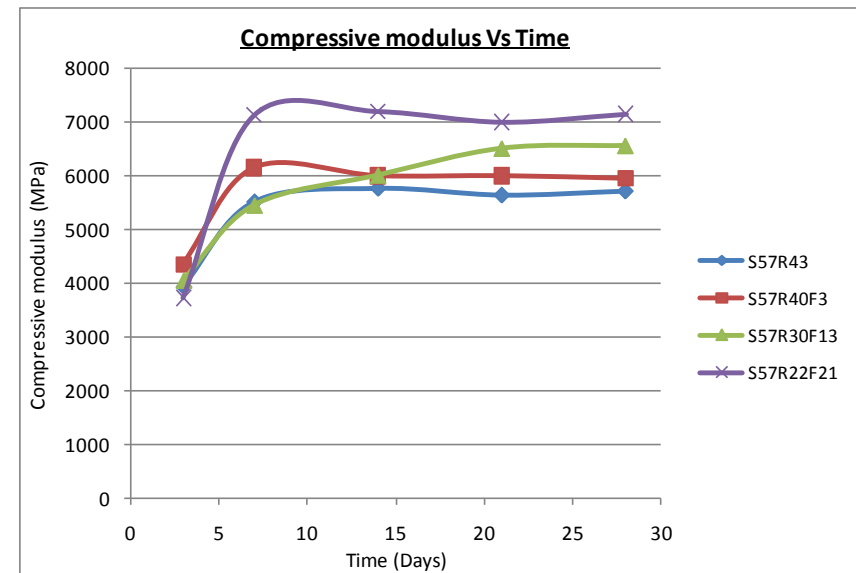
(b)

Figure 5.13: (a) Compressive stress Vs time, (b) Compressive modulus Vs time

As seen in figure 5.13(a), mix batches S57R43, S57R40F3 and S57R30F13, S57R22F21 initially have two different compressive strength regions, and then they seemed to be converged after 28 days. Maximum compressive strength of polyester based fillers was indicated in around 21 days and then it was reduced at 28 days which is somewhat different from the behaviour of Ordinary Portland Cement (OPC) concrete. Compared to OPC concrete, these fillers were given 21 days maximum compressive strength. For OPC concrete this was given in 28 days.

From figure 5.13(b), more than 90% of compressive modulus was rapidly developed between 3 and 7 days for all filler mixes. After 21 days, compressive moduli of all four samples varied in a similar way.

Table 5.12: Other properties

Sample identification	Flexural modulus (MPa) -28D	Modulus of rupture (MPa) -28D	Mean Density (kg/m^3)	Linear Shrinkage (%)	Volumetric Shrinkage (%)	Split Tensile Stress (MPa) -28D	Gel Time (Min)
S57R43	7500	34	1764.89	0.80	0.99	10.94	52
S57R40F3	8500	31.5	1774.72	0.67	0.96	10.63	53
S57R30F13	10000	24	1771.46	0.29	0.29	6.57	58
S57R22F21	14000	14	1866.63	0.66	0.95	5.46	60

Measurement of linear shrinkage and volumetric shrinkage were performed according to section 5.2.1. This test mix was observed to be shrunk into a smaller amount as it hardened. This phenomenon is similar to OPC concrete that shrinks as it is hardened. However when compared with earlier samples (based on weight percentage), these samples were giving around 80% less volumetric shrinkage. The measured volumetric shrinkage of the test mixes were between 0.29% to 0.99%, depending on the mix proportions.

2.5% initiator by weight of resin was given a reasonable gel time to allow for workmanship. These fillers had a lower density, ranging from 1750 kg/m^3 to 1875 kg/m^3 than that of OPC concrete.

A 28 day split tensile test was performed according to the ASTM D3967-08 standard. Cylindrical specimens having a diameter of 50 mm and a height of 100 mm were used in the test. Three samples were tested from each batch of filler material. Figure 5.14 shows typical failure pattern of the split tensile sample. Form table 5.12 indicates the split tensile stress capacity was reduced, with respect to the increased amount of fly ash.

Figure 5.14: Fracture pattern of split tensile sample

Flexural test was performed using the three point bending test, in accordance with ISO 178:1993, section 5.2.1. Five samples were tested from each batch. The specimen was simply supported and tested under 3-point loading with the span set at approximately 16 times the thickness of the sample. The load was applied at midspan of the specimen at a constant rate of 1 mm / min, using a 10 kN MTS testing machine. The load and midspan deflection were recorded up to the point of failure, to determine the strength and elastic properties of the polymer based filler material.
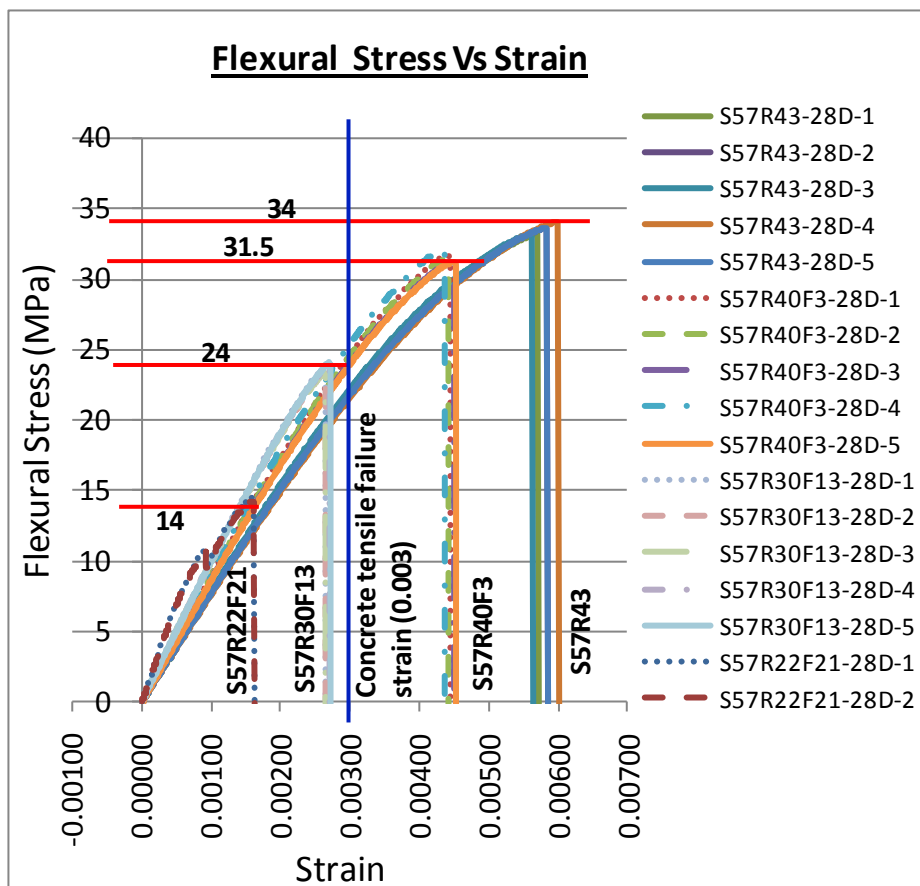

Figure 5.15: Flexural stress-strain relationship of the filler material

The experimental stress-strain relationship at the bottom face of filler material under flexural loading is shown in Figure 5.15. The experimental results showed that the filler material behaved almost linear elastic manner under flexural loading. The specimens failed in a brittle manner without any sign of cracking. Failure of the specimens is due to tensile failure at the bottom mid span of the specimen. Samples S57R22F21 and S57R30F13 having low tensile strain values at the failure which less than 0.003 (Concrete tensile failure strain). Compare to other two samples S57R22F21 and S57R30F13 behave more brittle manner. Flexural modulus was calculated using three point deflection formula. The highest modulus was given by S57R22F21. From figure 5.15 and 5.16, amount of fly ash directly affect both the flexural modulus and modular of rupture.
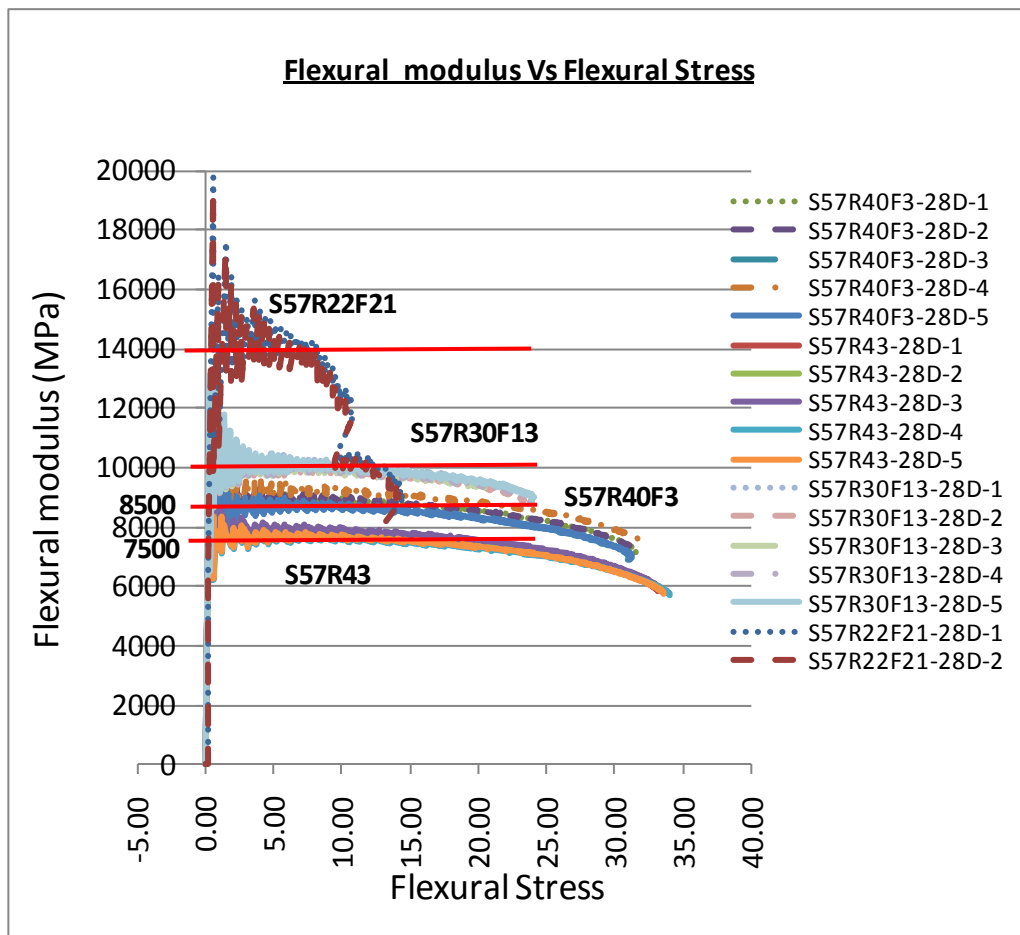

Figure 5.16: Flexural modulus Vs flexural stress relationship

5.6 Axial stress – strain relationship for unconfined polyester based filler material

In the past decade, most researchers focussed their study on the stress strain behaviour of concrete wrapped with FRP confinement. There was an absence of study on confinement and un-confinement behaviour of polymer base filler material. It may be difficult to define the relationship by one approach, because the shape of uni axial stress-strain curve of polyester base filler is influenced by many factors.

Several hypotheses and approaches are available and fully employed by many investigators for normal concrete. Some may differ in detail, and others may differ significantly, depending on how the factors affecting the relationship are evaluated, and the manner in which testing conditions can be controlled (Carreira, D.J et al. 1985).

However, there are several conditions that must be satisfied in any mathematical model, these are:

1. Point of origin, $f = 0$ at $\varepsilon = 0$.

2. Slope of the stress-strain curve at the origin, $\frac{df}{d\varepsilon} = E_c$ and $\varepsilon = 0$.

3. Point of maximum stress $f = f_o$ at $\varepsilon = \varepsilon_o'$ where $\frac{df}{d\varepsilon} = 0$.

4. The analytical curve must satisfy the experimental data to show the ascending and descending portions.

In this regard, a carefully conducted set of experiments must be carried out. Strains were measured at the regions of uniform strain. Two strain gauges of 10 mm gauge length were fixed at the middle third of the height of the specimen longitudinally in two diametrically opposite sides. Similarly another two strain gauges were placed laterally at the middle third in two diametrically opposite sides. All specimens were prepared according to these procedures and specimens ready to be tested are shown in Figure 5.17(a).

Loading and strain measurement were carefully controlled by introducing a 2 mm / min loading rate. Continuous record of load and strain readings were obtained up to failure. Maximum strength of polyester base filler is expressed by the cylinder strength ($f_o = f'_c$). The experimental results as shown figure 5.17(b) satisfy the above mentioned basic conditions with two different regions. A single equation of a

polynomial form for different types of polyester fillers can be obtained to predict the experimental behaviour (equation 5.12).
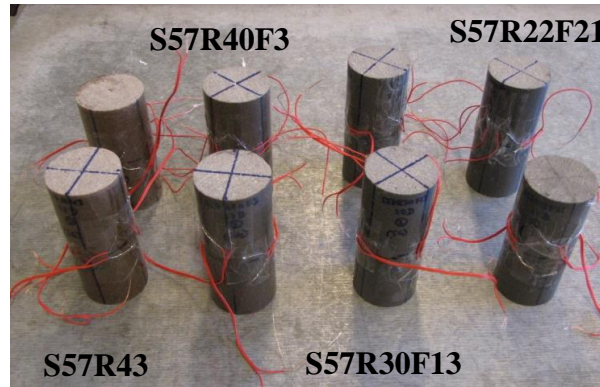
(a)
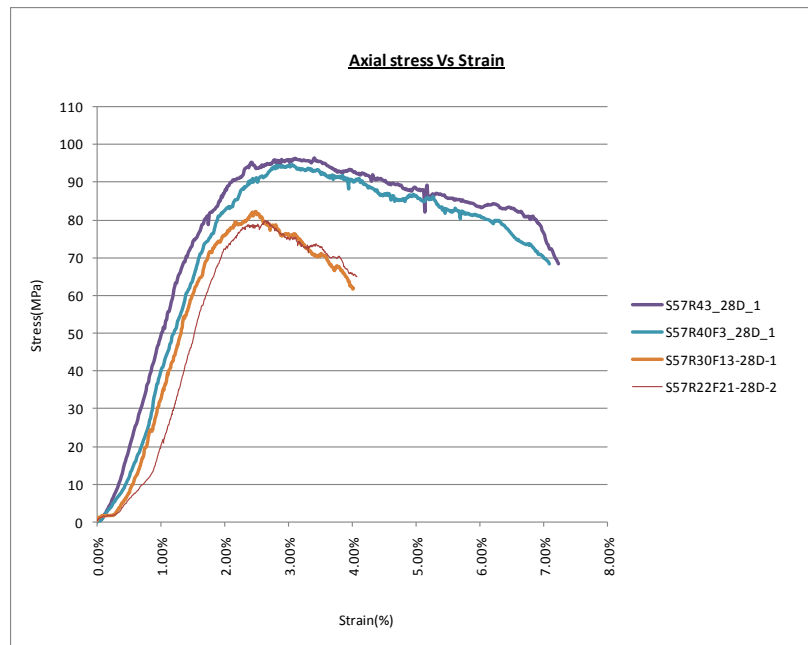
(b)

Figure 5.17: (a) Specimens before testing, (b) Axial stress Vs strain for deferent composition of fillers

$$\frac{f}{f_o} = A\left(\frac{\varepsilon}{\varepsilon_o}\right)^1 + B\left(\frac{\varepsilon}{\varepsilon_o}\right)^2 + C\left(\frac{\varepsilon}{\varepsilon_o}\right)^3 \text{------------------ (5.12)}$$

Coefficients A, B and C are evaluated by plotting the experimental results in non dimensional form as shown in figure 5.18(a) and 5.18(b) using the least squares polynomial curve fitting with, a third degree polynomial (n = 3) was selected in which equation (5.12) become:

$$\frac{f}{f_o} = 1.9044\left(\frac{\varepsilon}{\varepsilon_o}\right)^1 - 1.1311\left(\frac{\varepsilon}{\varepsilon_o}\right)^2 + 0.1972\left(\frac{\varepsilon}{\varepsilon_o}\right)^3 \rightarrow \text{Low fly ash region----- (5.13)}$$

$$\frac{f}{f_0} = 0.5704 \left(\frac{\varepsilon}{\varepsilon_o}\right)^1 + 1.4481 \left(\frac{\varepsilon}{\varepsilon_o}\right)^2 - 1.0216 \left(\frac{\varepsilon}{\varepsilon_o}\right)^3 \rightarrow \text{High fly ash region} ---- (5.14)$$
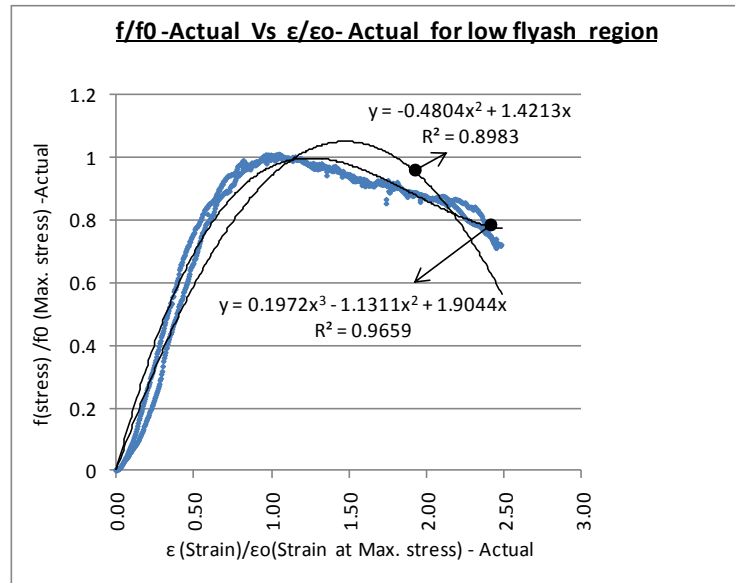
(a)
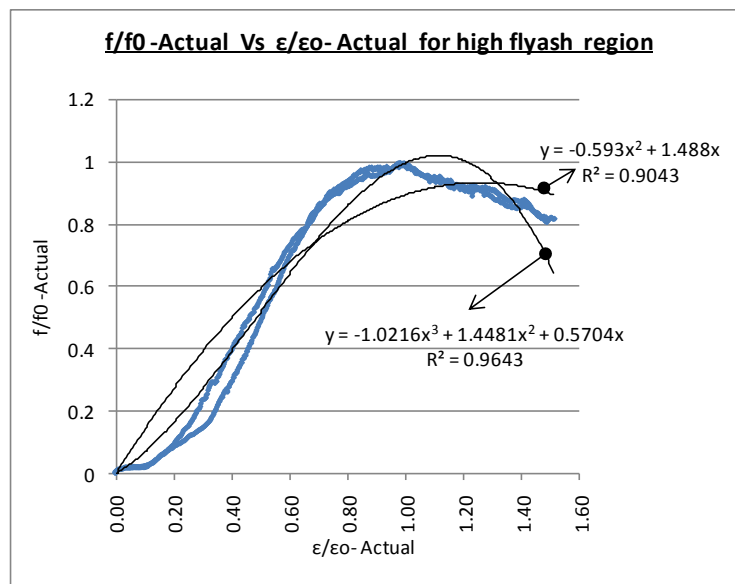
(b)

Figure 5.18: Second and third degree polynomial fittings for experimental results (a) low fly ash region, (b) high fly ash region

Figures 5.18(a) and 5.18(b) show comparison between second and third degree polynomials. Obviously (n =3) gives a better fitting. A fourth degree polynomial was also tried but was excluded from the analysis for its complexity. Curve fitting approach is not a very reliable way to predict the constitutive behaviour of a material. Because, generally ascending and descending branches of the stress strain curve are very difficult to represent by polynomial curve.

Another simple form proposed for concrete stress-strain relationship similar to the form proposed by (Desayi. P et al., 1964) and (Carreira, D.J et al., 1985):

$$\frac{f}{f_0} = \frac{R\left(\frac{\varepsilon}{\varepsilon_o}\right)}{1+(R-1)\left(\frac{\varepsilon}{\varepsilon_o}\right)^\beta} \quad \text{-------------------------------------- (5.15)}$$

In which, $\beta = \dfrac{R}{R-1}$

where R = material parameter depending on the shape of the stress-strain curve

$\quad = \dfrac{E_c}{E_o}$

Ec = modulus of elasticity of concrete,

Eo = max. stress f_o/ strain at max. stress ε_o.

Various values of R were chosen as an attempt to find the value of (R) that has a good fit with the experimental data for different proportions of fillers selected from table 5.13.

Table 5.12: Values of R based on the experimental results

Sample Identification	F_o(Mpa)	E_c(Mpa)	ε_o	E_o(Mpa)	$R=E_c/E_o$	Average R	Remarks
S57R43	96.25	5700	0.030	3262.712	1.747	1.782	Low fly ash region
S57R40F3	95.00	5950	0.029	3275.862	1.816		
S57R30F13	82.50	6550	0.025	3300.000	1.985	2.199	High fly ash region
S57R22F21	80.00	7150	0.027	2962.963	2.413		

Figure 5.19 shows a comparison between stress-strain relationships using equation 5.15 with different values of R. Evidently, equation 5.15 gives the best fitting when the value of R equals (1.782) for low fly ash region and R equals (2.199) for high fly ash region respectively which were found to be the average value of the set shown in table 5.13.
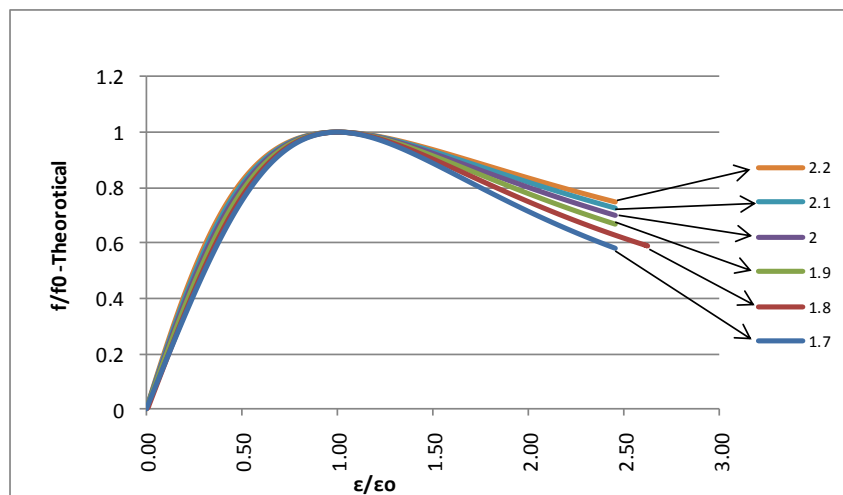

Figure 5.19: Non- dimensional stress- strain relationship from Eq. 5.15 for various values of R

Therefore, equation 5.15 becomes:

$$\frac{f}{f_0} = \frac{1.782\left(\frac{\varepsilon}{\varepsilon_0}\right)}{1+0.782\left(\frac{\varepsilon}{\varepsilon_0}\right)^{2.278}} \rightarrow \text{Low fly ash region----------- (5.16)}$$

$$\frac{f}{f_0} = \frac{2.199\left(\frac{\varepsilon}{\varepsilon_0}\right)}{1+1.199\left(\frac{\varepsilon}{\varepsilon_0}\right)^{1.833}} \rightarrow \text{High fly ash region----------- (5.17)}$$

These are also compared with equations 5.13, 5.14 and 5.16, 5.17 as shown in figures 5.20 (a), (b), (c) & (d) for different filler mixes used in this work. The comparison gives a good indication that the proposed equations 5.13 and 5.17 agree with the experimental results in low fly ash region. But, in a high fly ash region, equations 5.14 and 5.18 need some modification.
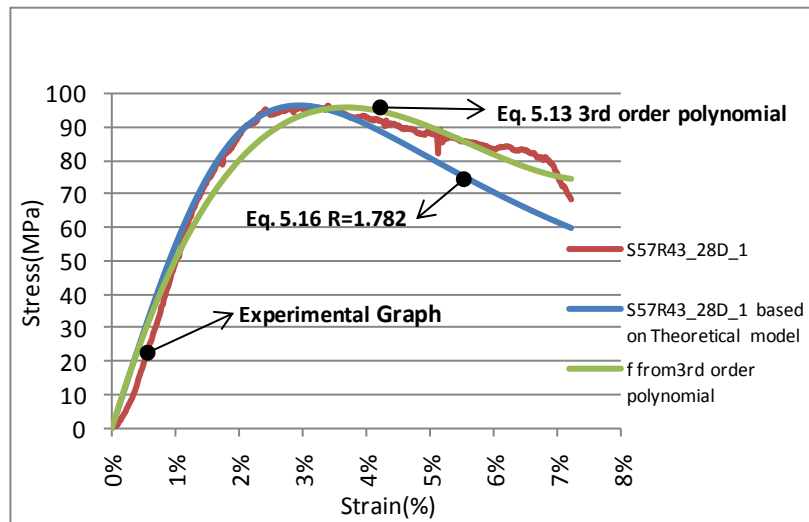
(a)
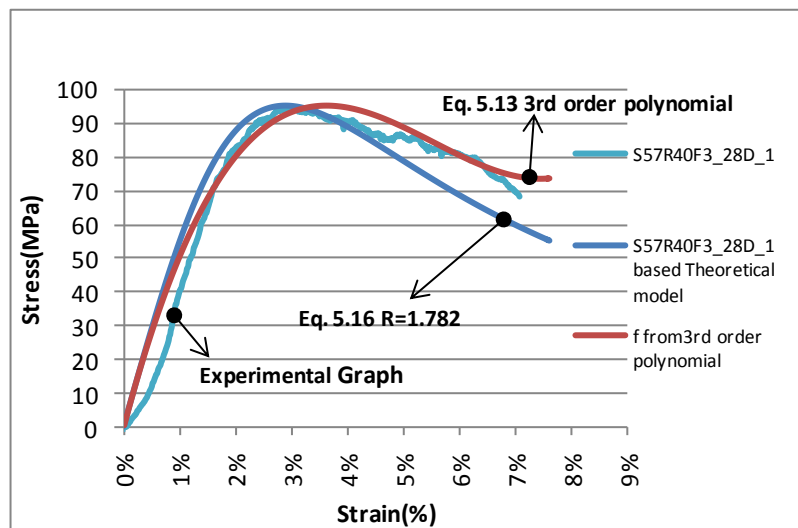
(b)

(c)
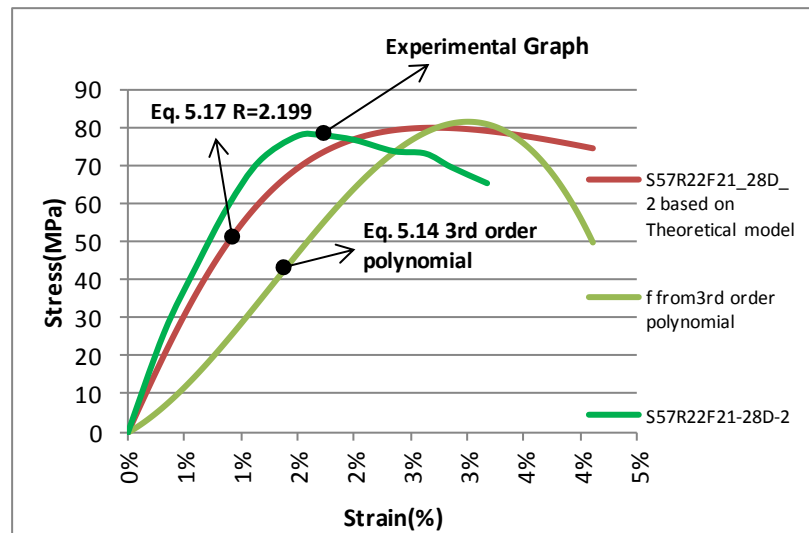
(d)

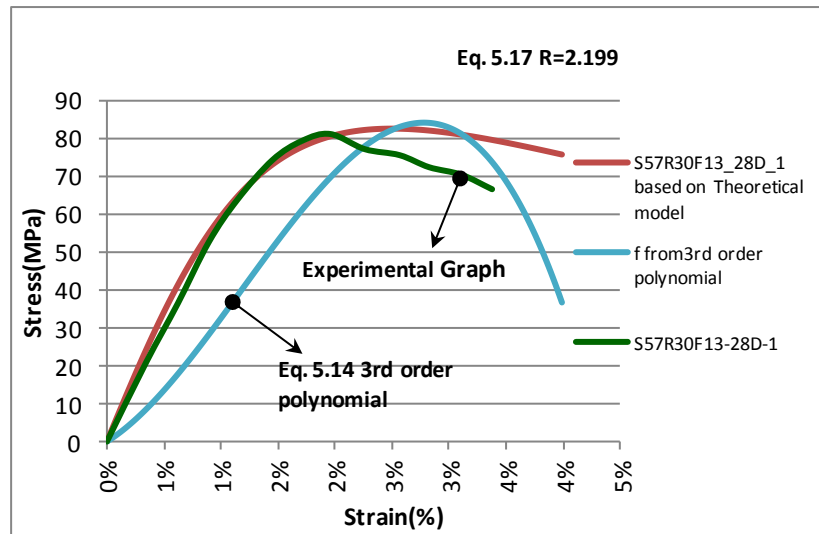Figure 5.20: Comparison of 3rd order polynomial, theoretical equation and experimental results for low fly ash region [(a) S57R43 & (b) S57R40F3] and high fly ash region [(c) S57R30F13 & (d) S57R22F21]

Finally the work is based on testing polyester base filler specimens made of local material to provide a relationship for stress-strain that designers can employ in the calculation of sectional capacities, which will finally lead to member and structure behaviour. Equations 5.13, 5.14 and 5.16, 5.17 are proposed to define the stress-strain curve based on the experimental work conducted. The comparison gives a good indication that the proposed R values agree reasonable with the experimental results for the low fly ash region while it will need some modification for the high flyash region. Generally the descending branch of the theoretical curve needs to be further analysed.

5.7 Conclusions

Preliminary development of polymer based filler materials was performed for the FRP tubular connector for timber pile rehabilitation. This research investigated the structural properties and unconfined stress – strain relationship of polymer based filler materials with different proportions of resin, sand, and fly ash. The following conclusions can be drawn from the work reported in this chapter.

- More than 60MPa compressive strength can be achieved easily in the filler material development when polyester resin content varied from 40% to 60% (w/w) with fly ash and sand. When polyester resin content varied from 16.5% -35% (w/w), more than 80MPa 28 days compressive strength can be achieved directly (table 5.11).

- Maximum compressive strengths of polyester based fillers were indicated in around 21 days, and different from Ordinary Portland Cement (OPC) concrete.

- More than 90% of compressive modulus (figure 5.13(b)), was rapidly developed between 3 and 7 days for all filler mixes. After 21 days, compressive moduli behaved uniformly.

- Polyester based fillers have considerably low density compare to that of OPC concrete.

- Amount of finer material (fly ash) used in the mixes directly affected the gel time and shrinkage.

- The addition of fly ash proved to improve the volumetric shrinkage and density of the polyester based fillers.

- If fly ash was introduced to the mixes, then mixes were transformed ductile to brittle behaviour with having less plastic region. Also split tensile stress capacity was reduced respective to the increased amount of fly ash.

- If polyester resin content lies in between 40% to 60% by total weight, then most fillers having more than 10% compressive strain plastic region. If polyester resin: Materials ratio 1:1, this plastic region becomes more uniform.

- One aim of the experimental program is to provide a relationship for stress-strain behaviour of polyester based filler material so that designers can use it in the calculation of sectional capacities. Equations 5.13, 5.14 and 5.16, 5.17 are proposed to define the stress-strain curve for unconfined polymer

concrete. A remarkable agreement was observed between the experimental and analytical curves for low fly ash region, and modification is required for the analytical curves in a high fly ash region.

Considering the above findings, most of the tested trial polyester filler materials can be used in this connector, based on their fair compressive and flexural stress-strain behavior, compared with traditional concrete. However, shrinkage and gel time, play an important role in selecting the appropriate mix configuration.

Chapter 6

CONCLUSIONS

6.1   Summary

The main tasks of this research project were to examine the structural behaviour of Glass Fibre Reinforced Polymer (GFRP) tubular piles and connector used for novel timber pile rehabilitation technique. To investigate these tasks, three objectives were considered. In the first objective, the affects of various loading scenarios on the capacity of the GFRP hollow tubular piles were investigated (in Chapter 3). Then as a second objective, numerical simulations were performed (in Chapter 4) using finite element analysis approach to verify experiments and study the behaviour of the overall pile rehabilitate system. Based upon the results of these numerical simulations, further research areas were highlighted for polymer based filler development. As a third objective, appropriate polymer based filler materials were developed (in Chapter 5) for the GFRP tubular connector, to transfer the vertical load from the super structure, to the original timber stump, by the connector. The third objective included investigations of suitable polymer based filler mixes, mix design approaches, and mathematical models to represent the behaviour of unconfined polymer based fillers, under compression loadings. As a result, this chapter presents conclusions based on the entire research, including experimental investigation, numerical simulations, and development of polyester based filler material.

6.2   Conclusions

Detailed experimental investigation was conducted (in Chapter 3), using coupon specimens to characterise the mechanical properties of the glass fibre composite laminates, and the full scale GFRP pile specimens to identify actual behaviour under serviceability loads. It should be noted that the predicted ultimate compressive capacities of the 300 mm external diameter short section of the pile and the ultimate moment capacity of 3.1 m long pile were 1690 kN, 180.8 kNm respectively. GFRP pile behave in a linear elastic manner in the serviceability loading range. Based on the experimental analyses, the compressive elastic modulus (E) and flexural stiffness (EI) of the pile are approximately 14300 MPa, 2.627 x 10^{12}

Nmm^2 respectively in the serviceability range, per the Shorncliffe pier loadings given by Brisbane City Council. Compare to the predicted ultimate compressive capacity of the pile (excluding the effect of buckling) 4 times higher than actual Shorncliffe pier loading. Therefore, the factor of safety of the GFRP pile against Shorncliffe pier under pure compression loading is around 4.

The predicted ultimate compressive capacities of the 470 mm external diameter short section of the pile and the ultimate moment capacity of 9.2 m long pile were 4222 kN, 469.8 kNm respectively. Based upon the experimental analyses, the compressive elastic modules (E) of the pile was approximately 15100 MPa, and flexural stiffness (EI) was around 1.09×10^{13} Nmm^2 in serviceability range against rural area timber bridge loadings under class 4 classification in AS 5100.7-2004. Compare with predicted ultimate compressive capacity of the pile (excluding the effect of buckling) 2.81 times higher than actual rural area bridge loadings. Therefore the factor of safety of the GFRP pile, against actual rural area bridge loadings under class 4 road classification in accordance with AS 5100.7-2004, is around 2.8.

Generally most of the calculated mechanical property values from the finite element models are approximately same order as the experimental investigation values. The use of FE method, thus, proved to be effective in determining the overall compressive modulus and flexural modulus of the GFRP composite piles under serviceability loadings. From FEA, it was found that glass-reinforced lamina bears 96% of the applied load, while 4% was carried by soric XF-reinforced lamina for particular lamina layup arrangement introduced to the GFRP pile. Lateral strain of the plies remains the same across the thickness, irrespective of the loading magnitude, while strain variations of the plies on the axial direction were developed, and more pronouncedly at the maximum applied load.

Overall performance of the pile rehabilitation system was evaluated (in Chapter 4) by considering two FE models, which represented two types of load scenarios. First scenario, behaviour of 300 mm external diameter 7.5 m long pile followed by connector against Shorncliffe pier loadings was evaluated. Here 1.2DL+0.4IL +1.65WL load case was identified as worst and lower margin safety factor of GFRP pile and connector were around 5.5, 1.75 respectively. Therefore against Shorncliffe pier loadings given by Brisbane City Council, this GFRP pile and the connector behave in the safe way. Second scenario, behaviour of 470 mm external diameter 7.5m long pile filled with polyester based filler against rural area bridge loadings was

evaluated. Here 1.2DL+1.8TL +1.65DEB L load case was identified as worst and lower margin safety factor of pile was around 2. It was also recommended that this pile is suitable for only remote areas, having only 2, A160 axial loads vehicle. Further development and analysis is required for GFRP piles, which is placed on a bridge having M1600 and S1600 traffic loads. FE modelling for polymer based filler was done against to the two-lane timber bridge loadings, per AS 5100 bridge code. From the FEA results any suitable filler material having more than 46 MPa compressive strength and 0.002 failure strain can be recommended as a filler for the connector. Therefore considering other factors such as durability, gel time, pumping ability and workability, further development of polyester based filler materials were chosen.

Then, polyester based filler materials were developed (in Chapter 5) using trial weight percentage and volumetric analysis approach. More than 60MPa compressive strength can be achieved easily in the filler material development when polyester resin content varied from 40% to 60% (w/w) with fly ash and sand. When polyester resin content varied from 16.5% -35% (w/w), more than 80MPa 28 days compressive strength can be achieved directly. Maximum compressive strengths of polyester based fillers were indicated in around 21 days and different from Ordinary Portland Cement (OPC) concrete. More than 90% of compressive modulus was rapidly developed between 3 and 7 days for all filler mixes. After 21 days, compressive modules behaved uniformly. Stress-strain behaviour of unconfined polyester based filler materials were developed, so that designers can use it in the calculation of sectional capacities, which will finally lead to member and structure behaviour. The following two equations were proposed by modifying Carreira et al. (1985) model, to define the stress-strain curve for unconfined polyester based fillers.

$$\frac{f}{f_0} = \frac{1.782\left(\frac{\varepsilon}{\varepsilon_0}\right)}{1+0.782\left(\frac{\varepsilon}{\varepsilon_0}\right)^{2.278}} \rightarrow \text{Low fly ash region}$$

$$\frac{f}{f_0} = \frac{2.199\left(\frac{\varepsilon}{\varepsilon_0}\right)}{1+1.199\left(\frac{\varepsilon}{\varepsilon_0}\right)^{1.833}} \rightarrow \text{High fly ash region}$$

A remarkable agreement was observed between the experimental and analytical curves for low fly ash region, and modification is required for the analytical curves in high fly ash region. Considering the above findings, most of the tested trial polyester filler materials can be used in this connector, based on their fair compressive and flexural stress-strain behaviour, compared with traditional concrete. However, shrinkage and gel time, play an important role in selecting the appropriate mix configuration.

6.3 Recommendations for future research

In order to fully develop this GERP composite pile and connector for timber pile rehabilitation, further research is recommended in the following areas:

- Evaluation of bond between polyester base fillers and GFRP material.
- Full scale testing for GFRP pile followed by connector to study entire behaviour under different loadings.
- The pile is connected to other parts of a structure, then entire behaviour is different and appropriate tests are recommended to evaluate GFRP connections and joints to verify the capacities.
- In principle, if axial compression is the controlling design load, then the continuous fibres of the GFRP system should be oriented in the hoop direction for maximum confinement. On the other hand, if applied moment is the dominating design factor, the continuous fibres of the GFRP system should be oriented in the axial direction of the pile and connector. Therefore, fibres oriented in other directions such as $\pm 45°$ to the axis of the piles may provide the optimum design solution. Further testing should be conducted to examine more optimal fibre orientations, and to quantify the effect of different fibre orientations on the pile and connector capacity.

This study has outlined the behaviour of fibre composite piles and connectors for timber pile rehabilitation. The concept developed, tested and verified in this study is viable for general timber pile rehabilitations in piers / jetties, and extending to rural two lane timber bridges.

LIST OF REFERENCES

1. ACI Committee 548, Guide for polymer concrete overlays, ACI 548.5R-94, 1998.

2. AS 5100.2-2004, Bridge Design – Design loads, Standards Australia.

3. AS 5100.7-2004, Bridge Design – Rating of existing bridges, Standards Australia.

4. ASTM D 6289-98, Standard Test Method for Measuring Shrinkage from Mold Dimensions of Molded Thermosetting Plastics, American Society for Testing and Materials.

5. ASTM D 695, Standard Test Method for Compressive Properties of Rigid Plastics. West Conshohocken, American Society for Testing and Materials.

6. ASTM D3967 - 08, Standard Test Method for Splitting Tensile Strength of Intact Rock Core Specimens, American Society for Testing and Materials.

7. ASTM Designation D5379M-98, Standard Test Method for Shear Properties of Composite Materials by the V-Notched Beam Method (Iosipescu Shear Test).

8. Avent, R.R. (1989). Durability of Posted and Epoxy-Grouted Timber Piles. *Journal of Structural Engineering*, 115(4), ASCE, April 1989, 826 - 833.

9. Binshan, S.Y., Alrik, L.S., & Lawrence, C.B. (1995). Mass and Volume Fraction Properties of Pultruded Glass Fibre-Reinforced Composites. *Research Report, Composites Volume 26, Elsevier Science Limited, U.K.*

10. Blaga, A., & Beaudoin, J.J. (1985). Polymer concrete. *Canadian Building Digest*, CBD-242, NRC-IRC Publication, Canada.

11. Browne, R.D., Adams, M., & French, E.L. (1975). Experience in the use of Polymer Concrete in the Building and Construction Industry. *Proceedings, First International Congress on Polymers in Concretes, London*, 1975

12. Carreira, D.J., & Chu, K.D. (1985). Stress-Strain Relationship for Plain Concrete in Compression. *ACI Journal Proceedings*, 82(6): 797-804 (1985).

13. Christensen, J.B., Gilstrap, J. & Dolan C.W. (1996). Composite materials reinforcement of existing masonry walls. *Journal of Architectural Engineering 20*(4):56-60.

14. Coburn, S. K. (2000). Corrosion Factors to be Considered in the Use of Steel Piling in Marine Structures. Pile Buck, Technical Guidelines, Palm City, FL, 10A-18C.

15. Department of Mains Roads, Queensland Australia. (February 2005). *Timber Bridges Maintenance Manual*, from http://www.tmr.qld.gov.au/Business-and-

industry/Technical-standards-and-publications/Timber-bridge-maintenance-manual.aspx

16. Desayi, P., & Krishnan, S. (1964). Equation for the Stress-Strain Curve of Concrete. *ACI Journal Proceedings*, 61(3): 345-350 (1964).

17. Dimmick, F.E. (1994). Restoration and Overlayment of Steep Curved Ramps by Using Epoxy Systems. *Concrete International*, 16(1): 32-38 (January 1994).

18. Dimmick, F.E. (1996). 15-Year Tracking Study: Comparing Epoxy Polymer Concrete to Portland Cement Concrete Applied on Slab-on Grade and Bridge Decks. *Properties and Uses of Polymers in Concrete*, SP-164, American Concrete Institute, Farmington, 1996.

19. Dudgeon, C.D. (1987). Engineered Materials Handbook. Metals Park. ASM International.

20. Fam A.Z. (July 2000). Concrete-Filled Fibre Reinforced Polymer Tubes for Axial and Flexural Structural Members. Ph.D. thesis, University of Manitoba, Winnipeg, Manitoba.

21. Fam, A.Z., & Rizkalla, S.H. (2001). Behaviour of Axially Loaded Concrete-Filled Circular Fibre-Reinforced PoIymer Tubes. *ACI Structura1 Journal*, 98(3), May-June 2001.

22. Fontana, J.J., Webster, R., & Kukacka, L.E. (1978). Rapid Patching of Deteriorated Concrete Using Polymer Concrete. *Proceedings, 2nd International Congress on Polymers in Concrete, University of Texas, Austin*, Oct. 1978, 105-119.

23. Fontana, Jack J., & Bartholomew, John. (1981). Use of Concrete Polymer Materials in the Transportation Industry. *Applications of Polymer Concrete, SP-69, American Concrete Institute, Farmington Hills, Mich.*, 1981, 21-30.

24. Fowler, D. W. (1999). Polymers in concrete: A vision for 21st century. *Cement and Concrete Composites*, 21, 449–452.

25. GangaRao, H., Sonti, S., Superfesky. M., (1996). Static Response of Timber Crossties Reinforced with Composite Fabrics. *International Society of the Advancement of Materials and Process Engineering Symposium and Exhibition*. Volume 41, 1291-1303.

26. Hamdy, M., & Radhouane, M. (2009). Behavior of FRP Tubes-Encased Concrete Columns under Concentric and Eccentric Loads. *COMPOSITES & POLYCON 2009*, American Composites Manufacturers Association, January 15-17, 2009.

27. Hamilton, H.R., & Dolan, C.W. (2000). Durability of FRP reinforcements for concrete. *Progress in Structural Engineering and Materials*, 2(2), 2000, 139–145.

28. Irene Scott & Ken, W. (2002). Application of Fibre Reinforce Polymer Composite in Bridge Construction. *IPWEA NSW Division Annual Conference 2002.*

29. ISO 1172:1999, Determination of the textile-glass and mineral filler content.

30. ISO 14126:1999, Fibre Reinforced Plastic Composites, Determination of Compressive Properties in the In-Plane Direction (Modified Method 2).

31. ISO 178:1993, Plastics Determination of Flexural Properties, Geneva, International Organisation for Standardisation.

32. Jane Proszek Gorninskia, Denise C. Dal Molinb & Claudio S. Kazmierczaka (2004). Study of the modulus of elasticity of polymer concrete compounds and comparative assessment of polymer concrete and Portland cement concrete. *Cement and Concrete Research*, 34 (2004) 2091–2095.

33. Kallol Sett & Vipulanandan, C. (2004). Properties of Polyester Polymer Concrete with Glass and Carbon Fibers. *ACI Materials Journal*, 101(1), January-February 2004.

34. Katsuki, F., Uomoto, T. (1995).Prediction of Deterioration of FRP Rods due to Alkali Attack. *Non-Metallic (FRP) Reinforcements for Concrete Structures, FRPCS-2,* Ghent, Belgium, 82-89.

35. Kshirsagar, S., Lopez-Anido, R., & Gupta, R.K. (2000). Environmental aging of fibre-reinforced polymer-wrapped concrete cylinders. *ACI Material Journal,* 97(6), 703–712.

36. Lopez-Anido, R., & Karbhari, V.M. (2000). Chapter 2: Fibre reinforced composites in civil infrastructure. *Emerging materials for civil engineering infrastructure - State of the art*, ASCE, Reston, 41–78.

37. Lopez-Anido, R., & Xu, H. (2002). Structural characterization of hybrid fibre-reinforced polymer - glulam panels for bridge decks. *Journal of Composites for Construction*, 6(3), 194–203.

38. Lopez-Anido, R., Antonis, P., Michael, S., Sandford, T.C., & Barry, G. (2005). Repair of Wood Piles Using Prefabricated Fibre-Reinforced Polymer Composite Shells. *Journal of Performance of Constructed Facilities*, 19(1), Feb 2005, 78-87.

39. Lopez-Anido, R., Gardner, D.J., & Hensley, J.L. (2000). Adhesive bonding of eastern hemlock glulam panels with E-glass/vinyl ester reinforcement. *Forest Products Journal*, 50(11/12), 43–47.

40. Lopez-Anido, R., Michael, A.P., & Sandford, T.C. (2003). Experimental characterization of FRP composite wood pile structural response by bending tests. *Marine Structures* 16(4), 257-274.

41. MacGregor, J.G., & Wight J.K. (2005). Reinforced Concrete Mechanics and Design. 4th Ed., Prentice Hall, Upper Saddle River, New Jersey.

42. Mander, J.B., Priestley, M.J.N., & Park, R. (1988). Theoretical Stress-Strain Model for Confined Concrete. *Journal of Structural Engineering*, ASCE, 114 (8), August 1988, 1804 - 1826.

43. Marinela Barbuța, Maria Harja, & Rina Baran (2010). Comparison of Mechanical Properties for Polymer Concrete with Different Types of Filler, J*ournal of Materials in Civil Engineering*, Vol. 22(7), July 1, 2010.

44. Mirmiran, A., & Shahawy, M. (1997). Behaviour of Concrete Columns Confined by Fibre Composites. *Journal of Structural Engineering*, Vol. 123, No. *5,* 1997, 583 – 590.

45. Muthukumar, M., & Mohan, D. (2004). Optimization of Mechanical Properties of Polymer Concrete and Mix Design Recommendation Based on Design of Experiments. *Journal of Applied Polymer Science*, Vol. 94, 1107–1116 (2004).

46. Muthukumar, M., Mohan, D., & Rajendran, M. (2003). Optimization of mix proportions of mineral aggregates using Box Behnken design of experiments. *Cement and Concrete Composites*, 25, 751–758.

47. Picher, F., Rochette, P & Labossiere, P. (1996). Confinement of Concrete Cylinders with CFRP*, Proceedings of the 1st International Conference on Composites in Infrastructure, H. Saadatmanesh and M. R. Ehsani, eds., University of Arizona, Tucson, Arizona,* 829-841.

48. Popovics, S. (1973).A numerical approach to the complete stress-strain curve of concrete. *Cement and Concrete Research*, 3(5), 583-599.

49. Railway and Truck Structures (1973), New Grout-Filled Timber Piles, February 1973, Vol. 69, No. 2, 28-29, Sirnmons-Boardman Pub. Corp., Bristol,Conn. USA.

50. Reis, J.M.L. (2006). Fracture and flexural characterization of natural fiber-reinforced polymer concrete. *Construction and Building Materials*, 20, 673–678.

51. Reis, J.M.L., & Ferreira, A.J.M. (2004). Assessment of fracture properties of epoxy polymer concrete reinforced with short carbon and glass fibers. *Construction and Building Materials*, 18, 523–528.

52. Ritter, Michael. A. (1990), Timber Bridges: Design, Construction, Inspection, and Maintenance, *Chapter 14: Maintenance and Rehabilitations of Timber Bridges,* 14:1-14:26.

53. San-Jose, J.T. (2006). Mechanical properties in resin polyester concrete, application to reinforced beams. *Science and Engineering of Composite Materials*, 13(4), 271–282.

54. STRAND 7 Release 2.3. (2005). Theoretical manual. Edition 1.

55. Teng, J.G., & Hu, Y.M. (2007). Behaviour of FRP-jacketed circular steel tubes and cylindrical shells under axial compression. *Construction and Building Materials* 21(2007) 827-838.

56. US ARMY (1985), Pile Construction, *Field Manual*, FM 5-134, Washington, DC, 8:1-8:10.

57. US Army Corps of Engineers, Naval Facilities Engineering Command, and Agency, A.F. C. E. S. (2001). Unified Facilities Criteria (UFC) - Operation and Maintenance: Maintenance of Waterfront Facilities. UFC 4-1 50-07, Washington, DC.

58. Vipulanandan, C., & Paul, E. (1991).Performance of epoxy and polyester polymer concrete. *ACI Materials Journal, 241–251, 1991.*

59. Vipulanandan, C., & Paul, E. (1993). Characterization of polyester polymer and polymer concrete. *Journal of Materials in Civil Engineering, ASCE*, 5(1), 1993, 62-82.

APPENDIX A

LAMINATES TEST DATA

APPENDIX B
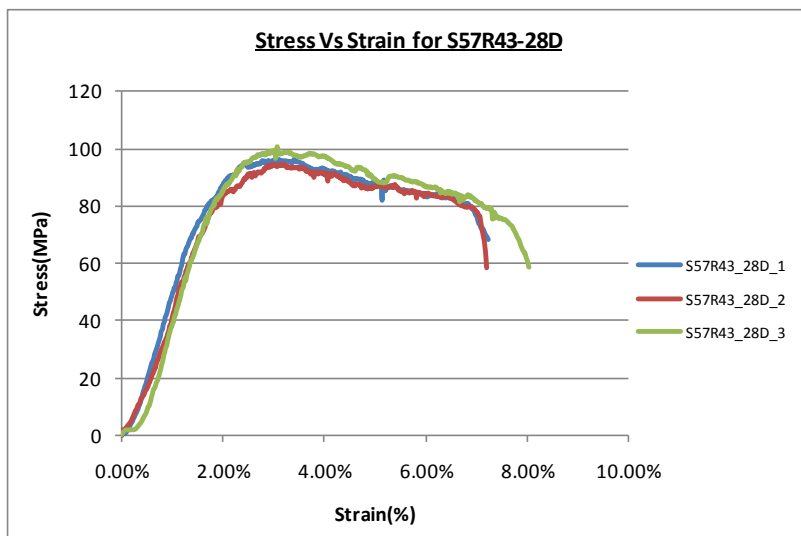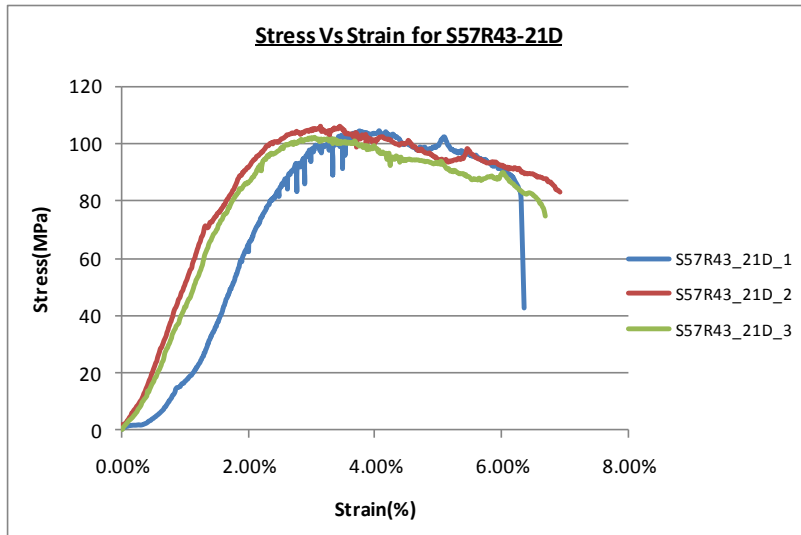
ADDITIONAL DATA OF FILLER MATERIAL DEVELOPMENT

(Supplement to Chapter 5)

Spread sheet developed using mixing formula

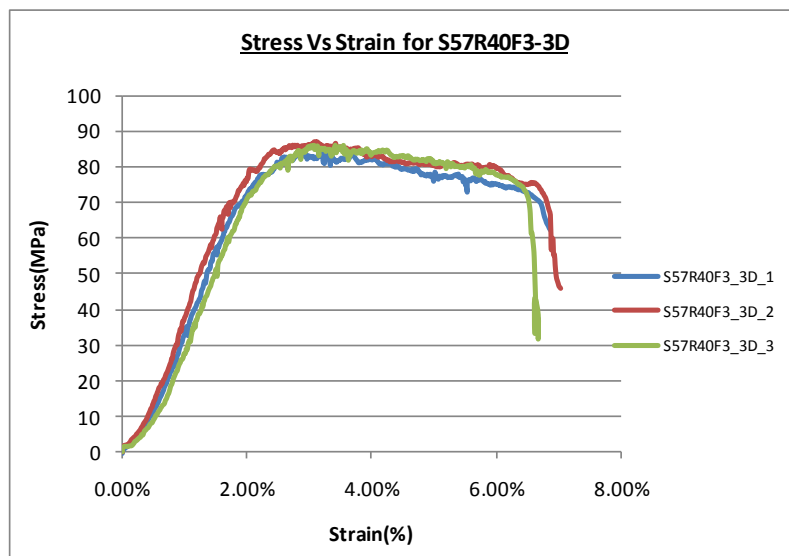|						Density	g/cc
Dia (mm)	50	Height(mm)	120		Sand	1494	1.494
Number of Samples	4				Fly Ash	1100	1.1
Volume of mould	235619.4 mm3				Resin	1100	1.1
					Catelist	1180	1.18
Total Volume	942.4778 cc				Caterlist %	0.025	
					contingency (%)	0.3	
					Volume Required==>	1225.221	

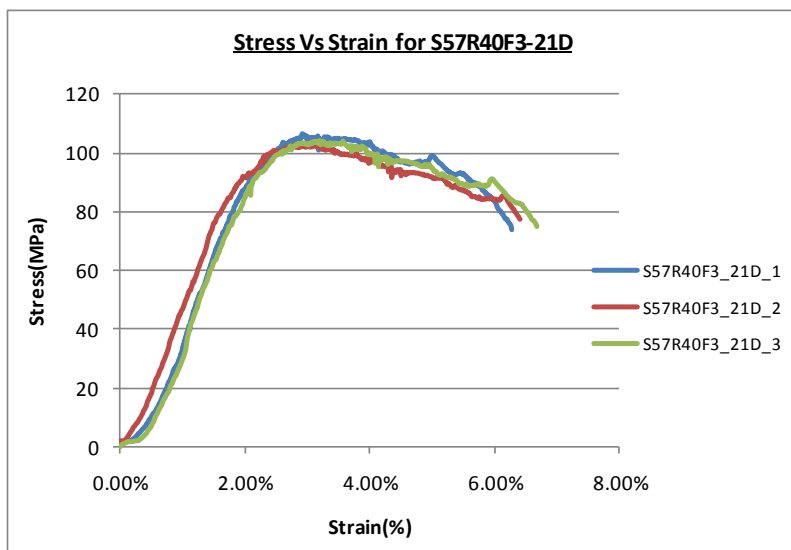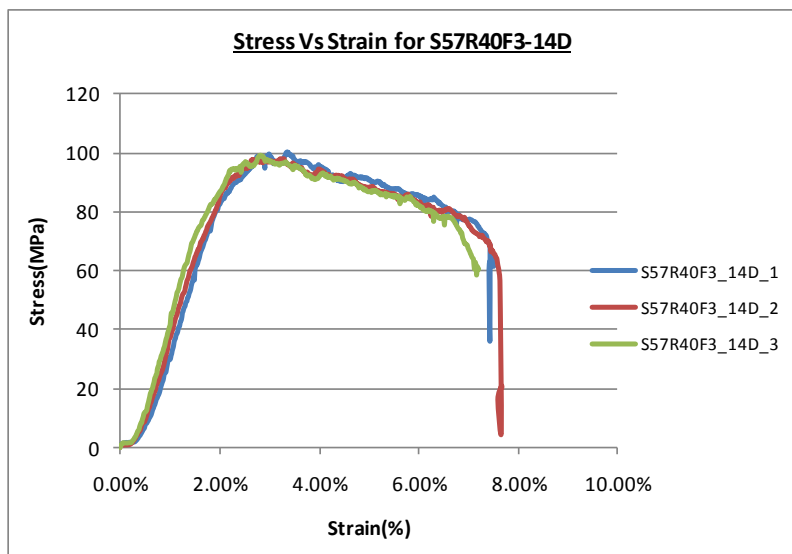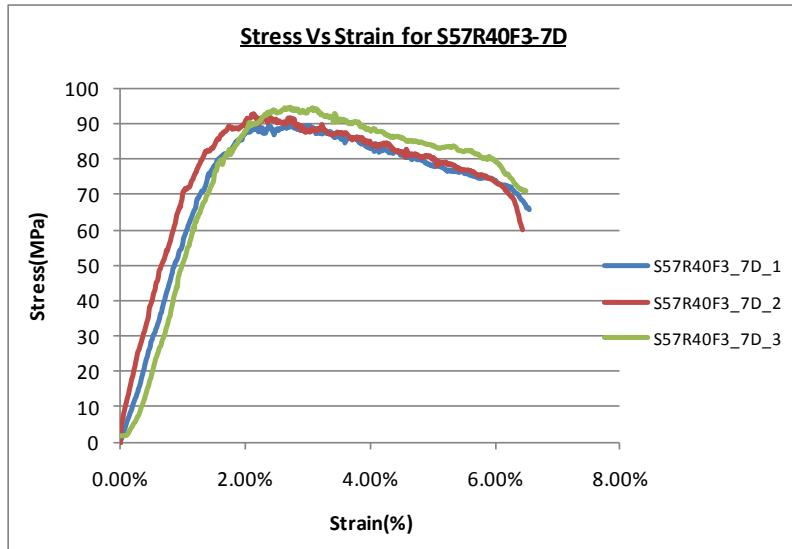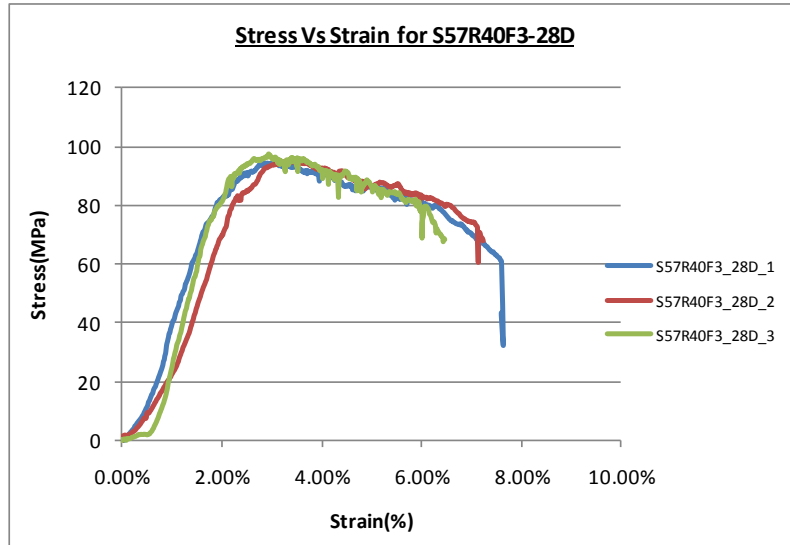| Sample #	% by volume			Amount(g)				% by weight			
	Sand	Resin+Catelist	FA	Sand	Caterlist	Resin	FA	Sand	Caterlist	Resin	FA
S57R43	57	43	0	1043.374	14.15828	566.3312	0	64.3	0.9	34.9	0
S57R40F3	57	40	3	1043.374	13.170	526.820	40.432	64.3	0.8	32.4	2.5
S57R35F8	57	35	8	1043.374	11.524	460.967	107.819	64.3	0.7	28.4	6.6
S57R30F13	57	30	13	1043.374	9.878	395.115	175.207	64.3	0.6	24.3	10.8
S57R25F18	57	25	18	1043.374	8.232	329.262	242.594	64.3	0.5	20.3	14.9
S57R20F23	57	20	23	1043.374	6.585	263.410	309.981	64.3	0.4	16.2	19.1
S57R15F28	57	15	28	1043.374	4.939	197.557	377.368	64.3	0.3	12.2	23.2
S57R10F33	57	10	33	1043.374	3.293	131.705	444.755	64.3	0.2	8.1	27.4
S57R5F38	57	5	38	1043.374	1.646	65.852	512.142	64.3	0.1	4.1	31.6

Stress Vs Strain variation for S57R43 with age

Stress Vs Strain for S57R43-3D

- S57R43_3D_1
- S57R43_3D_2
- S57R43_3D_3

Stress Vs Strain for S57R43-7D

- S57R43_7D_1
- S57R43_7D_2
- S57R43_7D_3

Stress Vs Strain for S57R43-14D

- S57R43_14D_1
- S57R43_14D_2
- S57R43_14D_3

Stress Vs Strain for S57R43-21D

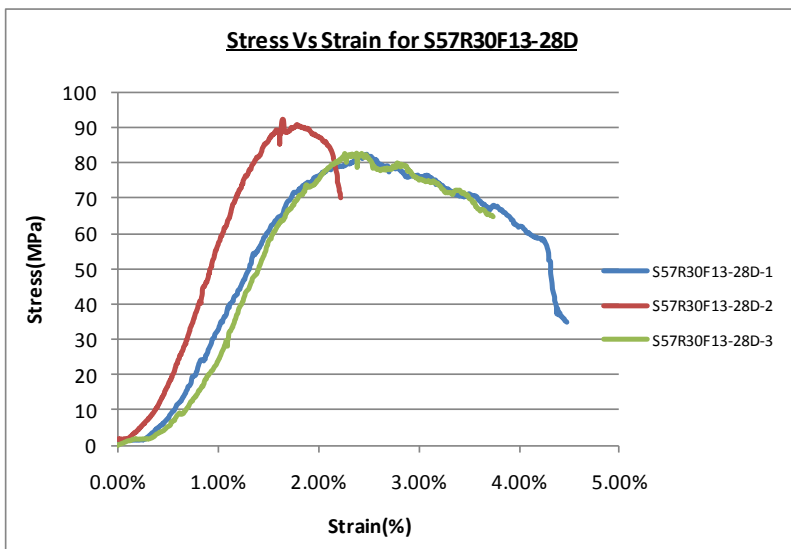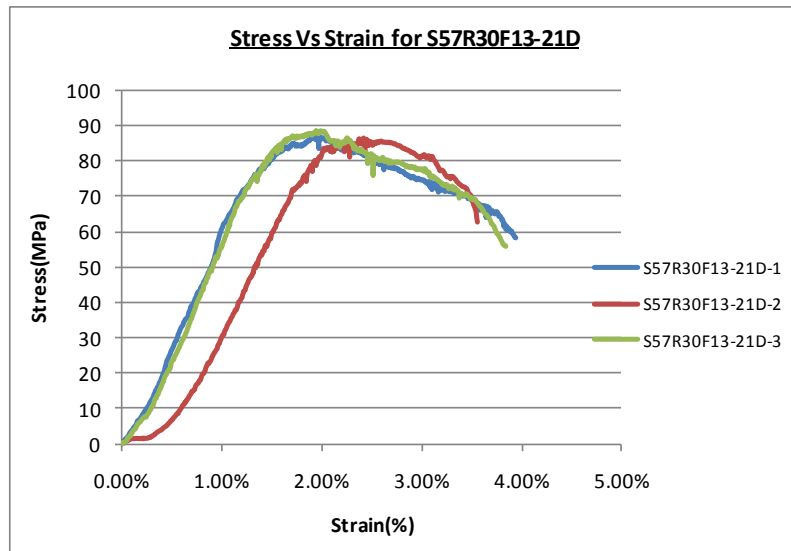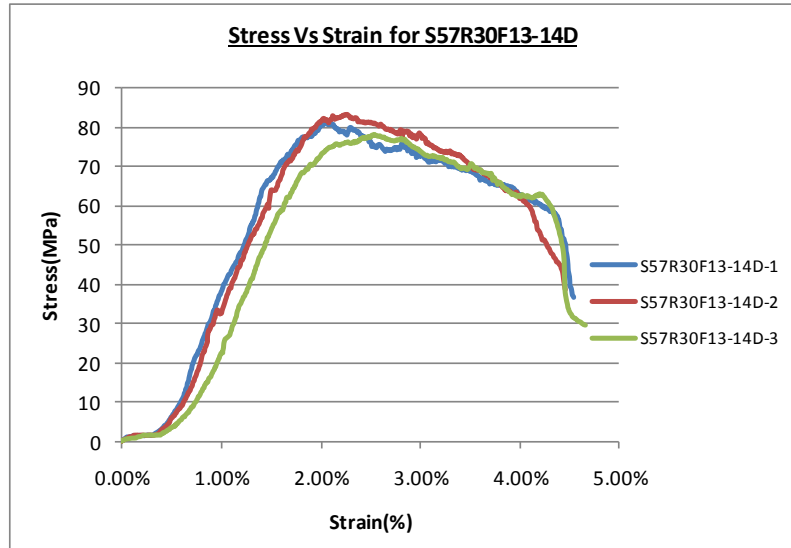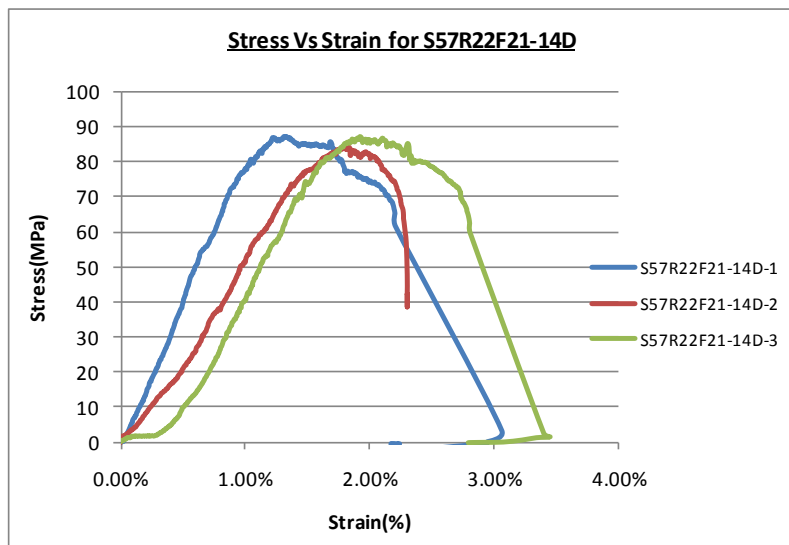Stress Vs Strain for S57R43-28D
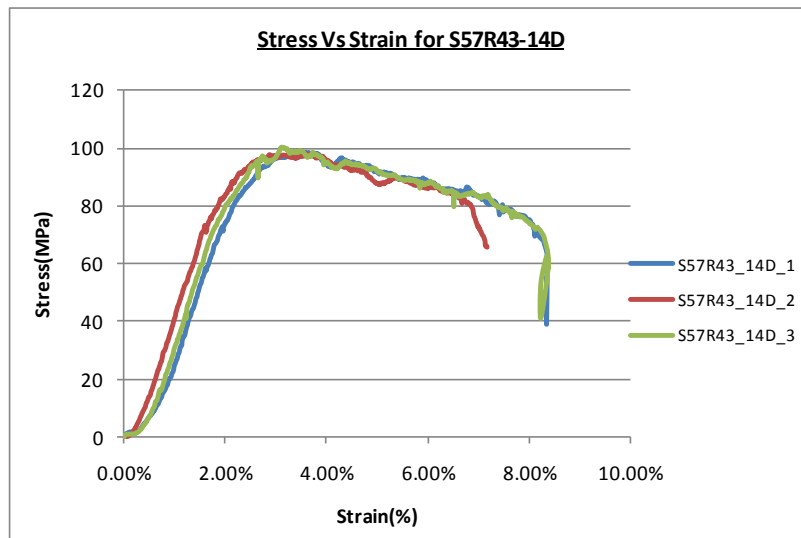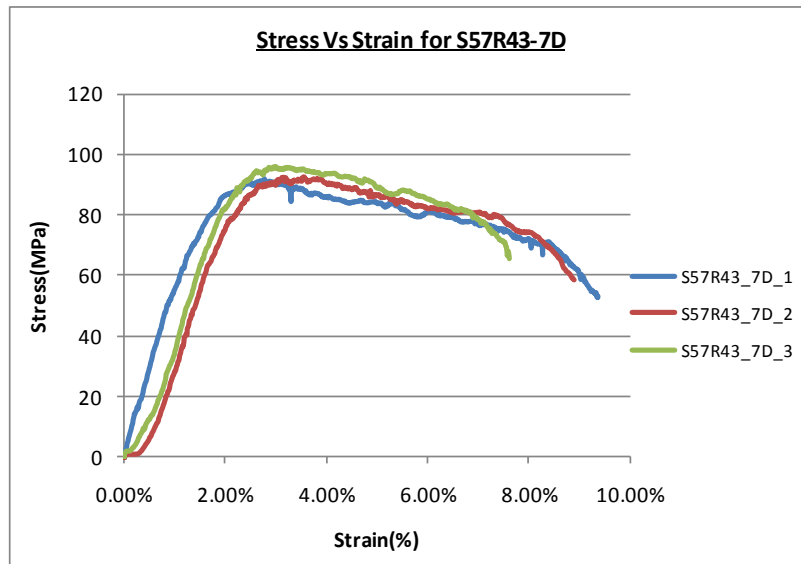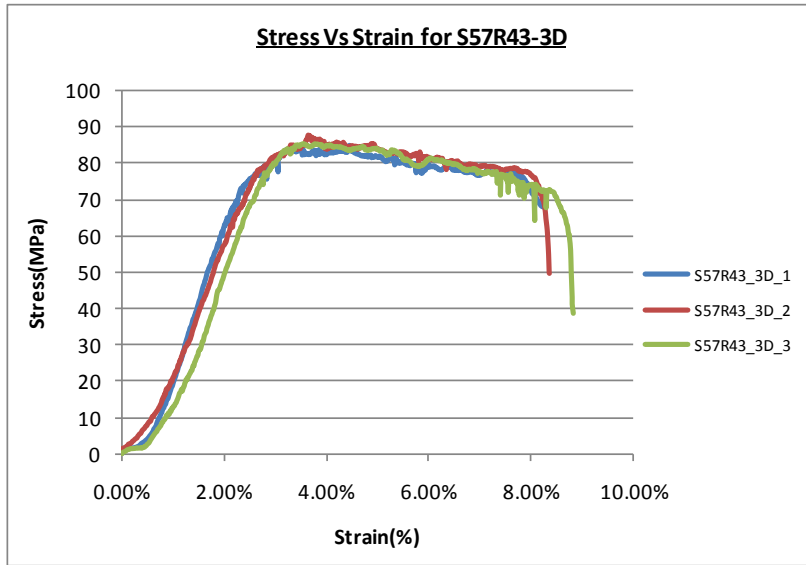
Stress Vs Strain variation for S57R40 with age

Stress Vs Strain for S57R40F3-3D

Stress Vs Strain for S57R40F3-7D

Stress Vs Strain for S57R40F3-14D

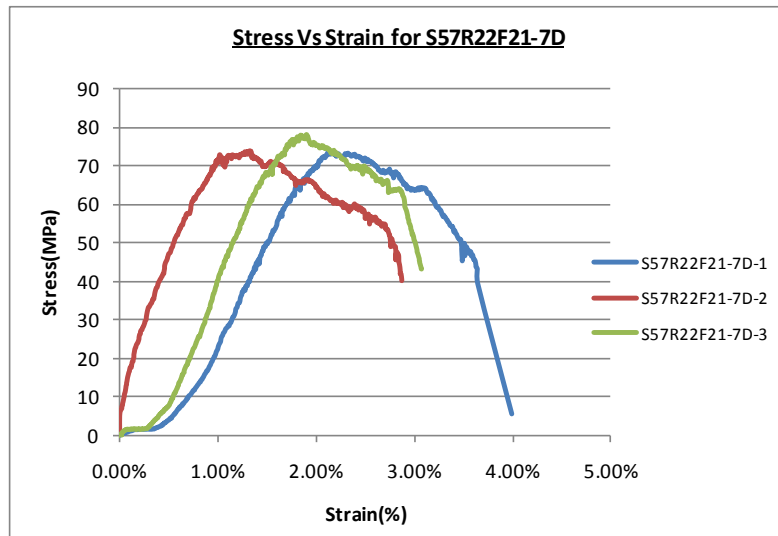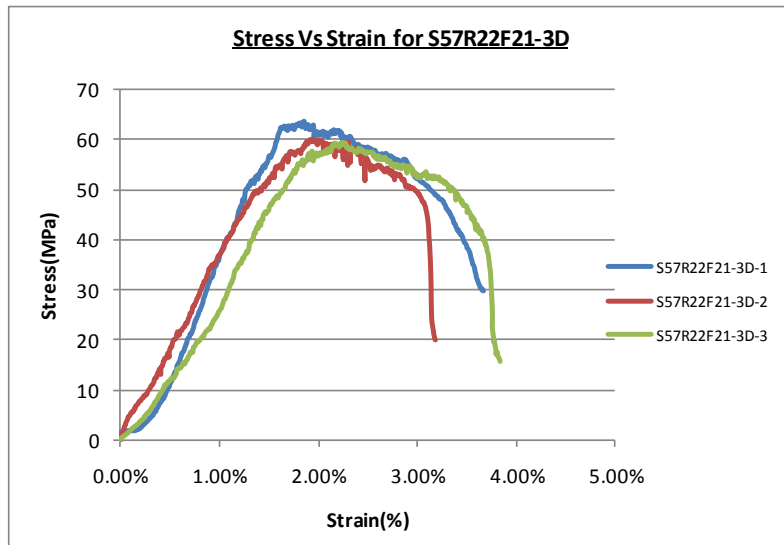Stress Vs Strain for S57R40F3-21D

Stress Vs Strain for S57R40F3-28D

Stress Vs Strain variation for S57R30F13 with age

Stress Vs Strain for S57R30F13-3D

Stress Vs Strain for S57R30F13-7D

Stress Vs Strain for S57R30F13-14D

Stress Vs Strain for S57R30F13-21D

Stress Vs Strain for S57R30F13-28D
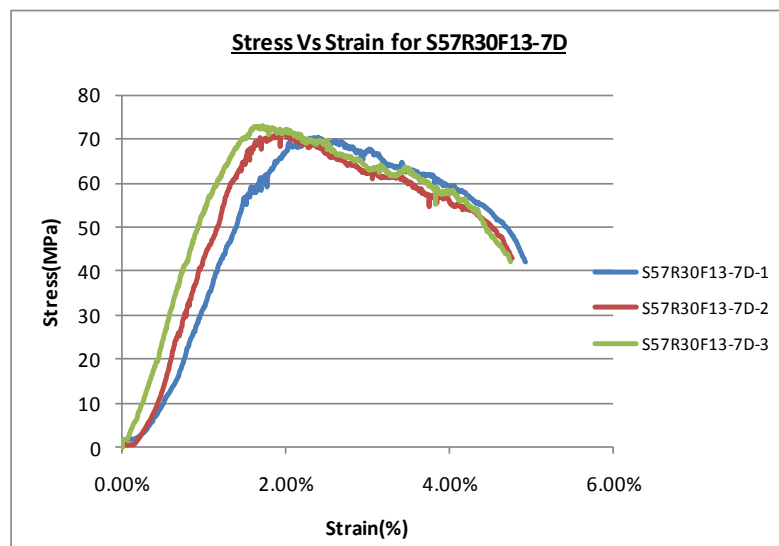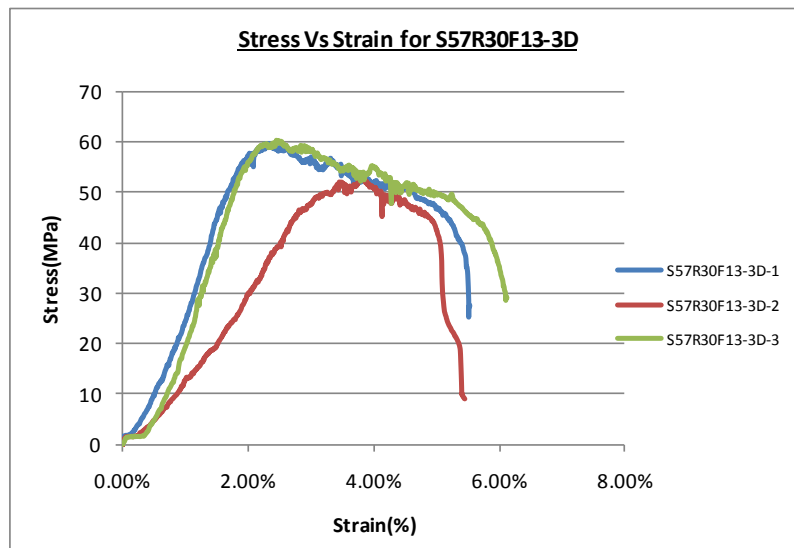
Stress Vs Strain variation for S57R21F21 with age

Stress Vs Strain for S57R22F21-3D
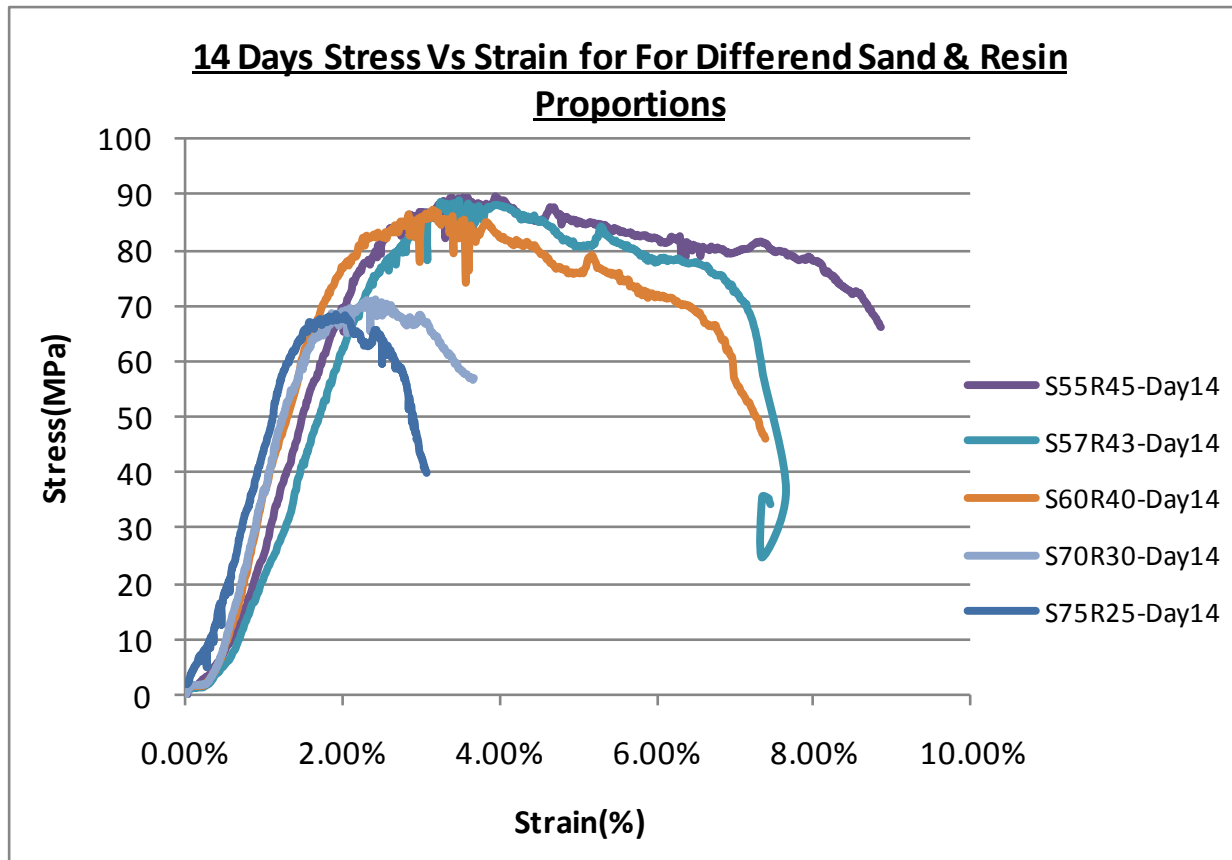

Stress Vs Strain for S57R22F21-7D

Stress Vs Strain for S57R22F21-14D

Stress Vs Strain for S57R22F21-21D

Stress Vs Strain for S57R22F21-28D
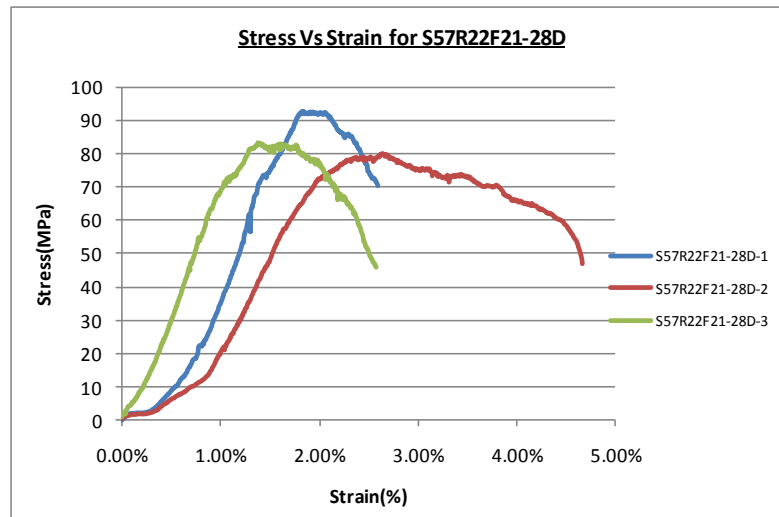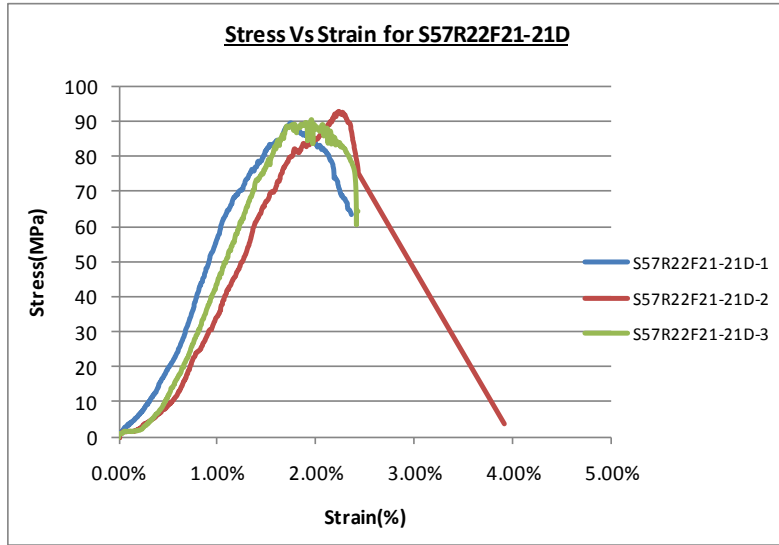
Stress – strain curves for initial trial proportions with sand and resin

14 Days Stress Vs Strain for For Differend Sand & Resin Proportions

28 Days Stress Vs Strain for For Differend Sand & Resin Proportions